อนุพันธ์แนฟทาลิไมด์ชนิดใหม่สำหรับการประยุกต์ในไดโอดอินทรีย์เปล่งแสง

นางสาวรุ่งทิวา อรุณฉาย

วิทยานิพนธ์นี้เป็นส่วนหนึ่งของการศึกษาตามหลักสูตรปริญญาวิทยาศาสตรมหาบัณฑิต
สาขาวิชาเคมี ภาควิชาเคมี
คณะวิทยาศาสตร์ จุฬาลงกรณ์มหาวิทยาลัย
ปีการศึกษา 2557

NEW NAPHTHALIMIDE DERIVATIVES FOR ORGANIC LIGHT-EMITTING DIODE APPLICATION

Miss Rungthiwa Arunchai

A Thesis Submitted in Partial Fulfillment of the Requirements

for the Degree of Master of Science Program in Chemistry

Department of Chemistry

Faculty of Science

Chulalongkorn University

Academic Year 2014

Thesis Title	NEW NAPHTHALIMIDE DERIVATIVES FOR ORGANIC LIGHT-EMITTING DIODE APPLICATION
By	Miss Rungthiwa Arunchai
Field of Study	Chemistry
Thesis Advisor	Associate Professor Paitoon Rashatasakhon, Ph.D.
Thesis Co-Advisor	Associate Professor Mongkol Sukwattanasinitt, Ph.D.

Accepted by the Faculty of Science, Chulalongkorn University in Partial Fulfillment of the Requirements for the Master's Degree

.....Dean of the Faculty of Science
(Professor Supot Hannongbua, Dr.rer.nat.)

THESIS COMMITTEE

.....Chairman
(Associate Professor Vudhichai Parasuk, Ph.D.)

.....Thesis Advisor
(Associate Professor Paitoon Rashatasakhon, Ph.D.)

.....Thesis Co-Advisor
(Associate Professor Mongkol Sukwattanasinitt, Ph.D.)

.....Examiner
(Anawat Ajavakom, Ph.D.)

.....External Examiner
(Nakorn Niamnont, Ph.D.)

รุ่งทิวา อรุณฉาย : อนุพันธ์แนฟทาลิไมด์ชนิดใหม่สำหรับการประยุกต์ในไดโอดอินทรีย์เปล่งแสง (NEW NAPHTHALIMIDE DERIVATIVES FOR ORGANIC LIGHT-EMITTING DIODE APPLICATION) อ.ที่ปรึกษาวิทยานิพนธ์หลัก: รศ. ดร.ไพฑูรย์ รัชตะสาคร, อ.ที่ปรึกษาวิทยานิพนธ์ร่วม: รศ. ดร.มงคล สุขวัฒนาสินิทธิ์, 84 หน้า.

สารประกอบแนฟทาลิไมด์-ไตรเฟนิลเอมีนชนิดใหม่จำนวนสามชนิด (TPN1, TPN2 และ TPN3) สามารถสังเคราะห์โดยปฏิกิริยาซูซูกิครอสคัปปลิงระหว่างเอ็นเฟนิล-1,8-แนฟทาลิไมด์ และไตรเฟนิลเอมีน ในสารละลายคลอโรฟอร์ม สารเหล่านี้ดูดกลืนแสงสูงสุดในช่วงความยาวคลื่น (λ_{max}) 430-433 นาโนเมตร ขณะที่การคายแสงของสารสูงสุดที่ความยาวคลื่น 564-599 นาโนเมตร ด้วยค่าควอนตัมยิว 0.18-0.29 ในสถานะของแข็งแบบฟิล์มบางซึ่งมีแรงการจัดเรียงตัวเพิ่มมากขึ้น และป้องกันการสั่นของโมเลกุล การดูดกลืนแสงเลื่อนไปที่ความยาวคลื่นมากขึ้น ในขณะที่พีคการคายแสงเลื่อนไปที่ความยาวคลื่นสั้นลง อนุพันธ์ทุกชนิดมีความเสถียรทางความร้อนที่สูง อนุพันธ์ถูกนำมาขึ้นรูปในไดโอดอินทรีย์เปล่งแสง (OLED) ที่มีโครงสร้างเป็น ITO/PEDOT:PSS/TPN1:CBP/BCP/LiF/Al พบว่าปล่อยแสงสีเขียวออกมา ให้ค่าความสว่างสูงสุดได้ 10,404 แคนเดลาต่อตารางเมตร ที่ 19 โวลต์ ค่าศักย์ไฟฟ้าเริ่มต้น 5.8 โวลต์ ผลการละลายของอนุพันธ์ทั้งสามต่อการขึ้นรูปไดโอดอินทรีย์เปล่งแสงพิสูจน์ได้โดยภาพจากเทคนิค AFM

ภาควิชา เคมี ลายมือชื่อนิสิต .....

สาขาวิชา เคมี ลายมือชื่อ อ.ที่ปรึกษาหลัก .....

ปีการศึกษา 2557 ลายมือชื่อ อ.ที่ปรึกษาร่วม .....

5472081423 : MAJOR CHEMISTRY

KEYWORDS: TRIPHENYLAMINE / NAPHTHALIMIDE / SUZUKI CROSS-COUPLING / OLED

RUNGTHIWA ARUNCHAI: NEW NAPHTHALIMIDE DERIVATIVES FOR ORGANIC LIGHT-EMITTING DIODE APPLICATION. ADVISOR: ASSOC. PROF. PAITOON RASHATASAKHON, Ph.D., CO-ADVISOR: ASSOC. PROF. MONGKOL SUKWATTANASINITT, Ph.D., 84 pp.

Three new triphenylamino naphthalimides (TPN1-3) are successfully synthesized by means of Suzuki cross-coupling between *N*-phenyl-1,8-naphthalimide and triphenylamine precursors. In $CHCl_3$ solution phase, their maximum absorption wavelengths are around 430-433 nm while the maximum emission wavelength at 564-599 nm with quantum yields in the range of 0.18 to 0.29 in $CHCl_3$. In solid thin-film state where the packing force enhances the conjugated system and prevents the molecular vibration, their absorption bands move towards longer wavelengths and the emission peaks shift to a shorter wavelengths. These compounds show excellent thermal stabilities with the 10% weight loss temperatures well above 350 °C. Results from the electrochemical investigation by cyclic voltammetry agrees with the data from computational calculations using Gaussian 09 code with B3LYP/6-31G(d,p) geometry optimizations. When the multi-layer OLED device of structure ITO/PEDOT:PSS/TPN1:CBP/BCP/LiF/Al is fabricated, a maximum brightness of 10,404 cd/m^2 of yellowish green light at an applied voltage of 19 V with a turn-on voltage of 5.8 V are observed. The effect of solubility of these compounds on device performance is proven by AFM images of the spin-casted thin films.

Department:	Chemistry	Student's Signature	.....
Field of Study:	Chemistry	Advisor's Signature	.....
Academic Year:	2014	Co-Advisor's Signature	.....

ACKNOWLEDGEMENTS

First of all, I would like to express my sincere gratitude to my thesis advisor, Associate Professor Paitoon Rashatasakhon, Ph.D. and my co-advisor, Associate Professor Mongkol Sukwattanasinitt, Ph.D., for valuable advice, guidance and kindness throughout this research.

Sincere thanks are also extended to Associate Professor Vudhichai Parasuk, Ph.D., Anawat Ajavakom, Ph.D. and Nakorn Niamnont, Ph.D., attending as the committee members, for their valuable comments and suggestions. I would like to especially thank Associate Professor Vinich Promarak, Ph.D. and Assistant Professor Taweesak Sudyoadsuk, Ph.D., Ubon Ratchathani University and also Professor Hideyuki Murata, Ph.D. and Assistant Professor Toshinori Matsushima, Ph.D., Japan Advanced Institute of Science And Technology for valuable guidance on OLED work.

In particular, I am thankful to Material Advancement via Proficient Synthesis (MAPS group), Department of Chemistry, Faculty of Science, Chulalongkorn University for providing the chemicals and facilities throughout the course of the study.

Gratitude is also extended to the members of my research group for their helpful discussion. Finally, I would like to specially thank my family and friends for their encouragement and understanding throughout. I would not be able to reach this success without them.

CONTENTS

Page

Page

LIST OF FIGURES

Page

LIST OF SCHEMES

Page

LIST OF TABLES

Page

LIST OF ABBREVIATIONS

A	Ampere
Å	Angstrom
Alq_3	Tris(8-hydroxyquinoline)aluminium
Al	Aluminium
^{o}C	Degree of celsius
cm^2	Square centimeter (s)
Ca	Calcium
Cd	Candela
$CDCl_3$	Dueterated chloroform
CRT	Cathode ray tube
CV	Cyclic voltammetry
d	Doublet
dd	Doublet of doublet
DSC	Differential scanning colorimeter
EMMs	Emitting materials
EL	Electroluminescent
EML	Emitting layer
ETL	Electron-transporting layer
EtOAc	Ethyl acetate
eV	Electron volt
g	Gram (s)
h	Hour (h)
HOMO	Highest occupied molecular orbital
HRMS	High resolution mass spectroscopy
H_2SO_4	Sulfuric acid
HTL	Hole-transporting layer
HTMs	Hole-transporting materials
Hz	Hertz
ITO	Indium tin oxide
J	Coupling constant
K_2CO_3	Potassium carbonate
KI	Potassium iodide
KIO_3	Potassium iodate
LCD	Liquid crystal display
LED	Light-emitting diode

lm	Lumen
LiF	Lithium fluoride
LUMO	Lowest unoccupied molecular orbital
Mg	Magnesium
m^2	Square meter (s)
m	Multiplet
mg	Milligram (s)
$MgSO_4$	Magnesium sulfate
min	Minute (s)
mL	Milliliter (s)
mmol	Millimole (s)
M	Molar
MS	Mass spectroscopy
m.p.	Melting point
nm	Nanometer (s)
NMR	Nuclear magnetic resonance
OLED	Organic light-emitting diode
$PdCl_2$(dppf)	[1,1'-Bis(diphenylphosphino)ferrocene]palladium(II) dichloride
PL	Photoluminescent
s	Singlet
t	Triplet
Tg	Glass transition temperature
TGA	Thermo gravimetric analysis
TLC	Thin layer chromatography
V	Volt (s)
W	Watt (s)
%	Percent (s)
δ	Chemical shift
ε	Molar absorptivity
λ	Wavelength
Φ	Fluorescence quantum yield

CHAPTER I
INTRODUCTION

1.1 Introduction

Monitors have evolved in their quality and technology. From the classical Cathode Ray Tube (CRT), through Plasma and Liquid Crystal Displays (LCD) to the latest Organic Light Emitting Displays (OLED) have been developed. [1] The CRT monitors are heavy, bulky, and high in energy consumption and heat generation. The CRTs have been replaced by LCD which is flatter and slimmer. LCD (liquid crystal display) refers to organic substances that reflect light when voltage is applied. LCD has some advantages over CRT; for instance, they generally create less eye-strain, light flickering, light weight, and most importantly, they consume much lower electrical power. However, LCD technology still has some disadvantages such as the inability to emit light by itself and must be illuminated reflectively of the background light source. Moreover, their performances depend on the environment; for example, low temperatures can cause slow response, high temperatures can cause poor contrast. [2] When LCD monitors were first introduced, the competing technology was called plasma. One of the key advantages of plasma displays was the capability of producing deeper black, which increases the contrast ratio. This makes the plasma displays suitable for bright rooms and outdoor areas, even though they consume much higher power than the LCDs.

One of the most critical parameters for monitors is the resolution. However, the designed quality, contrast ratio, dynamic range, linearity of reproduction, power consumption, and size are also important and contribute to the overall picture quality. Therefore, OLEDs have been improved and developed to fulfill these requirements.

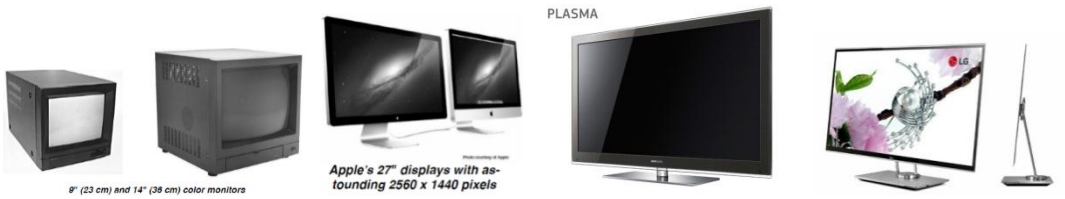

a b c d

Figure 1.1. (a) CRT, (b) LCD, (c) plasma, and (d) OLED displays in computer monitor [1]

1.2 Introduction to OLED

Organic light emitting diodes (OLEDs) are energy conversion devices (electricity-to-light) based on electroluminescence. OLEDs first attracted the researcher attention in the 1960s because of their potentially high luminescence quantum efficiencies and the ability to generate a wide variety of colors. OLEDs are extremely thin, practically two dimensional multi-layer devices of large square area. The thickness of all the active layers combined is only of the order of one hundred nanometers. There is no restriction on the size and shape of the OLED devices.

In 1987, Tang and Van Slyke, at Kodak, made a double layered device containing active "small molecules" with low-voltage (<10V) based on thin films of ~100 nm Alq_3 with good brightness (>1000 cd/m^2) and respectable luminous efficiency (1.5 lm/W) [3]. Shortly after, development on polymer light-emitting diodes commenced at Cambridge in Friend's group, and concurrently at Santa Barbara in Heeger's group [4].

During the last decades, great efforts were focused on the development of novel electroluminescent materials with intense luminescent efficiency, high thermal and optical stability, good charge carrier injection and transport, and desirable film morphology, as well as on the fabrication of high-performance OLED devices. Excellent red, green, and blue emitting materials are required to achieve full color displays and lighting applications [5]. **Figure 1.2** shows a comparison between an LCD with an OLED display [2]. It shows that the OLED display is easier to see at almost every angle with higher brightness and higher contrast than of LCD display which is an improvement of display technology.

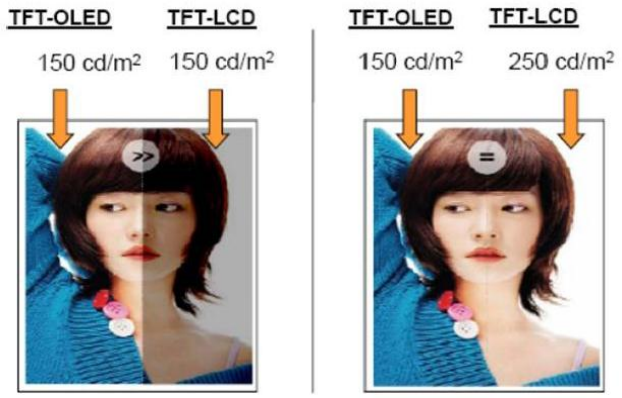

Figure 1.2. Comparison of brightness and contrast between OLED and LCD display [2]

1.3 OLED structure and operation

Structure of different OLEDs is shown in **Figure 1.3**. A single-layer OLED is made of a single organic layer sandwiched between the cathode and the anode. This device configuration is simple and suitable for materials which not only possess high photoluminescence quantum efficiency, but good hole- and electron-transporting properties.

If the emissive materials are lack of either hole- or electron-transporting property, the two-layer OLED could be constructed. For this, one organic layer is specifically chosen to transport holes and the other layer will function as the emissive layer with electron-transporting ability. Recombination of the hole–electron pair takes place at the interface between the two layers, which generates electroluminescence.

For most of the commercial OLED devices, both hole- and electron-transporting materials are fabricated along with the emissive material as seen in a three-layer OLED. The emitting layer is primarily the site of hole–electron recombination and thus for electroluminescence. This cell structure is useful for emissive materials that do not possess high carrier transport properties.

In a multi-layer OLED an electron injection layer is also included. Introduction of multilayer device structure eliminates the charge carrier leakage as well as exciton quenching, as excited states are generally quenched at the interface of the organic

layer and the metal. Multi layer OLEDs consist of different layers namely ITO glass plate, hole injection layer (HIL), hole transport layer (HTL), emitting layer (EML), electron transporting layer (ETL) and anode.

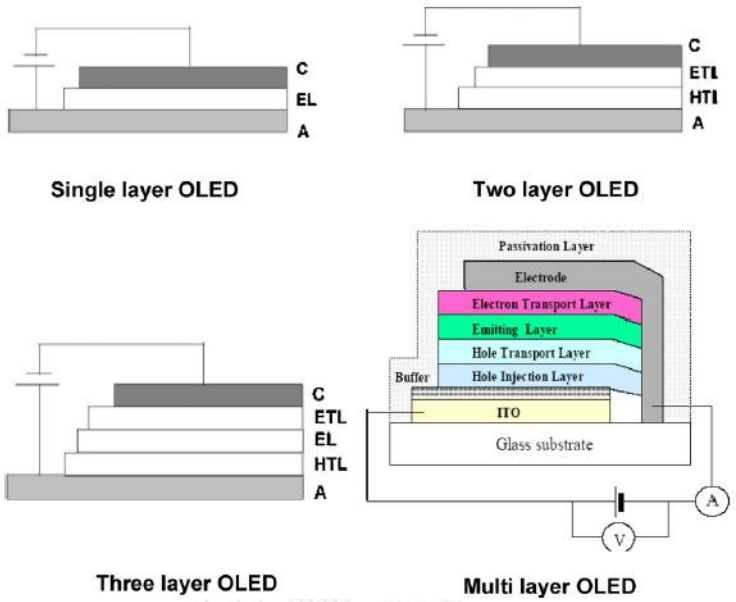

Figure 1.3. Structure of different OLEDs. Where C = cathode; EL = emitting layer; ETL = electron transport layer; HTL = hole transport layer; HIL = hole injection layer; A = anode.

When voltage is applied across the layer(s) of an OLED device, current flows through the device. Thus, the cathode gives electrons to the emissive layer and holes are injected from the anode, forming exciton pairs in the emissive layer. When the charges in exciton pairs are combined, they give rise to light emission. The color of the light depends on the type of organic molecule in the emissive layer. Emission color is basically determined by the energy difference of HOMO and LUMO of the emitting organic material. The intensity or brightness of the light depends on the amount of electrical current applied. Consequently by changing these active materials the emission color can be varied across the entire visible spectrum. Light emitting mechanism from an OLED device is shown in **Figure 1.4**.

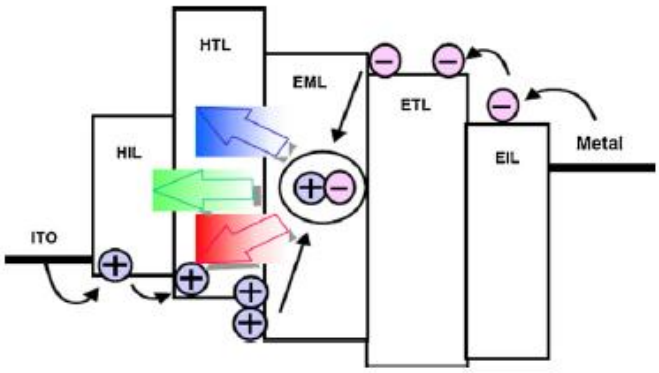

Figure1 4. Light-emitting mechanism in an OLED device [6]

1.4 Organic electroluminescent materials

OLED materials can be categorized into polymeric materials and low molecular-weight materials. [7, 8]

1.4.1 Polymers

The first polymers that were used is poly(phenylvinylene) (PPV), and due to the improved charge transport rates along the conjugated polymeric backbone compared to inter-molecular hopping rates, most subsequent PLED work has focused on conjugated polymers. Nevertheless, another class of polymers called polyfluorenes (PFs) has taken over as the dominant class of conjugated polymer in organic electronics. One non-conjugated polymer widely used is poly(N-vinylcarbazole) (PVK), used as both a hole-injecting material and as a host for dyes. Overall, polymers remain of great interest due to the low cost of manufacture and the potential of solution-processable deposition techniques, but one of the main barriers to commercialization is that they are generally far less pure than small molecules.

1.4.2 Low molecular-weight materials

The initial modern OLED breakthrough came with Alq_3. Small molecules have been researched in great detail, and improvements in efficiency and stability have surpassed polymers. Alq_3 is the only small molecule investigated as whole layers. Full-scale commercial displays have been made using patterned thermal evaporation through a mask of small molecules. However, the main limitation has not been

surpassed: the cost of the material evaporation, where over 80 % of the material is wasted. Organic light emitting diodes from polymers have more potential in this point, being suitable for solution processing, but the technology is not as well-developed as evaporation.

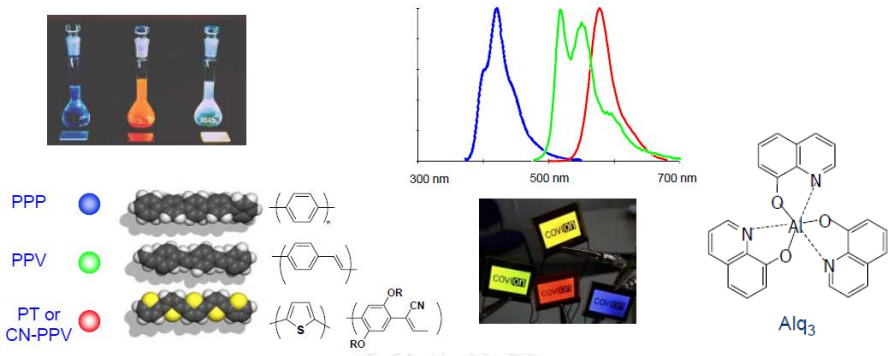

Figure 1.5. Chemical structures of emissive polymer (a) and emissive small molecule (b) [9]

1.5 Emitting materials (EMMs)

Organic fluorescence compounds are used as the emitter in OLED device. The fluorescence principle is described by the Jablonski diagram in **Figure 1.**6.

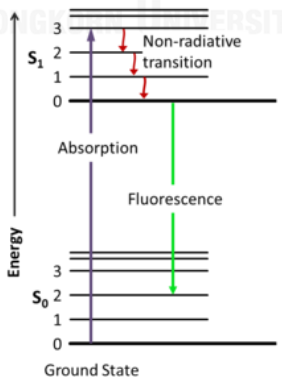

Figure 1.6. Jablonski diagram [10]

The examples of emitting materials are a red emitter 4-(dicyanomethylene)-2-methyl-6-[4-(dimethyl-aminostyryl)-4*H*-pyran] (DCM) [11] (**Figure 1.7**), a green emitter tris(8-hydroxyl-quinoline) aluminum (Alq_3) [12] and blue emitters NPD and polyfluorene (PF) derivatives (**Figure 1.7**). [13, 14]

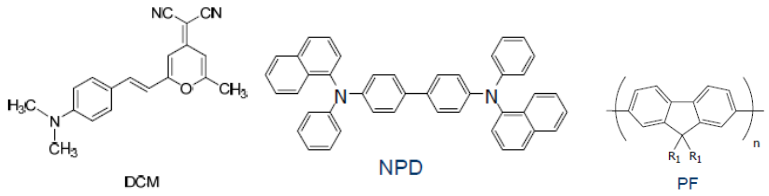

Figure 1.7. Chemical structures of DCM, NPD, and PF derivatives.

One of the measure problems in OLEDs is its low efficiency. Various techniques are used to improve the efficiency of OLED devices. An important aspect of host–guest systems is the choice of host and guest materials for both single and multidoped systems. [15, 16] The energy transfer from host to guest can be either Förster type energy transfer or Dexter type charge transfer or due to the formation of excimer or exciplex. The primary conditions for such energy transfers are overlap of the emission spectrum of the host and absorption spectrum of the guest (**Figure 1.8**). Therefore, the host material is always one with emission at higher energies, generally a blue-emitting material. The example of host materials that widely used are poly(*N*-vinylcarbazole) (PVK), 1,1,4,4-tetraphenyl-1,3-butadiene (TPD), 4,4',*N,N'*-dicarbazole-biphenyl (CBP) or 4,4'bis(*N*-(1-naphthyl)-*N*-phenyl-amino)-biphenyl (α-NPD).

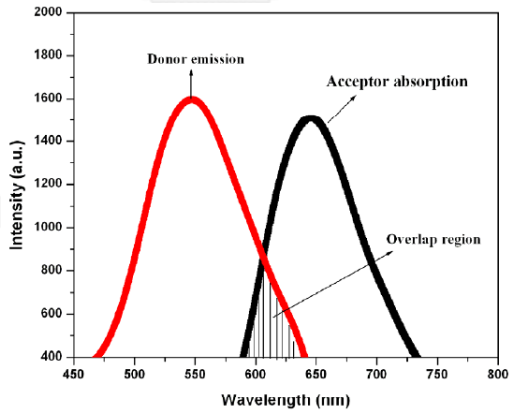

Figure 1.8. Spectral overlapping between emission of donor and absorption of acceptor [17]

1.6 OLED core fabrication technologies

OLED devices can be fabricated in two ways namely vacuum deposition technique and solution techniques including spin coat technique, ink jet technique, and casting. [18, 19]

As mentioned before, there are two choices for the organic layers, either small molecules or polymers. The method of application will depend on this choice. Polymers typically use spin coating. In spin coating, the organic material is deposited in liquid form on a substrate in excess. The substrate is rotated at high speed causing the liquid to spread out across the substance as seen in Figure 1.9 The liquid will form a thin layer and solidify as it evaporates. The thickness of the film is determined by the amount of time the substrate is rotated and the drying rate of the material. Films produced this way tend to have inconsistent thickness as well as poor surface smoothness. Due to this inconsistency, it is not the method of choice.

When using small molecule, evaporative techniques are commonly chosen. The small molecules are evaporated onto a substrate and form a thin film. This takes place in a vacuum; but it is time consuming as high vacuum state to be obtained and is difficult to deposit over large area. [20]

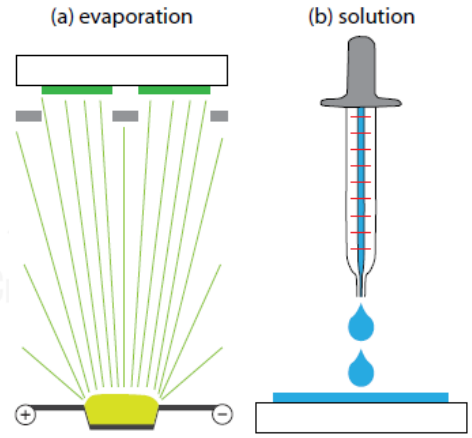

Figure 1.9. OLED deposition techniques. (a) thermal evaporation and (b) spin-coating from solution [18, 19]

1.7 Literature review

Literature review on triphenylamine:

In 2005, Fang and coworkers synthesized four triphenylamine groups-substituted fluorine (**XB10**). [25] The compound shows high thermal stability and high

glass transition temperature, *Tg*, of 165°C. Employing **XB10** as HTL, structure of ITO/TPD (30 nm)/**XB10** (30 nm)/Alq_3 (30 nm)/LiF (0.5 nm)/Al (120 nm) have been fabricated. The device gives very low turn-on voltage and high efficiency. When a hole block layer was fabricated [ITO/TPD (30 nm)/**XB10** (30 nm)/PBD (30 nm)/Alq_3(30 nm)/LiF (0.5 nm)/Al (120 nm)], the new compound can be used as a light-emitting layer for OLED to give a device emitting blue color.

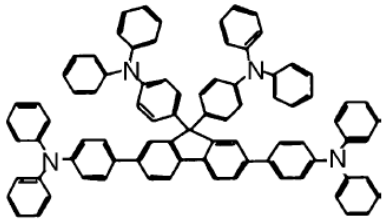

XB10

Figure 1.10. Structure of **XB10** [25]

In 2010, Sek and coworkers synthesized new p-type imines molecules which are unsymmetrical linear, symmetrical linear and star-shaped bearing a triphenylamine moiety as a core. [26] The imines are solution processable and form molecular glasses with T_g between 23 and 183°C. These imines exhibited violet or blue light emission depending on the shape, symmetry and conjugation of the compound. M3, D3 and T3 (**figure 1.11**) had high PL intensity and could be used in OLED as light emitting materials or as an active layer in organic solar cells.

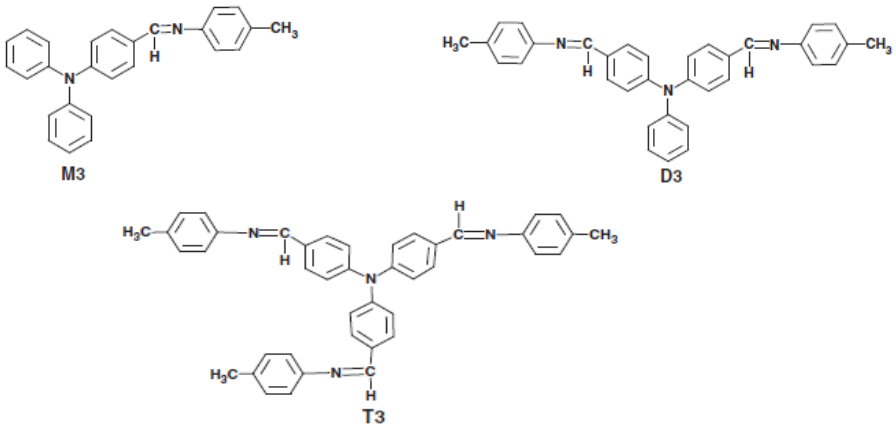

M3 D3 T3

Figure 1.11. Structure of molecules with triphenylamine moiety [26]

In 2013, Song and coworkers synthesized a series of green dopants based on 2,2-diphenylvinyl end-capped bithiophene and three different arylamine moieties (9-

phenylcarbazole, triphenylamine, and *N,N'*-di-(*p*-tolyl) benzeneamine) via the Suzuki coupling and Wittig reactions. [17] The strongest PL emitting compound with the 9-phenylcarbazole moiety had been used for fabricating an OLED device with yellowish green emission (CIE = 0.42, 0.54), maximum brightness and luminous efficiency of 5,100 cd/m^2 and 2.56 cd/A, respectively.

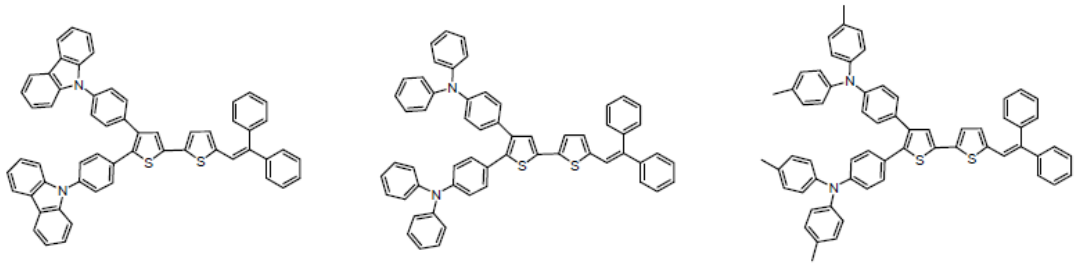

Figure 1.12. Structure of designed green dopants [17]

In 2013, Kochapradist and coworkers had studied the number of triphenylamine-substituted carbazoles, namely TnC (n = 2–4). [27] Increasing the number of triphenyl ne substituents in tl molecule not only ir roved the thermal stability, but also induced the formation of an amorphous form in the material. Their thermal properties and abilities as hole-transporting layers in Alq_3-based OLED, especially T4C having four triphenylamine substituents, were greater than both the common hole-transporters, *N,N'*-diphenyl-*N,N'*-bis(1-naphthyl)-(1,1'-biphenyl)-4,4'-diamine (NPB) and *N,N'*-bis(3-methylphenyl)-*N,N'*-bis(phenyl)benzidine (TPD). A green light-emitting device with a luminance efficiency as high as 5.07 cd/A was achieved.

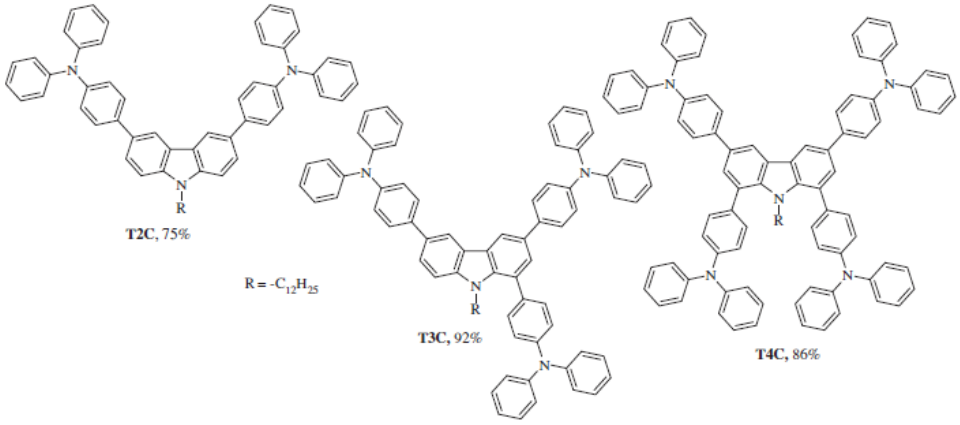

Figure 1.13. Structure of triphenylamine substituted carbazoles TnC [27]

Literature review on naphthalimide:

In 2004, Gan and coworkers studied the effect of substitution at the 4-position of 1,8-naphthalimide with electron-donating groups and changing emissive wavelengths from blue to red. [23] Novel naphthalimide derivatives were prepared by condensing 4-hydrazino-1,8-naphthalimides with the aldehydes (**NP-RED1-4**). Some of these dyes emit brilliant red fluorescence in solid films and were used as non-doping emissive materials to fabricate electroluminescence devices. The device had an EL peak at 620 nm with a maximum brightness of 15.5 cd/m^2 and a maximum current density of 2.9 mA/cm^2.

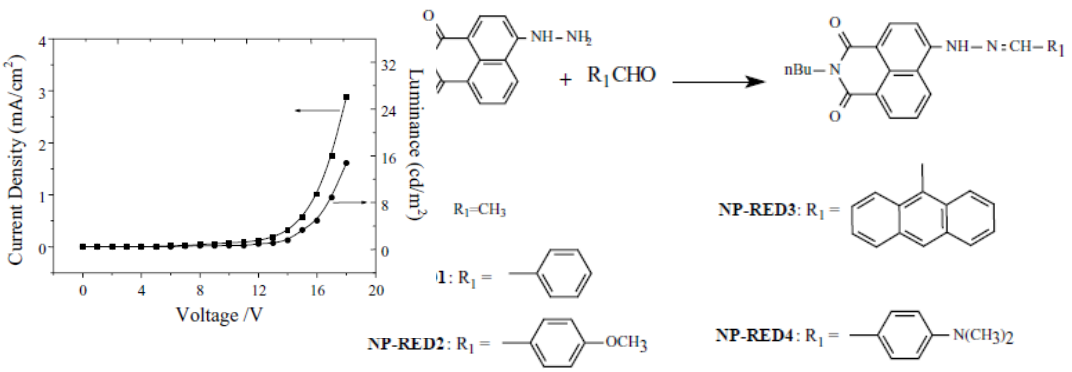

Figure 1.14. The synthesis of **NP-RED1-4** and luminescence–current density–voltage characteristics of a device with the configuration ITO/CuPc/NPB/NP-RED3/sodium stearate/Al [23]

In 2005, Wang and coworkers synthesized naphthalimide-fluorene molecule, 4-(*N*,*N*-dimethylamino)-*N*-(2'-fluorenyl)-1,8-naphthalimide (DFN). [28] The strong luminescence, good electron-affinity, and the temperature independence of fluorescence demonstrated the properties of DFN as electron transporting electroluminescent material. The OLED with a structure of ITO/*N*,*N*'-bis(3-methylphenyl)-*N*,*N*'-diphenyl-1,1'-biphenyl-4,4'-diamine/DFN/Al showed a yellow-green emission (CIE: x = 0.424, y = 0.543) with a brightness of 3563 cd/m^2. The external quantum efficiency and the highest luminous efficiency of the device reached 0.2% and 0.55 lm/W, respectively.

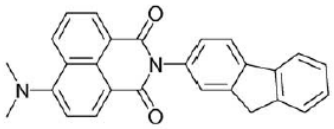

DFN

Figure 1.15. Structure of DFN [28]

In 2009, Mikroyannidis and coworkers synthesized two new linear divinylenes FN and PN that contained fluorene and phenylene, respectively, as central unit and naphthalimide terminal groups via Heck coupling and also two new star-shaped trivinylenes TPA-P and TPP-P that contained triphenylamine and 2,4,6-triphenylpyridine, respectively, as central core, and terminal phthalimide groups. [29] Trivinylenes showed higher thermal stability and higher T_g (118–126 °C) than divinylenes. FN, PN and TPA-P emitted green-orange light with maximum wavelengths at 518–586 nm, while TPP-P emitted blue light with maximum wavelengths at 444–462 nm due to the kinked central core of 2,4,6-triphenylpyridine. The maximum luminance among the four molecules was 583 cd/m^2 at current density of 186 mA/cm^2 and applied voltage of 19.5 V based on TPA-P, with a luminance efficiency maximum (η_{max}) of 1.7 cd/A.

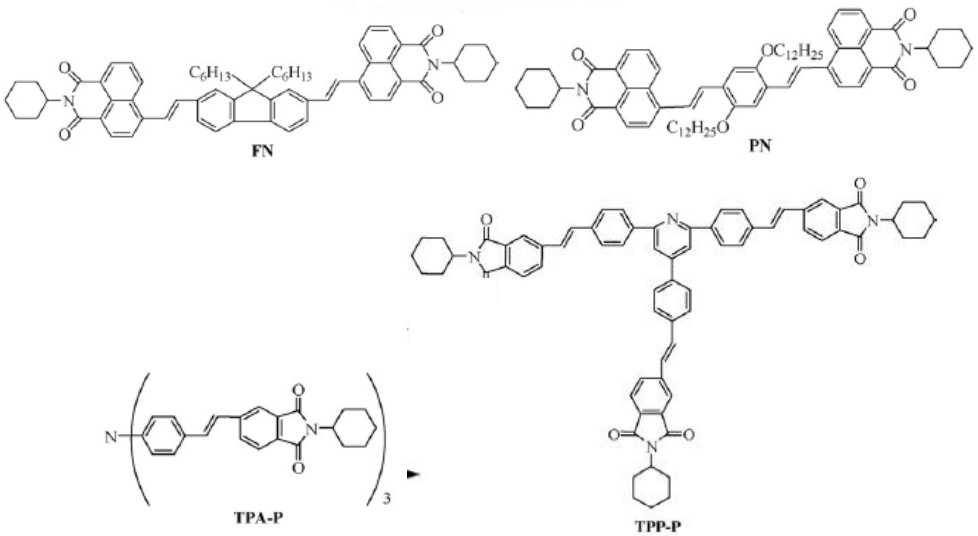

Figure 1.16. Structure of divinylenes **FN** and **PN,** and trivinylenes **TPA-P** and **TPP-P** [29]

In 2010, Liu and coworkers synthesized a series of starburst amorphous molecules derived from 1,3,5-tris(1-naphthyl)benzene by a palladium-catalyzed Miyaura borylation and palladium-catalyzed Suzuki coupling reactions. [30] These starburst naphthalimide derivatives formed amorphous film via vacuum vapor phase deposition. The relatively high T_g (up to 254 °C) and T_d temperature revealed their thin film thermal stability. The high current density and luminance of organic light emitting diodes fabricated indicated that these compounds owned good electron-transporting properties. These compounds hence had the potential to be used as electron-transporting materials in organic semiconducting devices.

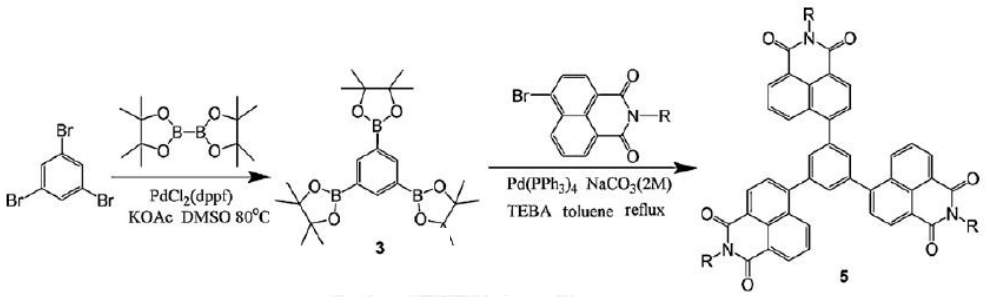

Figure 1.17. Synthesis of starburst naphthalimide derivatives [30]

In 2010, Coya and coworkers designed and synthesized new luminescent polymers containing two individual emission species-poly(fluorene-*alt*-phenylene) as a blue host and variable amounts of 1,8-naphthalimide as red dopant. [14] Optical studies in diluted solutions and thin solid films revealed that the emission spectrum could be tuned by varying the content of 1,8-naphthalimide moieties. Adjusting the polymer/naphthalimide ratio was possible to obtain single polymers which emitted white light. The single-layer electroluminescent simple devices with structure ITO/PEDOT:PSS/**P1**/Ba/Al were fabricated and emitted white light with CIE color coordinates (0.3, 0.42) and a high efficiency of 22.62 Cd/A.

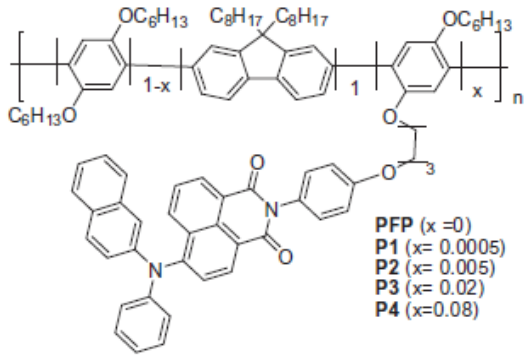

Figure 1.18. Structure of co-polymers **P1–P4** [14]

In 2012, Liu and coworkers synthesized two novel blue light-emitting sextuple hydrogen-bonding self-assembly molecular duplexes bearing 4-phenoxy-1,8-naphthalimide fluorophores - PhNIHB and 2TPhNIHB. [31] Their thermal and morphological stability were investigated. Non-doped diode with structure of ITO/PEDOT: PSS (40 nm)/PVK (40 nm)/blue emitter (70–80 nm)/CsF (1.5 nm)/Al (120 nm) was fabricated using solution process and 2TPhNI as emitter. The device gave yellow emission [CIE (0.38, 0.49)] with poor maximum luminous efficiency (LE_{max}) of 0.13 cd/A and external quantum efficiency (EQE_{max}) of 0.06%. However, the 2TPhNIHB-based device gave blue-green emission [CIE (0.25, 0.34)], with much greater efficiency relative to 2TPhNI-based one (LE_{max} of 0.37 cd/A and EQE_{max} of 0.35%).

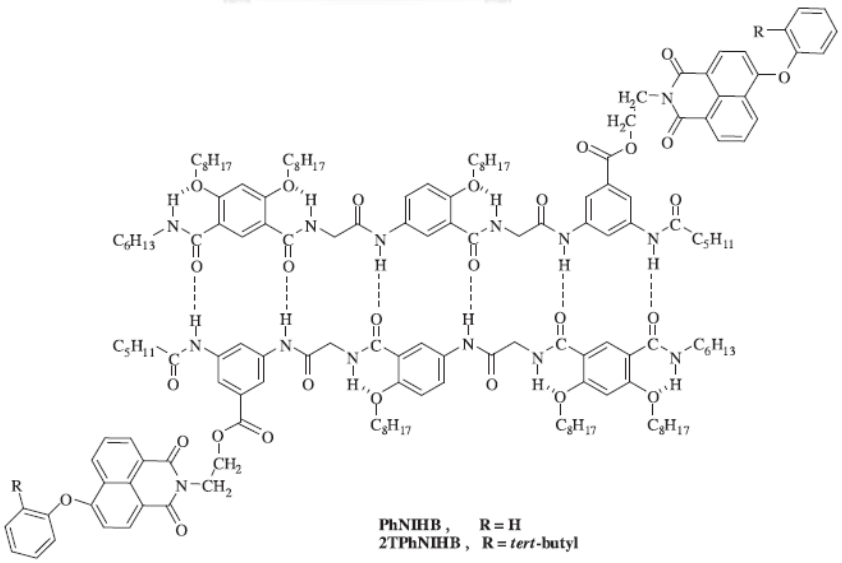

Figure 1.19. Structures of PhNIHB and 2TPhNIHB [31]

Literature review on triphenylamine and naphthalimide derivatives:

In 2006, Tu and coworkers had successfully developed pure-white-light electroluminescence by using single polymer of naphthalimide derivatives doped onto the polyfluorene backbones (**figure 1.20**), adjusted emission wavelength of 1,8-naphthalimide and optimized the content of 1,8-naphthalimide derivatives in the resulting polymers. [32] A device with a configuration of ITO/poly(3,4-ethylenedioxythiophene)/polymer/Ca/Al exhibited CIE coordinates of (0.32, 0.36), a maximum brightness of 11,900 cd/m^2, a current efficiency of 3.8 cd/A, a power efficiency of 2.0 lm/W, an external quantum efficiency of 1.50 %.

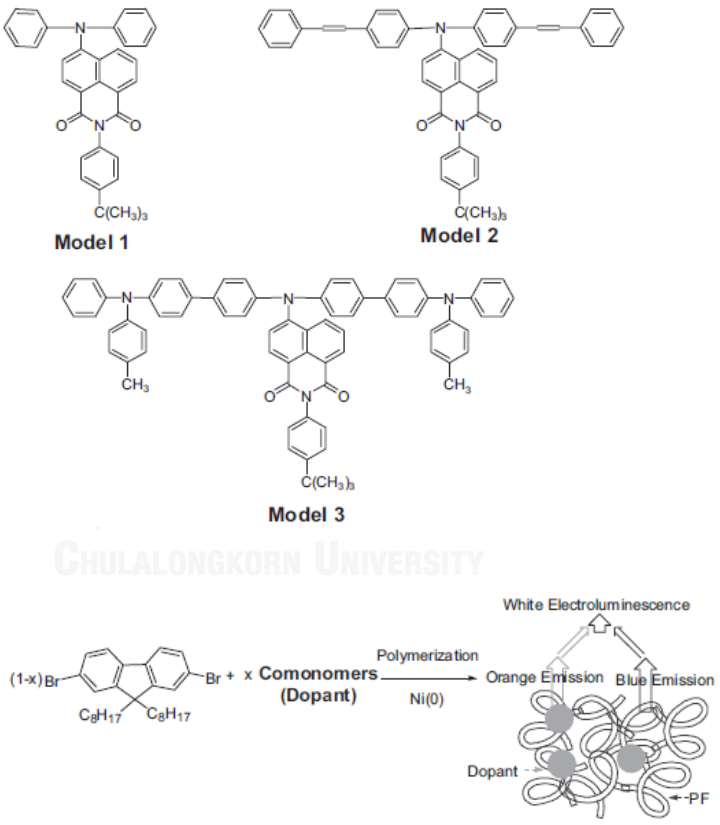

Figure 1.20. Structure of three kinds of polymers and their polymerization reaction [32]

In 2011, Gudeika and coworkers had successfully synthesized hydrazones containing electron-accepting 1,8-naphthalimide species and electron-donating triphenylamino moieties (**Figure 1.21**). [33] They exhibited initial mass loss temperatures in the range of 268-348°C and their T_g was in the range of 46-142°C.

Room temperature time-of-flight hole-mobilities in the solid solutions of the derivatives in the polymeric host bisphenol-Z polycarbonate (50%) exceeded 10^{-5} cm^2/V s at high applied electric fields.

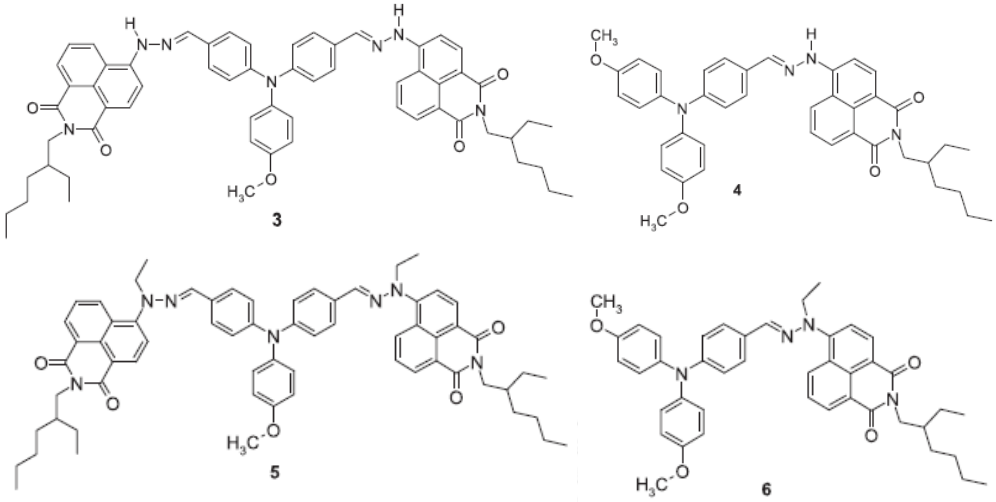

Figure 1.21. Structure of compounds studied by Gudeika [33]

In 2012, Xiao and Deng designed and synthesized a new symmetric starburst orange-red light material, tris(4-(2-(*N*-butyl-1,8-naphthalimide)ethynyl)-phenyl) amine(TNGT). [34] It showed a high fluorescence quantum yield and a slight concentration-quenching effect. A high brightness (6600 cd/m^2) and a high current efficiency [4.57 cd/A (at 420 cd/m^2)] with CIE (0.59, 0.40) were achieved at a relatively high doping concentration (20 wt%) in a TNGT-based OLED.

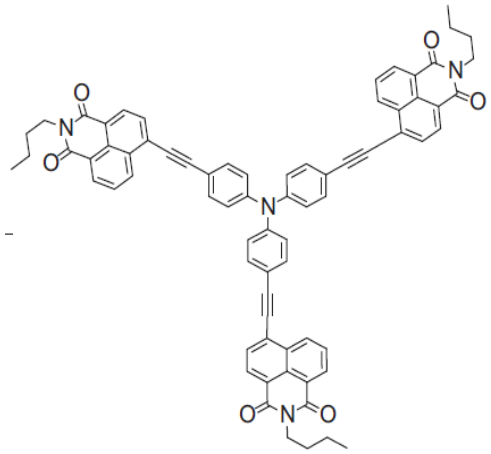

Figure 1.22. Structure of TNGT [34]

In 2013, Jin and Tang designed and studied a series of D–**π**–A bipolar molecules with triphenylamine (TPA) fragments as donors, 1,8-naphthalimide fragments as acceptors, and different **π**-conjugated bridges (CB) as **π**-conjugated bridges to explore their optical, electronic, and charge transport properties as charge transport and luminescent materials for organic light-emitting diodes (OLEDs). [35] The FMOs, NPA, and local density of states analysis revealed that the vertical electronic transitions of absorption and emission were characterized as intramolecular charge transfer (ICT). The calculated results showed that their optical and electronic properties were affected by the **π**-conjugated bridges of the bipolar molecules. The results suggested that **1**–**10** could be promising candidates for hole-transporting and luminescent materials for OLEDs.

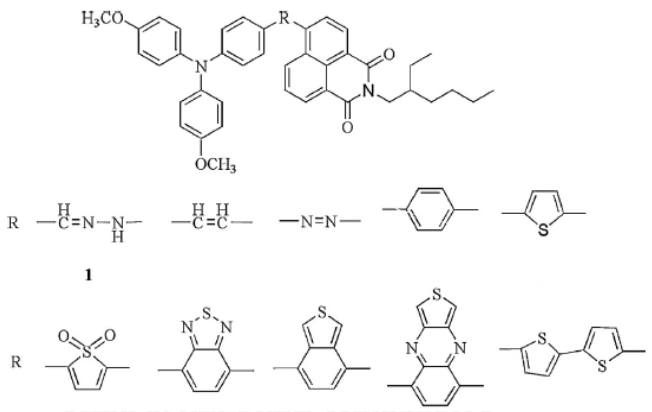

Figure 1.23. Structure of compounds studied by Jin and Tang [35]

In 2006, Mei and coworkers synthesized a series of copolymers (CNPFs) containing 1,8-naphthalimide moieties as color tuner via a Yamamoto coupling reaction of 2,7-dibromo-9,9-dioctylfluorene (DBF) and different amount of 4-(3,6-dibromocarbazol-9-yl)-*N*-(4'-tert-butyl-phenyl)-1,8-naphthalimide (Br–CN) (0.05–1 mol% feed ratio). [36] For photoluminescence, the color tuning went through the FÖrster energy transfer mechanism, while for electroluminescence (EL), the color tuning was dominated by a charge trapping scheme. It was found that by introduction of a very small amount of Br–CN (0.1–0.5 mol%) into polyfluorene, the emission color could be tuned from blue to pure green. A green emitting EL single-layer device based on CNPF containing 0.1 mol% of Br–CN showed good

performances with a low turn-on voltage of 4.2 V, a brightness of 9104 cd/m^2, the maximum luminous efficiency of 2.74 cd/A and the maximum power efficiency of 1.51 lm/W. They also improved the EL performances through balancing the charge trapping process by preparing a copolymer (BCNPF05) derived from 0.5 mol% of a triarylamine-containing 4-{3,6-bis-[4''-(4'''-bromophenyl-p-tolyl-amino)-phenyl]-carbazol-9-yl}-*N*-(4'-tert-butyl-phenyl)-1,8-naphthalimide (Br–BCN) and 99.5 mol% of 2,7-dibromo-9,9-dioctylfluorene. As expected, a single layer EL device based on BCNPF05 exhibited better performances with a brightness of 14228 cd/m^2, the maximum luminous efficiency of 4.53 cd/A and the maximum power efficiency of 1.57 lm/W.

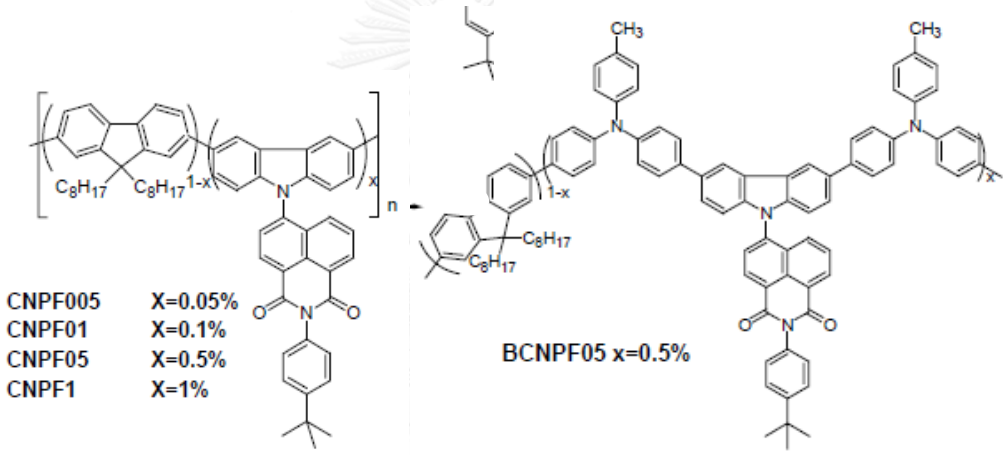

Figure 1.24. Structure of copolymer CNPFs and copolymer BCNPF05 [36]

1.8 Objective of this research

Triphenylamine (TPA) has been investigated for almost two decades because these compounds have shown good thermal and electrochemical stability, electron donating ability, and optoelectronic properties. Shirota and co-workers had led to the development of many classes of TPA-based compounds as hole-transporting or electroluminescent materials. [21, 22]

1,8-Naphthalimide derivatives have photophysical properties, which have been widely used as brilliant yellow dyes in synthetic fiber technology and as optical brightener, and as functional fluorescent imaging polymer. Naphthalimide derivatives

are also an attractive class of electron-deficient organic materials for OLEDs and are used as a new type of electron-transporting emitting materials for both small and polymer-based OLEDs with high performance, good light stability, high fluorescent quantum yield, and high electron affinity. However, most of the previous work concluded that 1,8-naphthalimides compounds could be utilized for green or blue devices due to the fact that naphthalimide derivatives emit light mainly in the blue and green-yellow regions. In fact substitution at the 4-position of 1,8-naphthalimide with electron-donating groups can increase fluorescent quantum yields and tune easily the emission wavelengths to longer ranges. [23, 24]

In this study, we incorporated 1,8-naphthalimide derivatives with triphenylamine (TPA) to be **TPN1-TPN3** which have shown excellent thermal and electrochemical stability, electron donating ability, and can be electroluminescent material in optoelectronic device with an aim to get OLED device with a high thermal stability and high quantum efficiency.

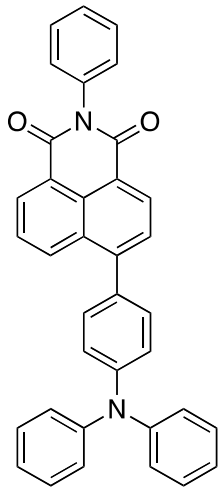

TPN1

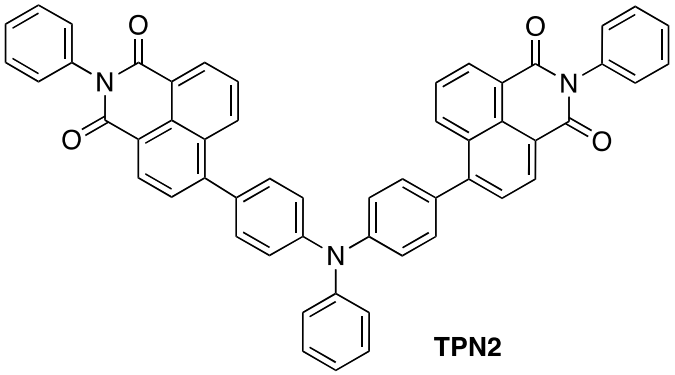

TPN2

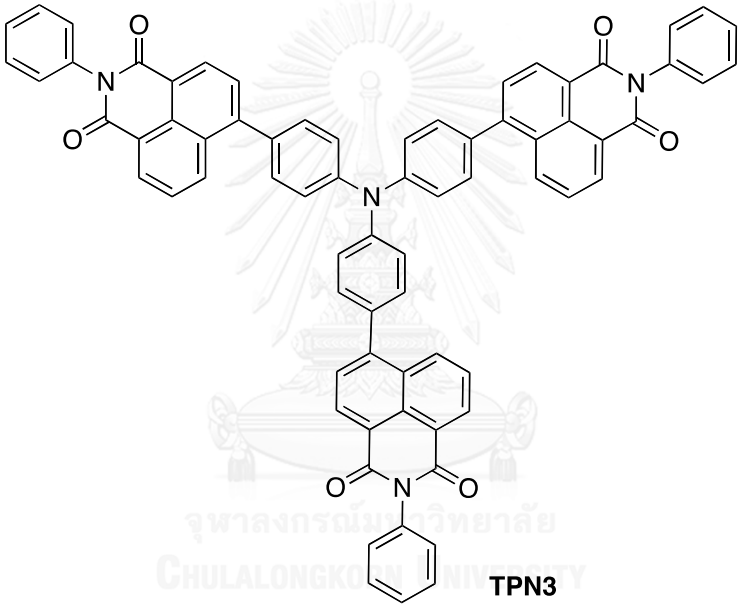

TPN3

In summary, the objectives of this work are following:

1. To synthesize molecules which can be emissive materials for OLED
2. To characterize and study the electronic, photophysical, electrochemical and thermal properties of the target molecules
3. To investigate their potential application as emitting materials for OLED

CHAPTER II

EXPERIMENTAL

2.1 Synthesis

2.1.1 Instruments and Equipment

Thin layer chromatography (TLC) was performed on aluminium sheets precoated with silica gel (Merck Kiesegel 60 F_{254}) (Merck KgaA, Darmstadt, Germany). Column chromatography was performed on silica gel (Merck Kieselgel 60G) (Merck KGaA, Darmstadt, Germany). All ^{1}H-NMR spectra were determined on Varian Mercury NMR spectrophotometer (Varian, USA) at 400 MHz with chemical shifts reported as ppm in $CDCl_3$. The ^{13}C-NMR spectra were measured on Bruker Mercury NMR spectrophotometer (Bruker, Germany) which equipped at 100 MHz with chemical shifts reported as ppm in $CDCl_3$. Mass spectra were recorded on a Microtof high resolution mass spectrometer (Bruker Daltonics). Absorption spectra were measured by a ShimadzuUV-2550 UV-Vis spectrophotometer. Fluorescence spectra were obtained from an Agilent technologies Cary Eclipse spectrofluorometer. The FT-IR spectra were recorded between 400 cm^{-1} to 4,000 cm^{-1} in transmittance mode on a Fourier Transform Infrared Spectrophotometer: Impact 410 (Nicolet Intruments Technologies, Inc, WI, USA).

The fluorescence quantum yields (Φ) were determined by comparison with a standard of known fluorescence quantum yield according to the following equation [35].

$$\Phi_{\mathrm{x}} = \Phi_{\mathrm{ST}} \left(\frac{Slope_x}{Slope_{ST}}\right)\left(\frac{\eta_x^2}{\eta_{ST}^2}\right)$$

Where the subscripts X refer to the unknown samples and ST refers to the standard quinine sulfate solution in 0.01 M H_2SO_4, whose fluorescence quantum yield is known to be 0.54 [36], Φ is the fluorescence quantum yield, *Slope* is the slope from the plot of integrated fluorescence intensity versus absorbance, and η is the refractive index of the solvent. The refractive indexes of $CHCl_3$ and 0.01 M H_2SO_4 were 1.445 and 1.333, respectively. The maximum absorbance of all samples should never exceed 0.1. The fluorescence emission spectra of the same solutions using appropriate excitation wavelengths selected were recorded based on the maximum absorption wavelength (λ_{max}) of each compound. Graphs of integrated fluorescence

intensities were plotted against the absorbance at the respective excitation wavelengths. Each plot should be a straight line with 0 interception and gradient *m*.

The electrochemical analysis by cyclic voltametry was performed using an AUTOLAB spectrometer. All measurements were made at room temperature on sample solutions in freshly distilled acetonitrile: dichloromethane (20% V/V) with 0.1 M tetra-n-butylammoniumhexafluorophosphate as electrolyte. A platinum working electrode, a platinum wire counter electrode, and a $Ag/AgNO_3$ (Sat.) reference electrode were used in all cyclic voltammetry experiments.

Thermal properties, Differential Scanning Calorimeter (DSC) results were performed on NETZSCH DSC 204F1 and Thermogravimetric Analysis (TGA) results were studied using NETZSCH TG 209F3.

2.1.2 Synthetic procedures

4,4'-(dibromo)triphenylamine (3)

A solution of NBS (0.74 g, 4.16 mmol) in DMF (8 mL) was added dropwise into a solution of triphenylamine (0.51 g, 2.08 mmol) in DMF (6 mL), and then stirred at $0^{\circ}C$ for 4 h. The solvent was removed, the residue was washed with water (15 mL), saturated aqueous NaCl (10 mL), and CH_2Cl_2 layer was dried over anhydrous $MgSO_4$. Then the solvent was removed and the residue was purified by silica gel chromatography eluted with haxane to get pellucid liquid (0.38 g, 46%). ^{1}H-NMR (400 MHz, $CDCl_3$, ppm) δ 7.31 (m, 4H), 7.24 (m, 2H), 7.05 (m, 3H), 6.91 (m, 4H). [37]

4,4',4''-(triiodo)triphenylamine (4)

A solution of triphenylamine (1.07 g, 4.35 mmol), potassium iodide (1.38 g, 8.35 mmol) and potassium iodate (1.80 g, 8.43 mmol) in acetic acid (25 mL) was refluxed for 20 min. The reaction was allowed to cool to room temperature and diluted with CH_2Cl_2, $Na_2S_2O_{3(aq)}$, and water. The aqueous layer was separated and extracted with CH_2Cl_2 again. The combined organic layer was dried over $MgSO_4$, filtered, and concentrated under reduced pressure to give a brown solid (2.57 g, 95%). ^{1}H- NMR (400 MHz, $CDCl_3$, ppm) δ 7.59 – 7.47 (m, 6H), 6.85 – 6.77 (m, 6H). [38]

4-bromo-*N*-(phenyl)-1,8-naphthalimide (5)

4-bromo-1,8-naphthalic anhydride (1.21 g, 4.37 mmol) and aniline (0.73 g, 7.88 mmol) were dissolved in glacial acetic acid (20 mL). The mixture was stirred and heated under refluxing condition overnight. After that the reaction mixture was allowed to cool to room temperature, the mixture was poured into ice and the resulting precipitate was filtered, washed with cool water, and dried over a steam bath. White powder, 95%, ^{1}H-NMR (400 MHz, $CDCl_3$, ppm) δ 7.32 (d, *J* = 7.4 Hz, 2H), 7.49 (t, *J* = 7.4 Hz, 1H), 7.56 (t, *J* = 7.5 Hz, 2H), 7.93 – 7.82 (m, 1H), 8.07 (d, *J* = 7.9 Hz, 1H), 8.45 (d, *J* = 7.9 Hz, 1H), 8.62 (d, *J* = 8.5 Hz, 1H), 8.69 (d, *J* = 7.3 Hz, 1H). [39]

***N*-Phenyl-1,8-naphthalimide-4-boronic acid pinacol ester (3)**

Under N_2 atmosphere, a solution of 4-bromo-*N*-(phenyl)-1,8-naphthalimide (1.45 g, 4.13 mmol) in DMF (15 mL) were added bis(pinacolato)diboron (2.54 g, 9.99 mmol), potassium acetate (0.98 g, 9.98 mmol), and $PdCl_2$(dppf) (0.15 g, 0.20 mmol) at room temperature. The mixture was heated at 75 $^{\circ}$C and stirred overnight. After cooling to room temperature, the mixture was extracted with EtOAc. The combined organic extracts were washed with water and brine, dried ($MgSO_4$), filtered and concentrated under reduced pressure. The residue was purified by silica-gel column chromatography (n-hexane/EtOAc = 20/1) to give 6 (0.56 g, 34%) as a pale yellow solid; ^{1}H-NMR (400 MHz, $CDCl_3$, ppm) δ 9.18 (d, *J* = 8.5 Hz, 1H), 8.64 (d, *J* = 7.3 Hz, 1H), 8.60 (d, *J* = 7.2 Hz, 1H), 8.33 (d, *J* = 7.3 Hz, 1H), 7.81 (t, *J* = 7.8 Hz, 1H), 7.56 (t, *J* = 7.6 Hz, 2H), 7.48 (t, *J* = 7.1 Hz, 1H), 7.34 (d, *J* = 7.9 Hz, 2H), 1.47 (s, 13H), 1.26 (s, 7H). [30, 40, 41]

TPN1

Under a N_2 atmosphere, a mixture of 4-(*N*,*N*-diphenylamino)-phenylboronic acid (0.10 g, 0.36 mmol), 4-bromo-*N*-(phenyl)-1,8-naphthalimide (0.14 g, 0.41 mmol), and Pd(dppf)Cl_2 (22 mg, 0.03 mmol) in toluene (10 mL) was stirred. Then an aqueous solution of K_2CO_3 (2 M 1 mL) was added via syringe. The reaction mixture was heated at 60 ℃ for 72 h. After cooling to room temperature, the reaction was diluted with water and extracted with CH_2Cl_2. The combined organic phase was dried over anhydrous $MgSO_4$, filtered, and concentrated under reduced pressure. The crude product was purified by column chromatography using CH_2Cl_2 as the eluent to afford

TPN1 as yellow solid (0.15 g, 84%). IR (ATR, cm^{-1}): ν 3059, 1655, 1585, 1488, 1368, 1231. ^{1}H-NMR (400 MHz, $CDCl_3$, ppm) δ 8.71 – 8.65 (m, 2H), 8.48 (dd, *J* = 8.5 and 1.0 Hz, 1H), 7.76 (t, *J* = 7.9 Hz, 2H), 7.58 (dd, *J* = 10.3 and 4.7 Hz, 2H), 7.52 – 7.46 (m, 1H), 7.44 – 7.38 (m, 2H), 7.38 – 7.29 (m, 6H), 7.24 (ddd, *J* = 7.5, 5.2, and 2.5 Hz, 6H), 7.11 (t, *J* = 7.3 Hz, 2H). ^{13}C-NMR (100 MHz, $CDCl_3$, ppm) δ 164.5, 164.3, 148.5, 147.4, 147.2, 135.6, 133.2, 131.9, 131.6, 131.3, 130.8, 130.2, 129.5, 129.4, 129.3, 128.70, 128.65, 127.8, 126.8, 125.1, 123.7, 123.1, 122.5, 121.4. HRMS: *m/z* calcd for $C_{36}H_{24}N_2O_2$: 516.1838; found: 539.1736 $[M+Na]^+$

TPN2

This compound was prepared from 4,4'-(dibromo)triphenylamine (1 eq) and boronate ester **A** (2.6 eq) using the same conditions for the synthesis of **TPN1**. The crude product was purified by column chromatography using pure CH_2Cl_2 as the eluent to afford as yellow solid in 30% yield. IR (ATR, cm^{-1}): ν 3059, 1655, 1585, 1488, 1368, 1231. ^{1}H-NMR (400 MHz, $CDCl_3$, ppm) δ 8.70 (d, *J* = 7.5 Hz, 4H), 8.48 (t, *J* = 7.4 Hz, 2H), 7.79 (dt, *J* = 8.3 and 4.1 Hz, 4H), 7.58 (t, *J* = 7.4 Hz, 4H), 7.50 (dd, *J* = 8.0 and 3.7 Hz, 6H), 7.44 (d, *J* = 8.4 Hz, 1H), 7.37 (dt, *J* = 8.4 and 5.5 Hz, 10H), 7.21 (dd, *J* = 8.0 and 6.5 Hz, 2H). ^{13}C-NMR (100 MHz, $CDCl_3$, ppm) δ 164.5, 164.3, 147.9, 146.9, 135.5, 133.1, 133.0, 131.7, 131.3, 131.2, 131.1, 130.2, 129.8, 129.4, 129.3, 128.8, 128.7, 127.9, 126.9, 125.8, 124.5, 123.9, 123.6, 123.1, 121.6. HRMS: *m/z* calcd for $C_{54}H_{33}N_3O_4$: 787.2471; found: 810.2368 $[M+Na]^+$.

TPN3

This compound was prepared from 4,4',4''-(triiodo)triphenylamine (1 eq) and boronate ester **A** (9.0 eq) using the same conditions for the synthesis of **TPN1**. The crude product was purified by column chromatography using pure CH_2Cl_2 to CH_2Cl_2/EtOAc (20/1) as the eluent to afford as orange solid in 56% yield. IR (ATR, cm^{-1}): ν 3059, 1655, 1585, 1488, 1368, 1231. ^{1}H-NMR (400 MHz, $CDCl_3$, ppm) δ 8.71 (d, 6H), 8.51 (d, *J* = 7.7 Hz, 3H), 7.82 (d, *J* = 7.3 Hz, 6H), 7.50 (m, br, 21H), 7.35 (d, *J* = 7.2 Hz, 6H). ^{13}C-NMR (100 MHz, $CDCl_3$, ppm) δ 164.4, 164.2, 147.6, 146.6, 135.4, 133.9, 132.9, 131.7, 131.3, 131.2, 130.2, 129.4, 129.3, 128.74, 128.66, 127.9, 126.9, 124.5, 123.2, 122.4, 121.8. HRMS: *m/z* calcd for $C_{72}H_{42}N_4O_6$: 1058.3104; found: 1081.3005 $[M+Na]^+$.

2.2 OLED device fabrication

2.2.1 Commercially available materials

The commercial sources and purities of materials used in these experiments are shown in **Table 2.1**. All materials were analytical grade and used without further purification, unless indicated.

Table 2.1. Commercially available materials for OLED device fabrication

Materials	Purity (%)	Company
1″ × 1″ Indium oxide doped tin oxide (99.3 wt % In_2O_3:0.7 wt % SnO_2)-coated glasses (5-15 Ω/sq)	99.5	Kintec
Poly(3,4-ethylenedioxythiophene)–poly(styrene) (0.5 wt % PEDOT: 0.5 wt % PSS)	1.3	Baytron
2,9-dimethyl-4,7-diphenyl-1,10-phenanthroline (BCP)	99.99	Sigma-Aldrich
Lithium fluoride (LiF)	99.98	ACROS
Aluminium (Al) wire	99.97	BDH
4,4'-bis(*N*-carbazolyl)-1,1'-biphenyl (CBP)	-	-

2.2.2 Reagents

The reagents were obtained from various suppliers as shown in **Table 2.2**. All reagents were analytical grade and used without further purification, unless indicated.

Table 2.2. List of reagents.

Reagents	Purity (%)	Company
Hydrochloric acid (HCl) 37%	36.5	Carlo Erba
Nitric acid (HNO_3) 69%	68.5-69.5	BDH
Sodium hydroxide (NaOH)	99.99	Carlo Erba
Acetone	99.5	BDH

2.2.3 Instruments

The following instruments were used in this study:

(1) Photoluminescence (PL) spectrophotometer (Perkin–Elmer, Model LS 50B)

(2) Spin-coater (Chemat Technology, Model KW-4A)

(3) Thermal evaporator (ANS Technology, Model ES280)
(4) Digital source meter (Keithley, Model 2400)
(5) Multifunction optical meter (Newport, Model 1835-C)
(6) Calibrated photodiode (Newport, Model 818 UVCM)
(7) USB Spectrofluorometer (Ocean Optics, Model USB4000FL)

2.2.4 Organic thin film preparation and characterization

The preparation process of organic thin films is described in **Figure 2.1**.

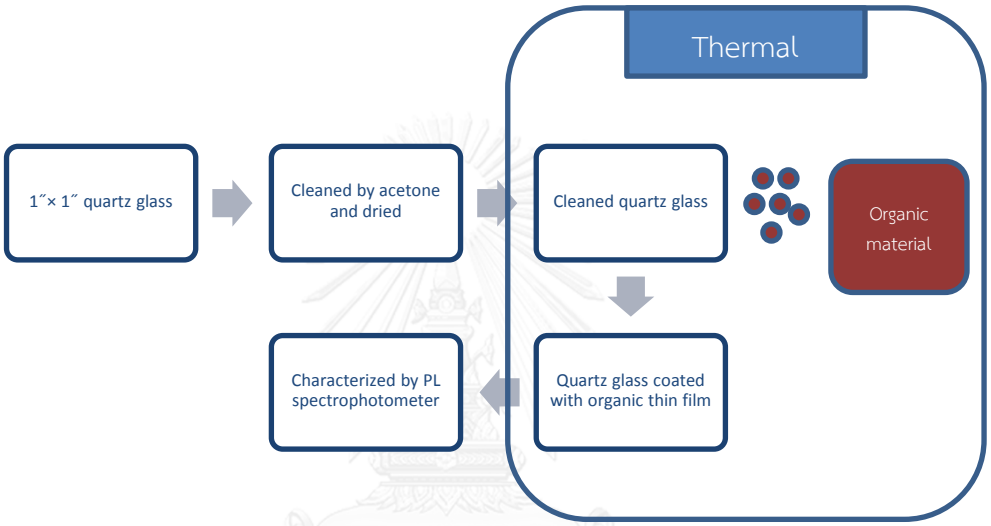

Figure 2.1. Preparation and characterization of organic thin film

In order to study the photophysical properties of solid state materials, organic thin films coating on quartz glass substrates (1″ × 1″) were prepared by thermal evaporation. Prior to film deposition, the substrates were cleaned with acetone in ultrasonic bath followed by drying on a hotplate. The clean quartz glass substrate was then placed on a substrate holder and the organic material was loaded into an evaporation source (alumina filament boat) located in the vacuum chamber of the thermal evaporator (**Figure 2.2b**). The vacuum chamber was evacuated to about 1 × 10^{-5} mbar by the vacuum pump system (**Figure 2.2a**). The organic material was thermally evaporated to the substrate surface at an evaporation rate of 0.2 – 0.4 Å/sec controlled by a calibrated quartz crystal oscillator (Maxtek thickness monitor, Model TM-350).

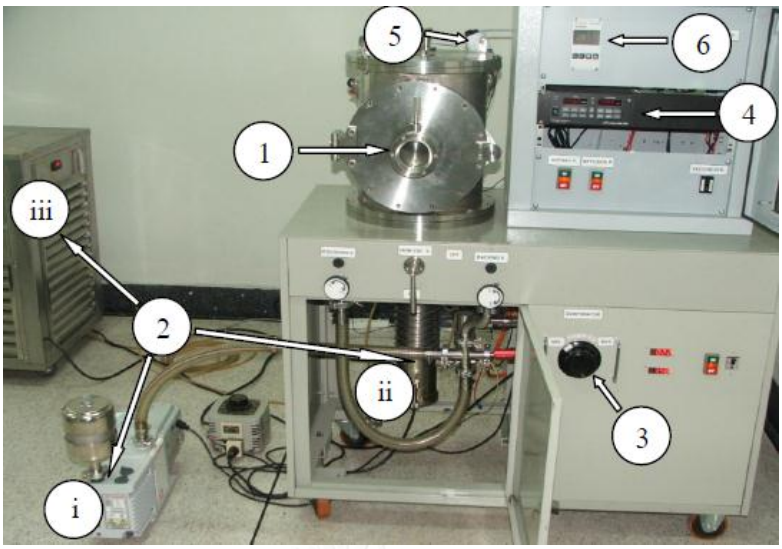

(a)

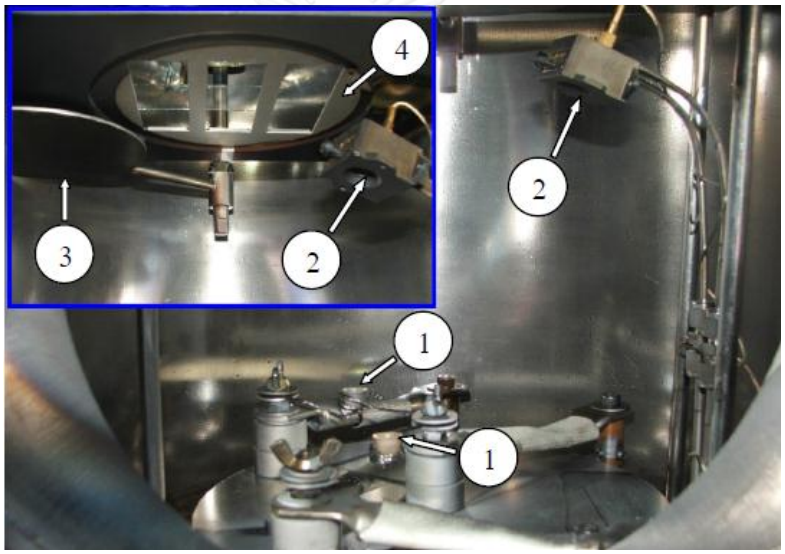

(b)

Figure 2.2. (a) A thermal evaporator which consists of (1) vacuum chamber, (2) high vacuum pump system; (i) backing pump, (ii) diffusion pump and (iii) cooler of diffusion pump, (3) volume control of evaporation source heater, (4) thickness monitor of quartz crystal oscillator, (5) vacuum gauge, and (6) vacuum gauge monitor and (b) vacuum chamber consisting of (1) evaporation source heaters (alumina filament bolts), (2) sensor of the quartz crystal oscillator, (3) source shutter, and (4) substrate holder.

2.2.5 OLED device fabrication

The OLEDs fabrication process is described in **Figure 2.3**.

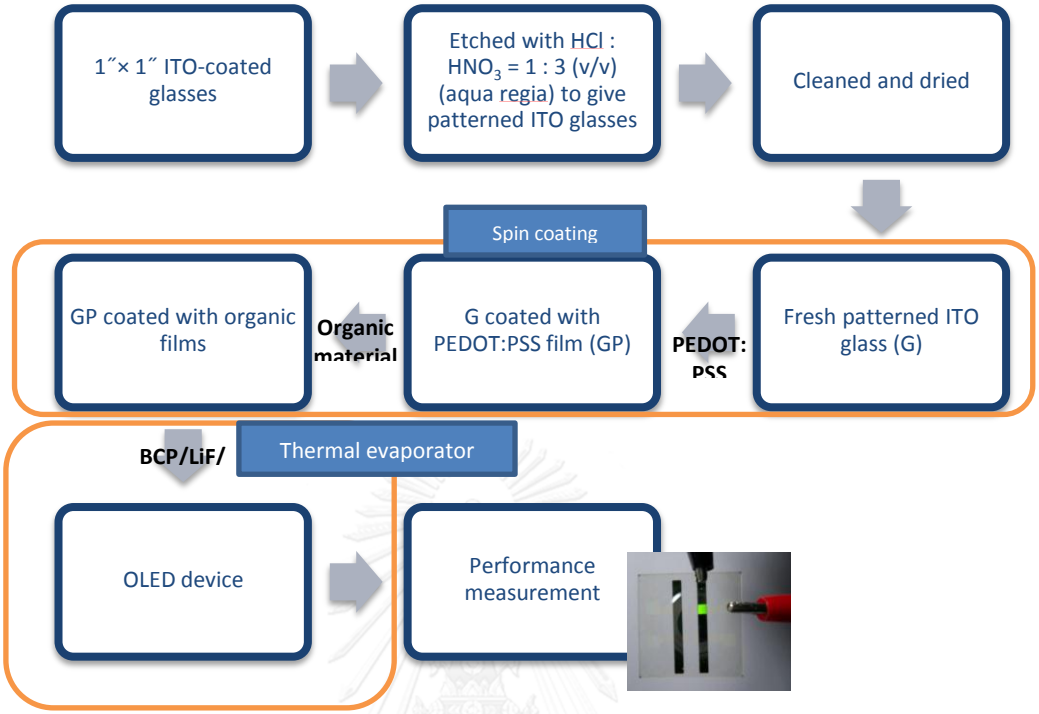

Figure 2.3. Fabrication and measurement of OLED

2.2.6 Patterning process for ITO-coated glasses

The ITO-coated glasses (**Figure 2.4a**) were firstly etched to give a pattern of ITO sheet on glass. Prior to the patterning process, the ITO sheet on glass was covered with a 2 x 10 mm of negative dry film photo resist. The covered ITO glass (**Figure 2.4b**) was immersed in the solution of HCl:HNO_3 (1:3 v/v) (aqua regia) for 10 min, with stirring during the etching process. The etched ITO glass was cleaned by thoroughly rinsing with water and subsequently soaking in 0.5 M NaOH for 10 min to remove the negative dry film from an ITO-coated glass surface. Finally, these substrates were thoroughly rinsed with water to give the patterned ITO glasses as shown in **Figure 2.4c**.

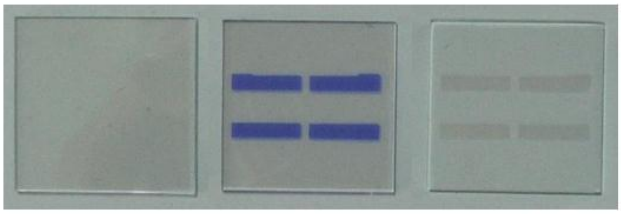

Figure 2.4. (a) ITO-coated glass, (b) ITO-coated glass covered with 2 x 10 mm of negative dry film photo resist and (c) patterned ITO glass

2.2.7 Cleaning process for the patterned ITO glasses

The cleanliness of the ITO surface was an important factor in the performance of the OLEDs devices. The patterned ITO glasses were cleaned for 10 min with detergent in ultrasonic bath followed by a thorough rinse with DI water and then ultra-sonicated in acetone for 10 min. Finally, the substrates were dried in vacuum oven at 100°C to give fresh patterned ITO glasses.

2.2.8 Spin-coating method of PEDOT:PSS

A PEDOT:PSS solution was diluted with DI water and stirred for 1 day. The spin-coating method was performed on a spin coater as shown in **Figure 2.5**. The diluted PEDOT:PSS solution was filtered through a 0.45 μm pore size nylon filter (Orange scientific) and spin-coated onto a fresh patterned ITO glass surface at 3000 rpm for 30 second. Finally, the patterned ITO glass coated with the PEDOT:PSS film was baked at 120°C for 15 min for curing.

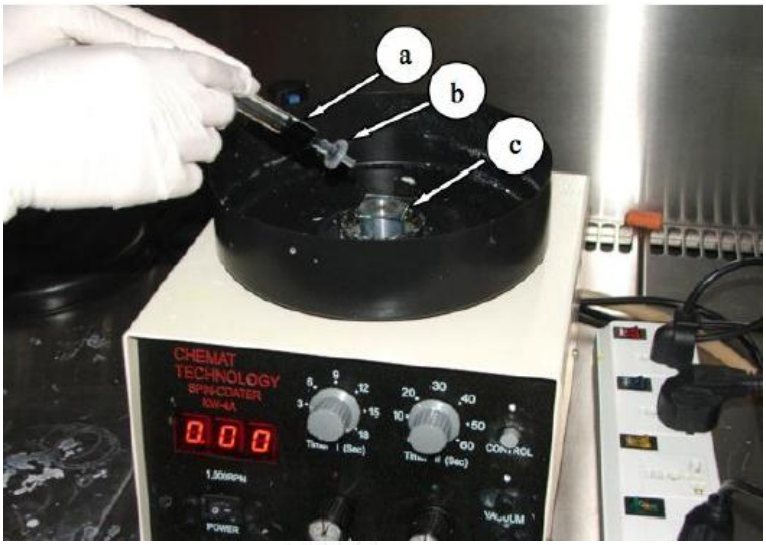

Figure 2.5. Spin-coating method by using a spin coater. (a) PEDOT:PSS solution in the syringe, (b) nylon filter, and (c) fresh patterned ITO glass.

2.2.9 Organic thin film deposition

The deposition of other organic layers was the next step in the fabrication of OLEDs. The organic layers were deposited using spin coating method (**Figure 2.5**) with the same procedure described in section 2.2.5. Prior to the deposition, the patterned ITO glass coated with PEDOT:PSS film was placed on a substrate holder. The organic material was dissolved in the solution of $CHCl_3$:toluene (4:1 %v/v) and then filtered through a 0.45 μm pore size nylon filter (Orange scientific) and spin-coated onto a patterned ITO glass coated with PEDOT:PSS film surface at 3000 rpm for 30 sec. Finally, the ITO glass coated with the organic film was baked at 100°C for 10 min.

2.2.10 Hole blocking and cathode deposition

After organic thin film deposition by the technique of spin coating, the next step is increasing hole blocking layer before closing with cathode deposition. 2,9-dimethyl-4,7-diphenyl-1,10-phenanthroline (BCP) was evaporated from a tungsten boat to deposit at the device. Finally, an ultra thin LiF layer and Al cathode contact were sequentially co-evaporated from two tungsten boats through a shadow mask (**Figure 2.6**) with 2 mm wide slits arranged perpendicularly to the ITO fingers, to

obtain the OLED with an active area of 2 × 2 mm^2 (**Figure 2.7**). The operating vacuum for evaporation of this cathode was under 1 × 10^{-5} mbar at high evaporation rates of 5 – 10 Å/sec. The thickness of LiF and Al of all devices were 0.5 and 150 nm, respectively.

Figure 2.6. Instrument for cathode deposition. (a) tungsten boats and (b) 2 mm wide fingers of a shadow mask.

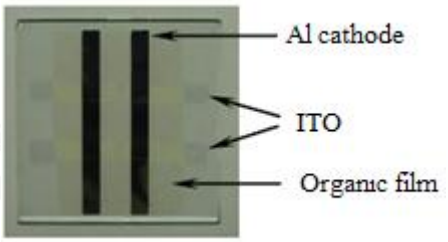

Figure 2.7. OLED device with 4 pixels. A pixel active area of a device is 2 x 2 mm^2.

2.2.11 Device measurement

The instruments for OLED device measurements are shown in **Figure 2.8**.The computer was used for controlling of the digital source meter, the multifunction optical meter, and the USB spectrofluorometer as well as recording the data. The digital source meter applied the voltages to the device and measured the resulting currents. The multifunction optical meter connected with the calibrated photodiode

served in the measurement of the luminance (brightness). The USB spectrofluorometer was used for the EL spectra acquisition.

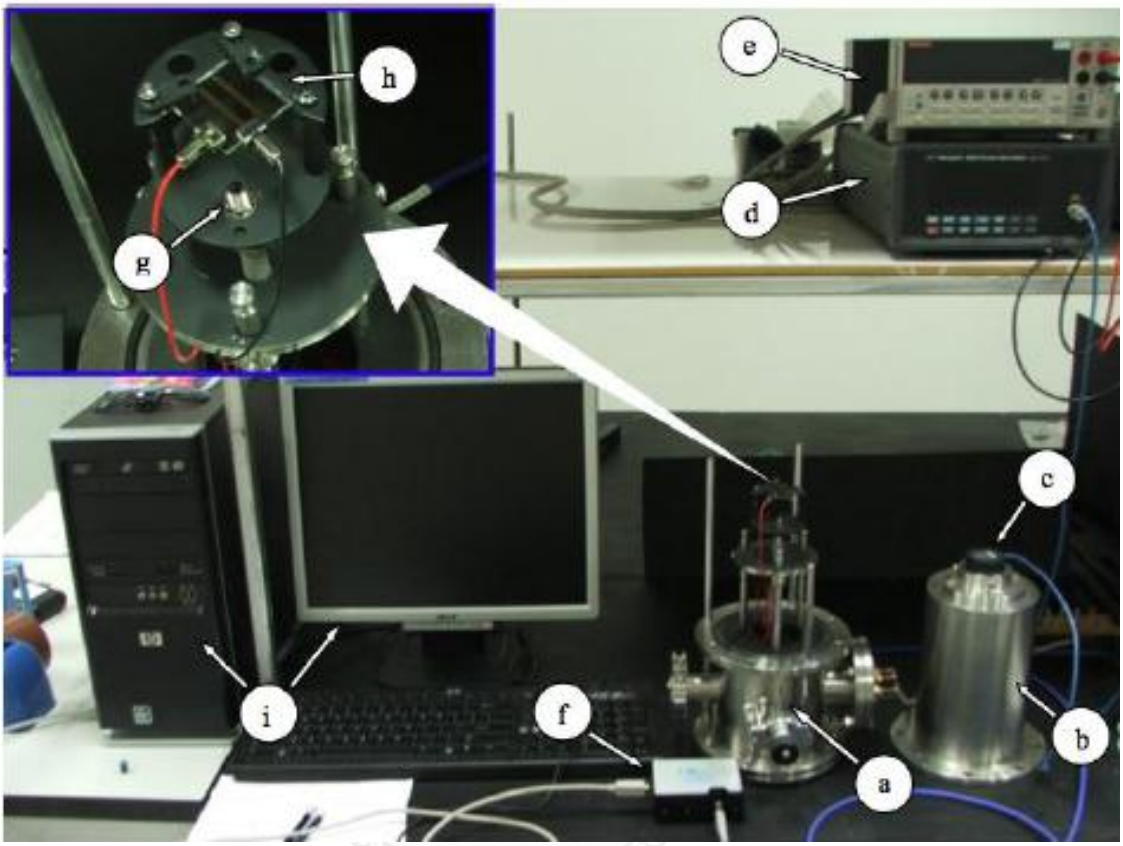

Figure 2.8. Instruments for determination of OLED device performance: (a) OLED test box, (b) lid of OLED test box, (c) calibrated photodiode, (d) multifunction optical meter, (e) digital source meter, (f) USB spectrofluorometer, (g) probe of USB spectrofluorometer, (h) OLED device holder, (i) computer controller and recorder for digital source meter, multifunction optical meter, and USB spectrofluorometer

All device measurements were performed in an OLED test box by blocking the incident light at room temperature under ambient atmosphere. When voltages were applied, the currents, brightness, and EL spectra were recorded at the same time to give the current density–voltage–luminance (*J-V-L*) characteristics and EL spectra. The turn-on voltage was defined at the brightness of 1 cd/m^2. The current density was calculated as the following formula (1):

$$J = \frac{I}{A} \qquad (1)$$

Here, *I* (mA) is the current and *A* (cm^2) is the pixel active area of the device. The luminous efficiency of the device was calculated as the following formula (2):

$$\eta_{lum} = \frac{L}{J} \quad (2)$$

Here, *L* (cd/m^2) is the luminance and *J* (mA/cm^2) is the current density.

The quantum efficiency of a device can be differentiated into two categories; internal and external quantum efficiencies.

Internal quantum efficiency (IQE)- This is the total number of photons generated inside the device per electron– hole pair injected into the device. It is represented by η_{int}. For OLEDs the internal quantum efficiency in the case of fluorescent materials is given by (OIDA 2002)

$$\eta_{int} = \gamma \eta_s \Phi_f, \quad (1)$$

where γ is the fraction of injected charges that produce excitons and is called the charge balance factor, η_s is the fraction of singlet excitons called singlet exciton efficiency and Φ_f is the fraction of energy released from material as light and called the quantum efficiency of fluorescence.

External quantum efficiency (EQE)- This is defined as the total number of photons emitted from the device per electron–hole pair injected into the device. It is represented by η_{ext}. The external quantum efficiency is related to the internal quantum efficiency and is given by (OIDA 2002)

$$\eta_{ext} = R_e \eta_{int}, \quad (2)$$

where R_e is the extraction or outcoupling efficiency representing the number of photons emitted from the device per number of photons generated in the device.

Power Efficiency

The luminous efficacy or power efficiency is the lumen output per input electrical power of the device. It is measured in lumen per watt (lm/W) or candela per ampere (cd/A). It is represented by η_p.

CHAPTER III

RESULTS AND DISCUSSION

3.1 Synthesis

The naphthalimide derivatives (TPN1, TPN2, TPN3) were synthesized from triphenylamine core and naphthalimide branch *via* Suzuki cross-coupling reaction. The synthesis began with a halogenation of triphenylamine moiety to give **2** and **3** in 46% and 95% yield, respectively. The structures of **2** and **3** were confirmed by ^{1}H and ^{13}C-NMR, which were in good agreement with the literature reports. [37, 38]

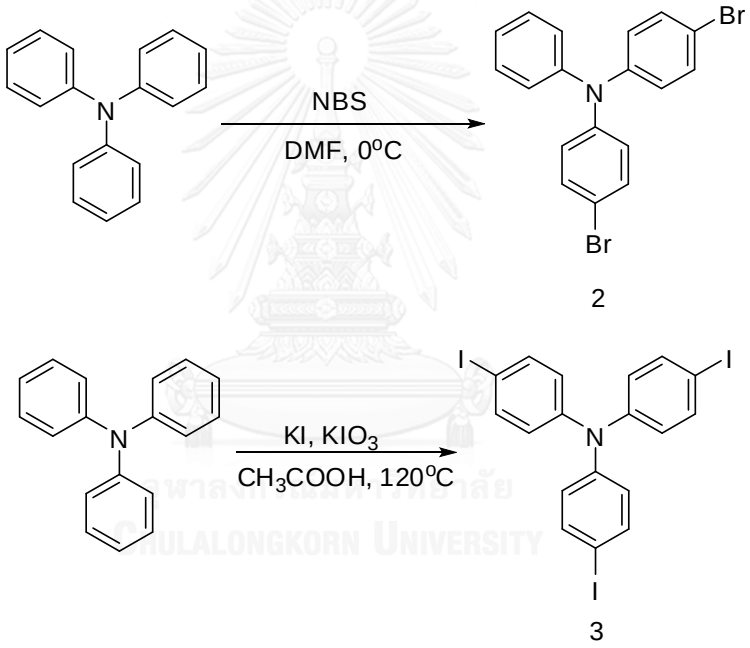

Figure 3.1. The synthesis of cores by bromination and triiodination

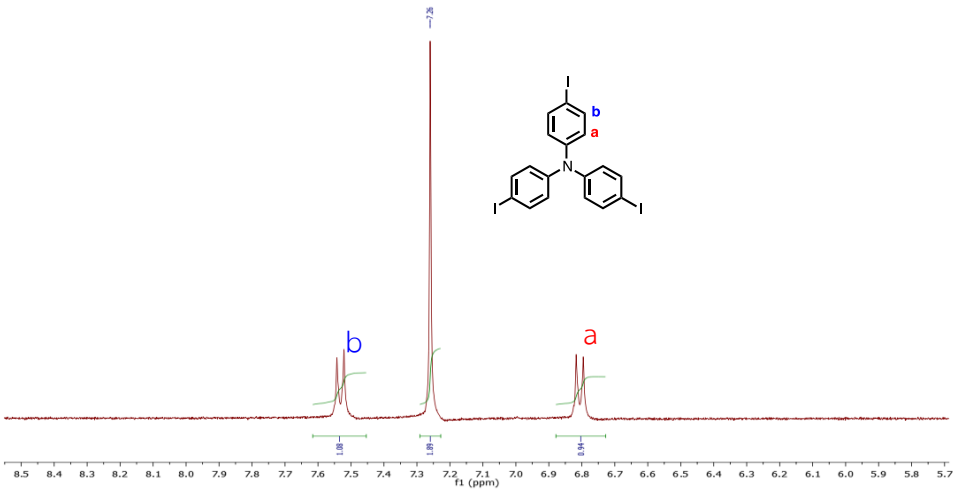

Figure. 3.2. ^{1}H- NMR of 4,4',4''-(triiodo)triphenylamine (**3**) in $CDCl_3$

The second step involved condensation reaction of 4-bromo-1,8-naphthalic anhydride with aniline to give **4** in 95% yield (**Figure 3.3**). The conversion of 4-bromo-*N*-(phenyl)-1,8-naphthalimide (**4**) into the pinacol boronate ester (**5**) was carried out using the procedure reported in the literature. [30, 40, 41]

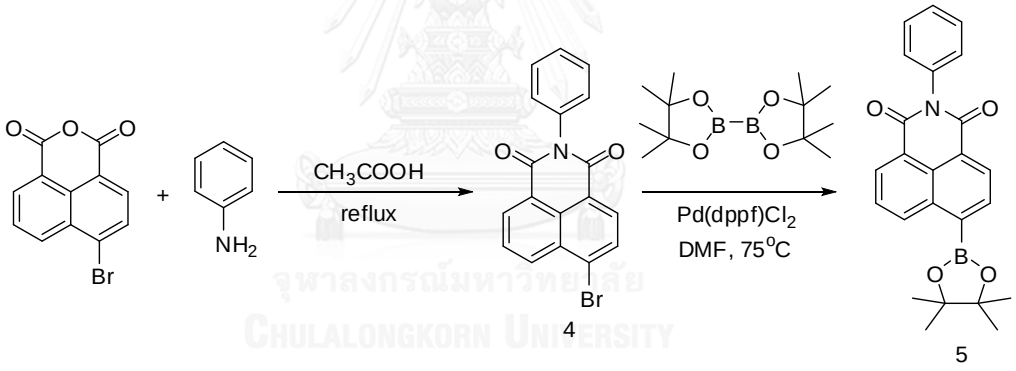

Figure 3.3. The synthesis of naphthalimide derivative as a branch

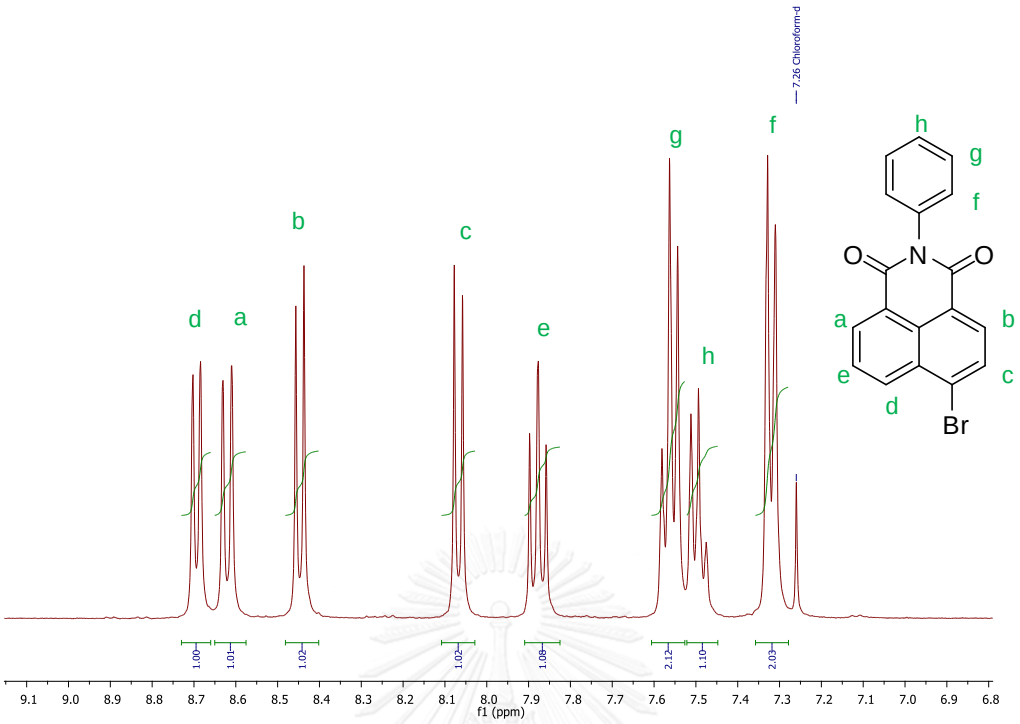

Figure 3.4. Expanded ^{1}H- NMR of 4-Bromo-*N*-(phenyl)-1,8-naphthalimide (**4**) in $CDCl_3$

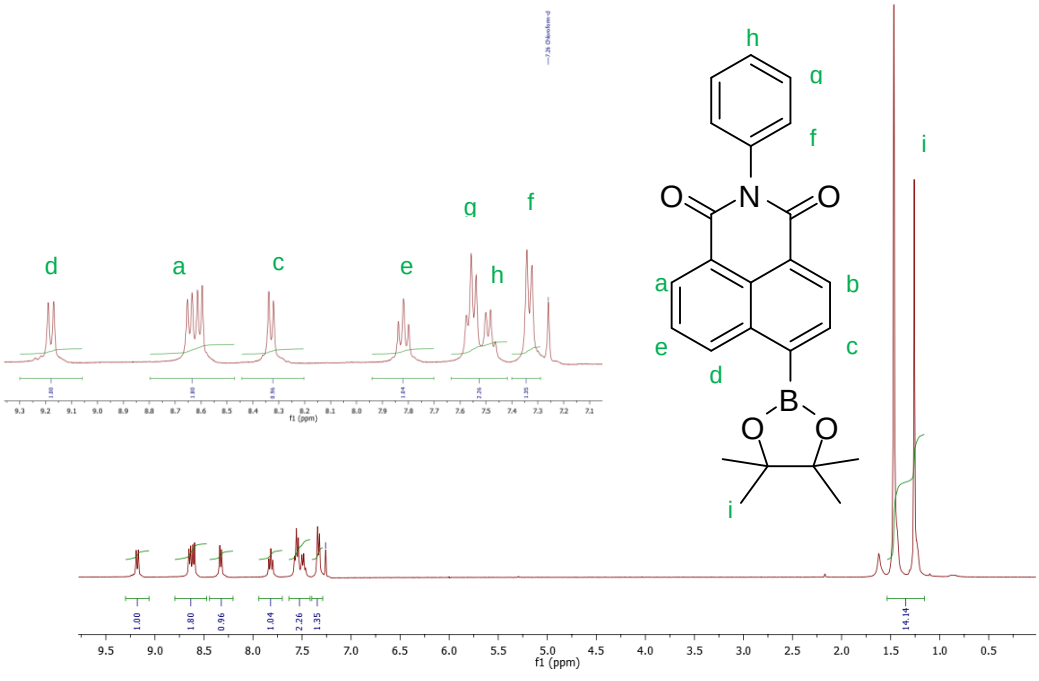

Figure 3.5. ^{1}H- NMR of *N*-phenyl-1,8-naphthalimide-4-boronic acid pinacol ester (**5**) in $CDCl_3$

The synthesis of our target compounds (**TPN1-TPN3**) relied on the Suzuki cross-coupling reactions (**Scheme 1**). Such reaction between the readily accessible 4-

bromo-*N*-(phenyl)-1,8-naphthalimide and the commercially available 4-(*N*,*N*-diphenylamino)-phenylboronic acid under the catalysis of (dppf)$PdCl_2$ provided **TPN1** in excellent yield of 84%. [42, 43] The conversion of 4-bromo-*N*-(phenyl)-1,8-naphthalimide into the pinacol boronate ester (**5**) was carried out using the procedure reported in the literature. **[30, 40, 41]** The Suzuki reaction between **5** and 4,4'-(dibromo)triphenylamine or 4,4',4''-(triiodo)triphenylamine afforded **TPN2** or **TPN3** in moderate yields. [40, 44] The characterization by IR, NMR, and HR-MS confirmed the successful synthesis of these target compounds.

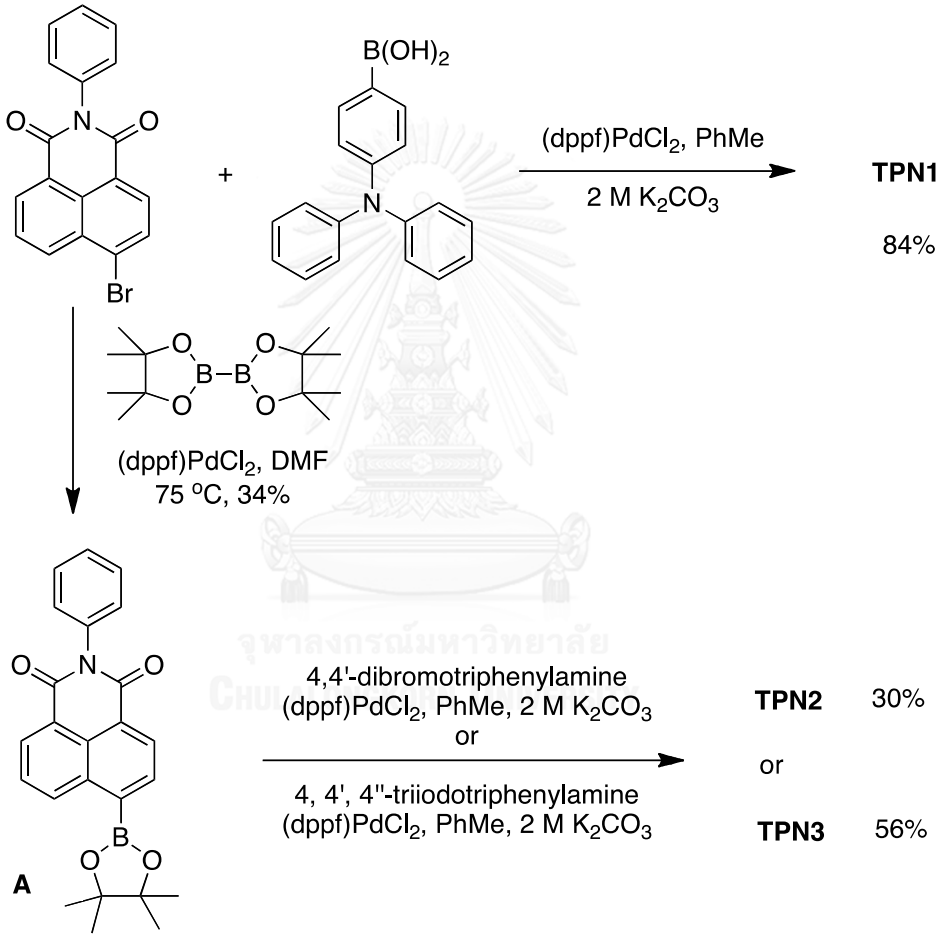

Scheme 1 Synthesis of **TPN1-3**

The ^{1}H-NMR spectra of **TPN1-TPN3** are shown in **figure 3.6-3.8**. All signals can be assigned to all protons in each corresponding structure. Initially, triphenylamine proton showed signals around 7.1-7.5 ppm and proton on naphthalimide ring showed peak at 8.71, 8.51, 7.82, and 7.50 ppm.

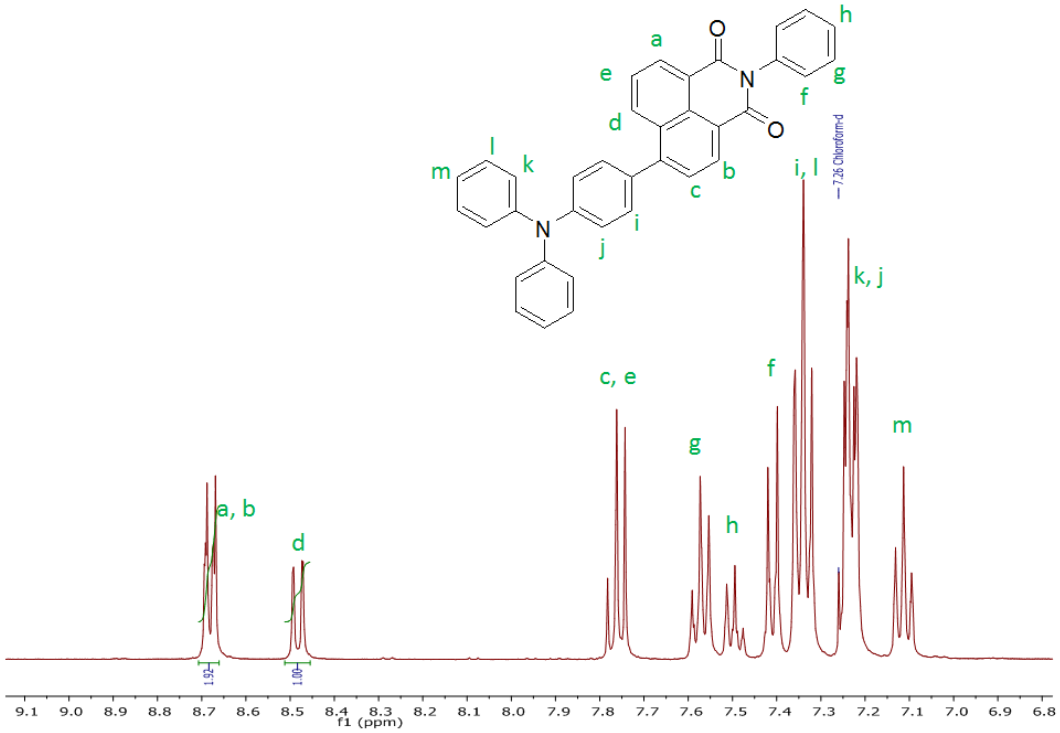

Figure 3.6. Expanded ^{1}H-NMR of **TPN1** in $CDCl_3$

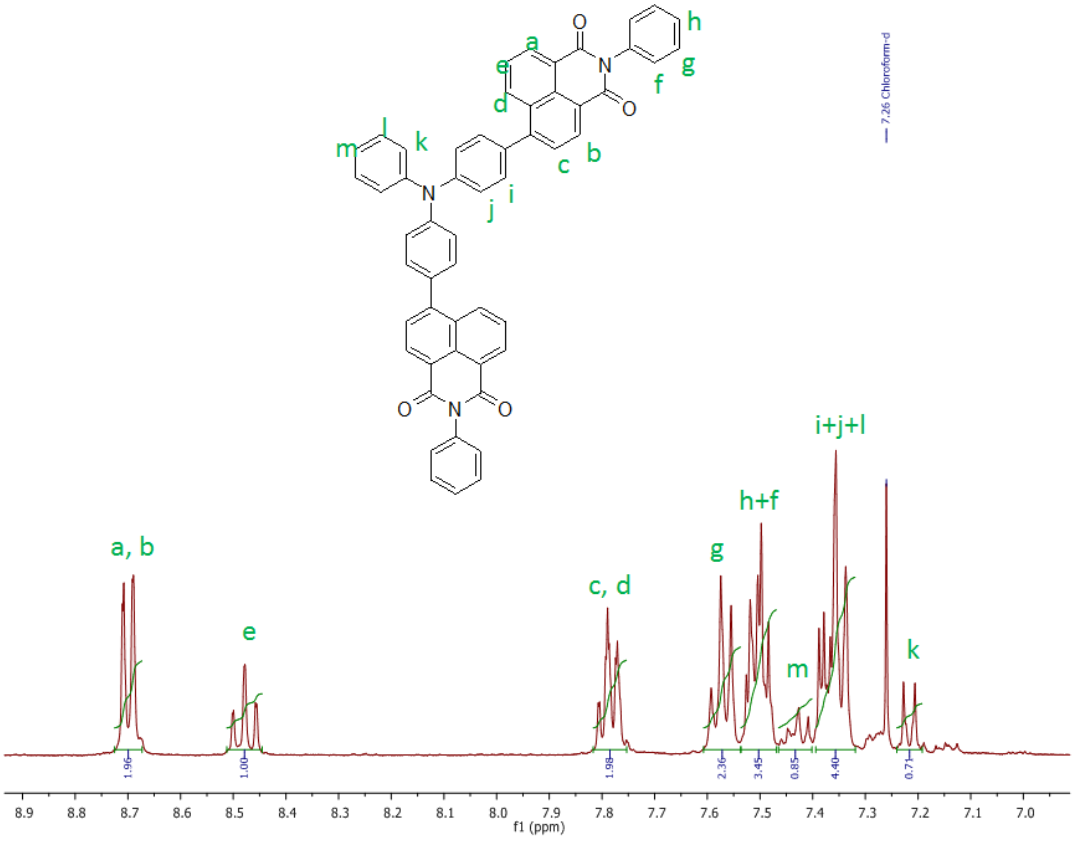

Figure 3.7. Expanded ^{1}H-NMR of TPN2 in $CDCl_3$.

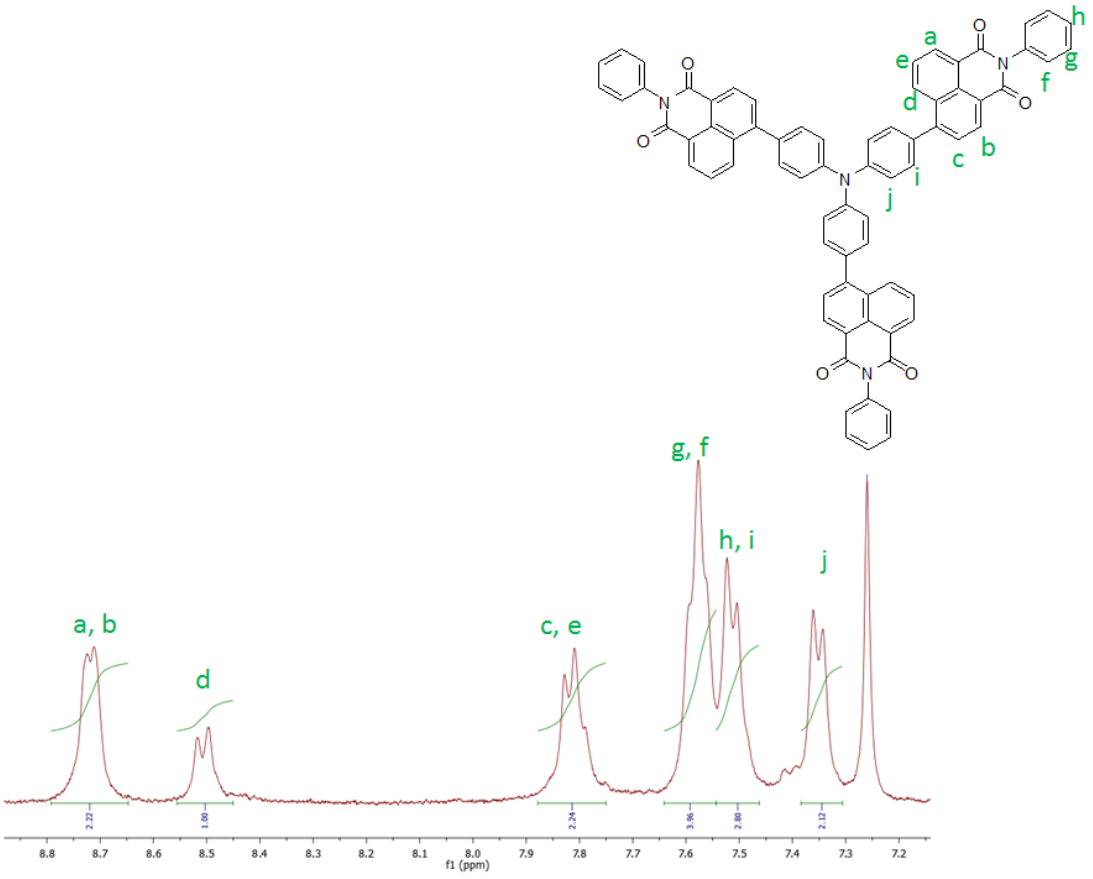

Figure 3.8. Expanded ^{1}H-NMR of TPN3 in $CDCl_3$

The Miyaura borylation reaction enables the synthesis of boronates by cross-coupling of bis(pinacolato)diboron with aryl halides. [30, 40, 41] Boronic acids, and boronate esters are common boryl groups incorporated into organic molecules through borylation reactions. Similarly, boronic esters possess one alkyl substituent and two ester groups. The mechanism is shown in **figure 3.9**.

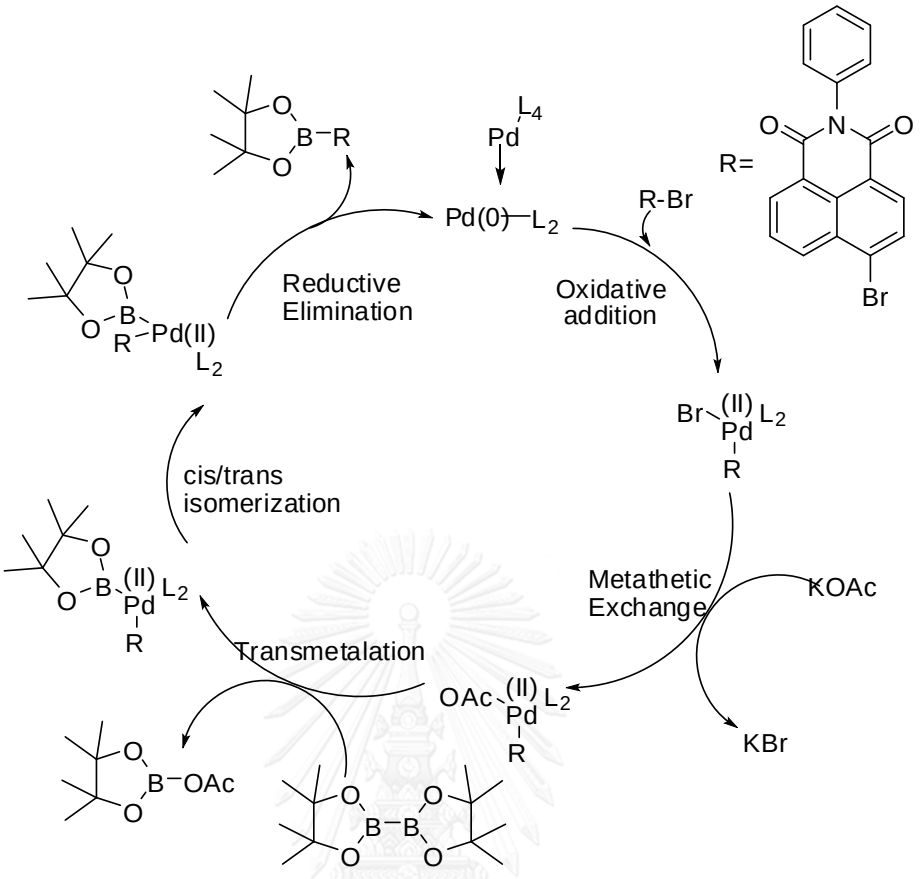

Figure 3.9. The mechanism of Miyamura reaction

The mechanism of Suzuki-cross coupling reaction (**Figure 3.10**) involves a three-stepp cycle: The first step is the oxidative addition of palladium to the halide to form the organopalladium species. Reaction with base gives intermediate which via transmetalation with the boron-ate complex forms the organopalladium species. Reductive elimination of the desired product restores the original palladium catalyst which completes the catalytic cycle.

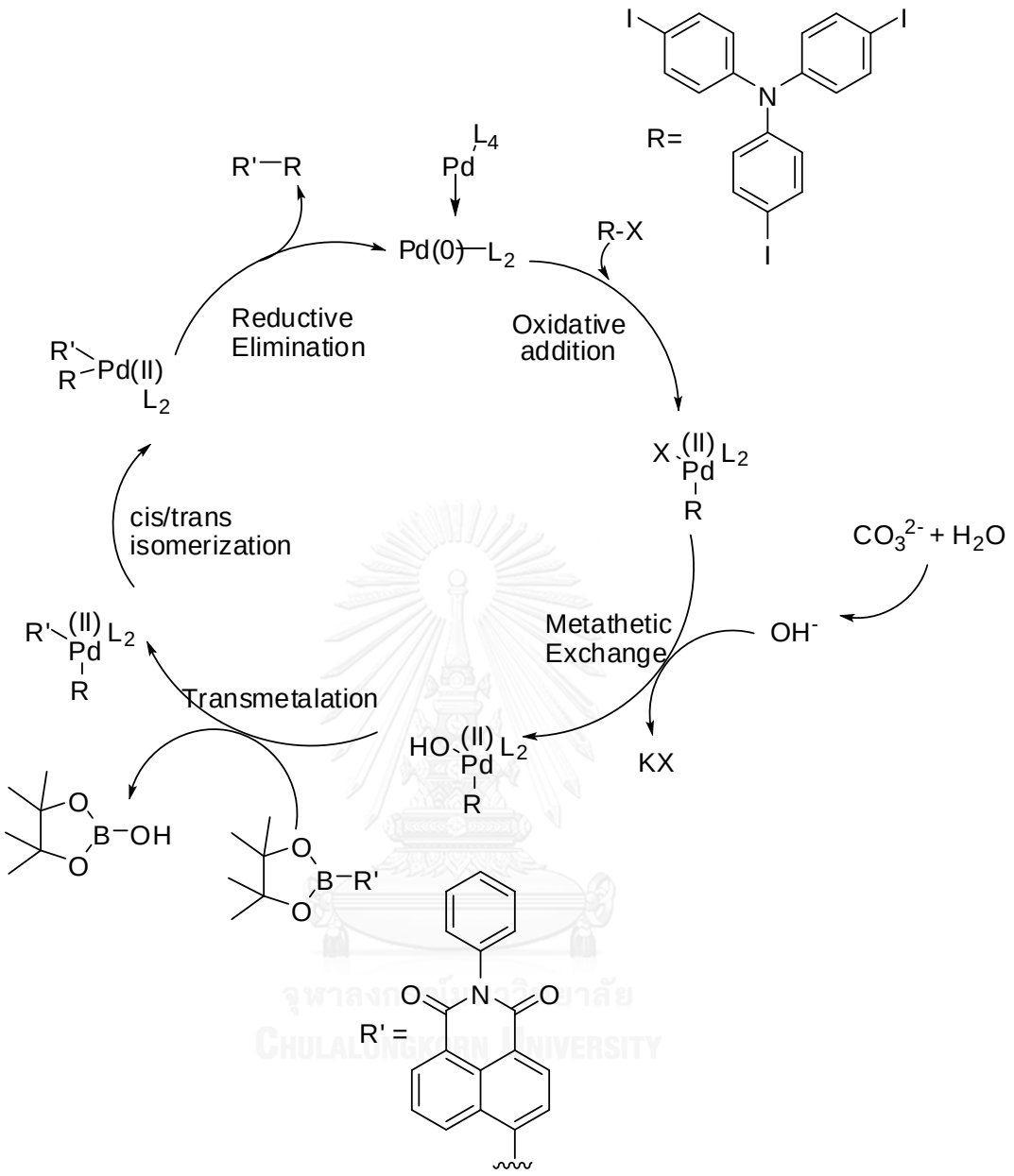

Figure 1.10. The mechanism of Suzuki-cross coupling reaction [42]

With **TPN3** in hands, the solubility in organic solvent can be enhanced by o-alkylation at the position 4 of *N*-phenyl ring using K_2CO_3 and *n*-butyl bromide in acetone at 60 $^{\circ}C$ with stirring for overnight. The product was purified by silica gel column chromatography in 48% yield as a brown solid. In borylation step, unfortunately, this condition was not effective for the synthesis because the products are mixture between minor alryl boronic pinacol ester and major homo-

coupling one which has an evidence to confirm in paper as reference (**figure 3.12**). [30]

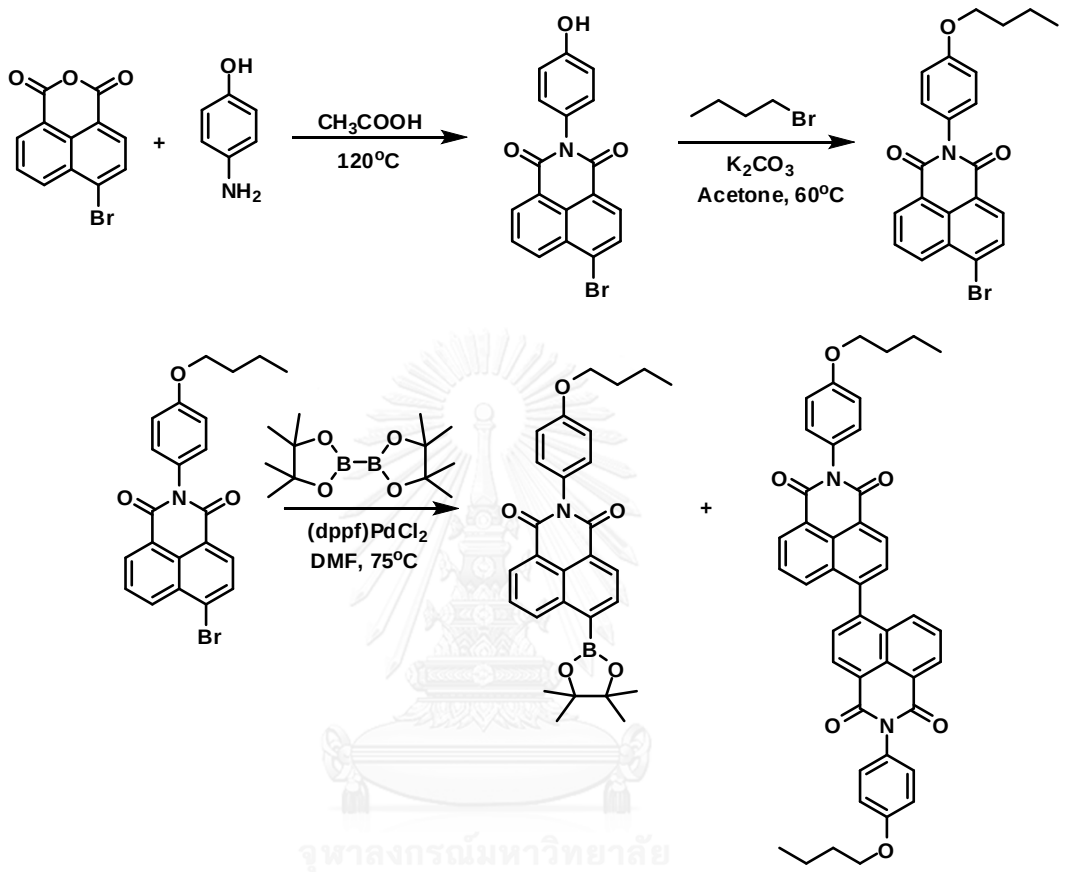

Scheme 2 Synthesis of **O-alkylation-TPN**

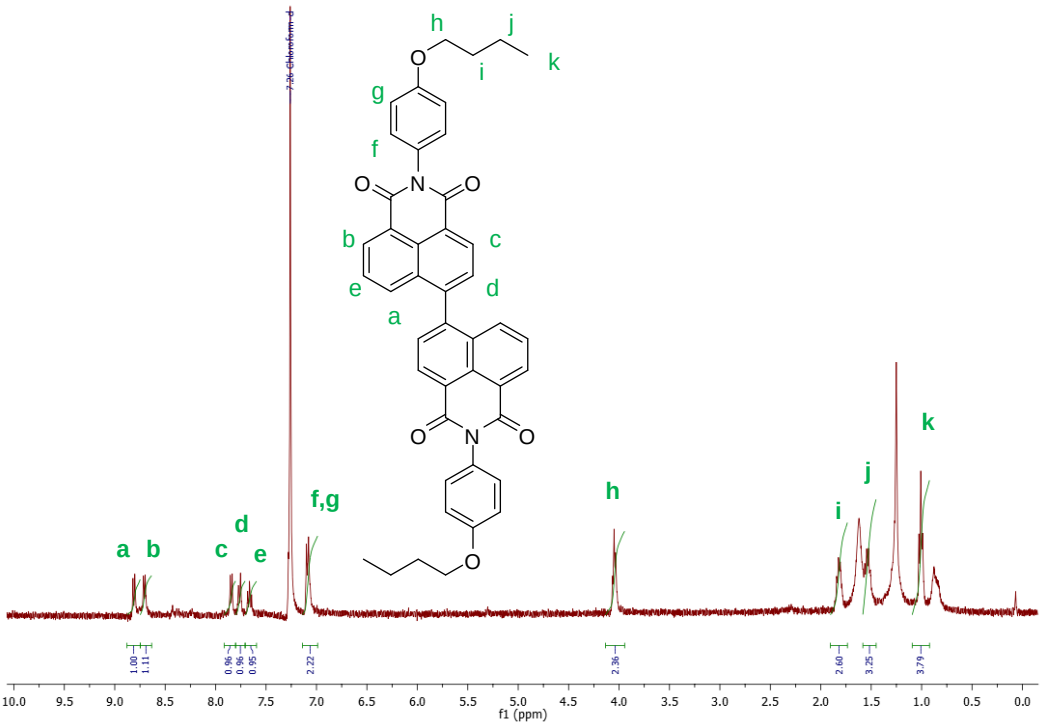

Figure 3.11. ^{1}H-NMR of homo-coupling product in $CDCl_3$

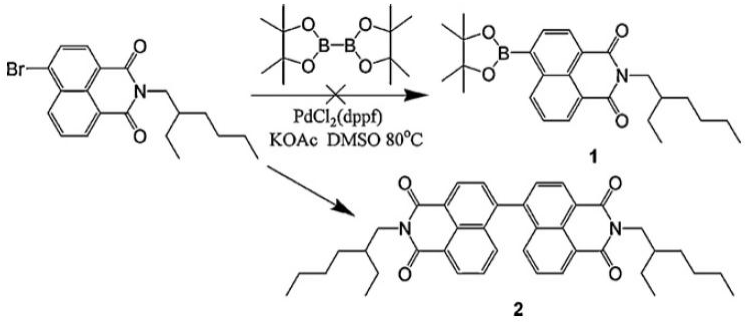

Figure 3.12. Homo-coupling product in borylation reaction [30]

3.2 Optical property

The UV-Vis absorption and emission spectra of **TPN1**, **TPN2**, and **TPN3** were obtained both in $CHCl_3$ and thin film. The results are summarized in **Table 3.2** and illustrated in Figure 3.12-13. In solution phase, they exhibited the characteristic absorption peaks in 312-326 and ~435 nm. Absorption band in the range of 312-326 nm correspond to the **π-π*** transition. The latter absorption band can be assigned to an intramolecular charge transfer (ICT) from the donor (Triphenylamine) to the acceptor (Naphthalimide). The spectra of the three compounds were all normalized

to the maximum absorption whether in solution or thin film state. The absorbance of the three compounds increased along with the number of naphthalimide derivative units both in solution and in film, suggesting that the molar extinction coefficient increased by introducing more naphthalimide derivative units into the one molecule. The optical band gap energies of **TPN1**, **TPN2**, and **TPN3** were then calculated from the onset wavelength of absorption spectra to be 2.48, 2.52 and 2.54 eV, respectively. With the increasing number of naphthalimide branchs, dihedral angles between the donor and acceptor segments are enlarged, which reduced the conjugation degree and thus increases the HOMO (highest occupied molecular orbital)-LUMO (lowest unoccupied molecular orbital) gap [45]; therefore, the optical band gap energy is much higher for this reason. For the thin films were obtained by thermal evaporation technique, the solid phase absorption spectra of all three compounds exhibited a significant bathochromic shift indicating a better **π**-electron delocalization in the conjugated systems which is probably a result of a greater planarity between the triphenylamine and naphthalimide units forced by the solid-state packing. [46]

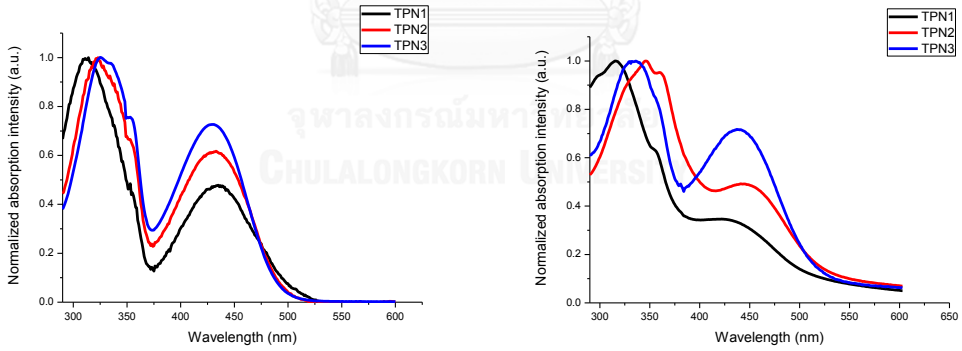

Figure 3.13. Absorption spectra of **TPN1**, **TPN2** and **TPN3** in $CHCl_3$ (left) and thin film (right)

The normalized fluorescence spectra are shown in **Figure 3.13**, obtained from $CHCl_3$ solution. **TPN1**, **TPN2**, and **TPN3** exhibited the maximum emission wavelength at 599, 580, and 564 nm, respectively. With increasing the number of naphthalimide branches, the fluorescence emission peaks are gradually blue shift due to decreasing electron delocalization within molecule which was consistent with the optical band gap energy value. The solid state, emission spectra of compounds exhibited a

hypsochromic shift compared to the solution phase spectrum. This result may also be attributed to the aforementioned solid-state packing force and the restricted structural relaxation. The quantum yield was measured in $CHCl_3$ solution at room temperature using quinine sulfate solution in 0.01 M H_2SO_4 (Φ_F = 0.54) as a standard.

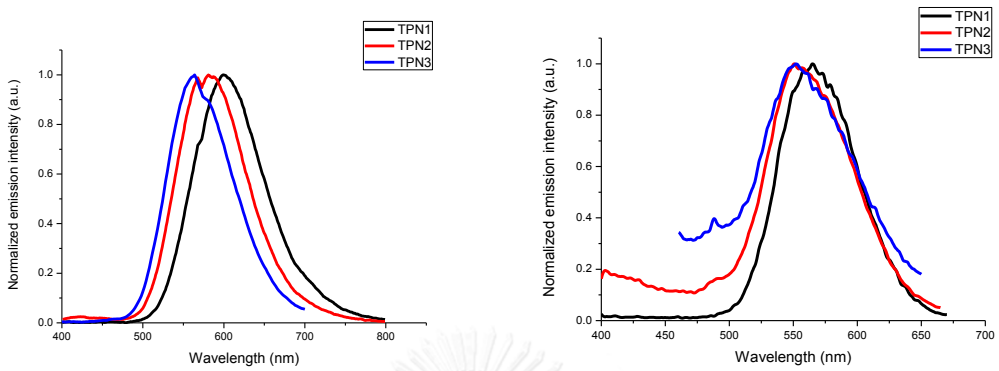

Figure 3.14. Emission spectra of **TPN1**, **TPN2** and **TPN3** in $CHCl_3$ (left) and thin film (right)

Table 3.1. Optical properties of **TPN1**, **TPN2** and **TPN3** measured in $CHCl_3$ solutions and in thin films.

Cpds	Absorption-λ_{max} (nm)			Emission-λ_{max} (nm)		Φ^e	E_g^f (eV)
	log ε ($M^{-1}cm^{-1}$)	Solution[a]	Thin film[b]	Solution[c]	Thin film[d]		
TPN1	4.37	312	317	599	555	0.18	2.48
TPN2	4.57	322	347	580	551	0.29	2.52
TPN3	4.65	326	334	564	550	0.18	2.54

[a] The absorption spectra from the UV-Vis spectra was measured in $CHCl_3$. [b] The absorption spectra from the UV-Vis spectra measured in thin film. [c] The PL emission excited at the absorption maxima in dilute $CHCl_3$ solution. [d] The PL emission excited at the absorption maxima in thin film. [e] PL quantum yield determined in $CHCl_3$ solution (A<0.1) at room temperature using quinine sulfate solution in 0.01 M H_2SO_4 (Φ_F = 0.54) as a standard. [f] The optical energy gap estimated from the onset of the absorption spectra (Eg = 1240/λ_{onset}).

3.3 Thermal properties

For optoelectronic applications, the thermal stability of organic materials must be considered; it causes device stability and lifetime. The heat generation due

to the thermionic emission and the electrical stress causes chemical decomposition of the materials stacked in the OLEDs and creates an undesirable reaction at the interfaces between the materials. The degradation of organic optoelectronic devices depends on morphological changes resulting from the thermal stability of the amorphous organic layer. Morphological change might be promoted by rapid molecular motion near the glass transition temperature (*Tg*). The thermal properties of all compounds were determined by differential scanning calorimetry (DSC) and thermogravimetric analysis (TGA) under nitrogen atmosphere.

The thermal properties of **TPN1**, **TPN2** and **TPN3** are shown in **Figure 3.21** and summarized in **Table 3.4**. The TGA curves revealed that all three compounds were thermally stable with high 10% weight loss temperatures ($T_d^{10\%}$) at 398, 453 and 527°C, respectively. The excellent thermal stability with high T_d readily leads to high stability OLEDs, which is favorable to improve the performance and lifetime of OLEDs during operation. From DSC experiments, there was one sharp endothermic peak for **TPN1** at 264°C due to melting temperature (T_m) and there was no endothermic baseline shift due to glass transition temperature (T_g); it revealed that **TPN1** has high crystalline. For **TPN2**, endothermic peak was observed at 385°C (T_m) and T_g at 254°C. For **TPN3**, T_g at 254°C was also observed at the same position as **TPN2** and there was endothermic peak at 477°C which is melting temperature (T_m). From these results, the amorphous compounds **TPN2** and **TPN3** have the ability to form a molecular glass with a high T_g. Moreover, the ability to form a molecular glass with the possibility to prepare good thin films by both evaporation and solution casting processes is highly desirable for applications in electroluminescent devices.

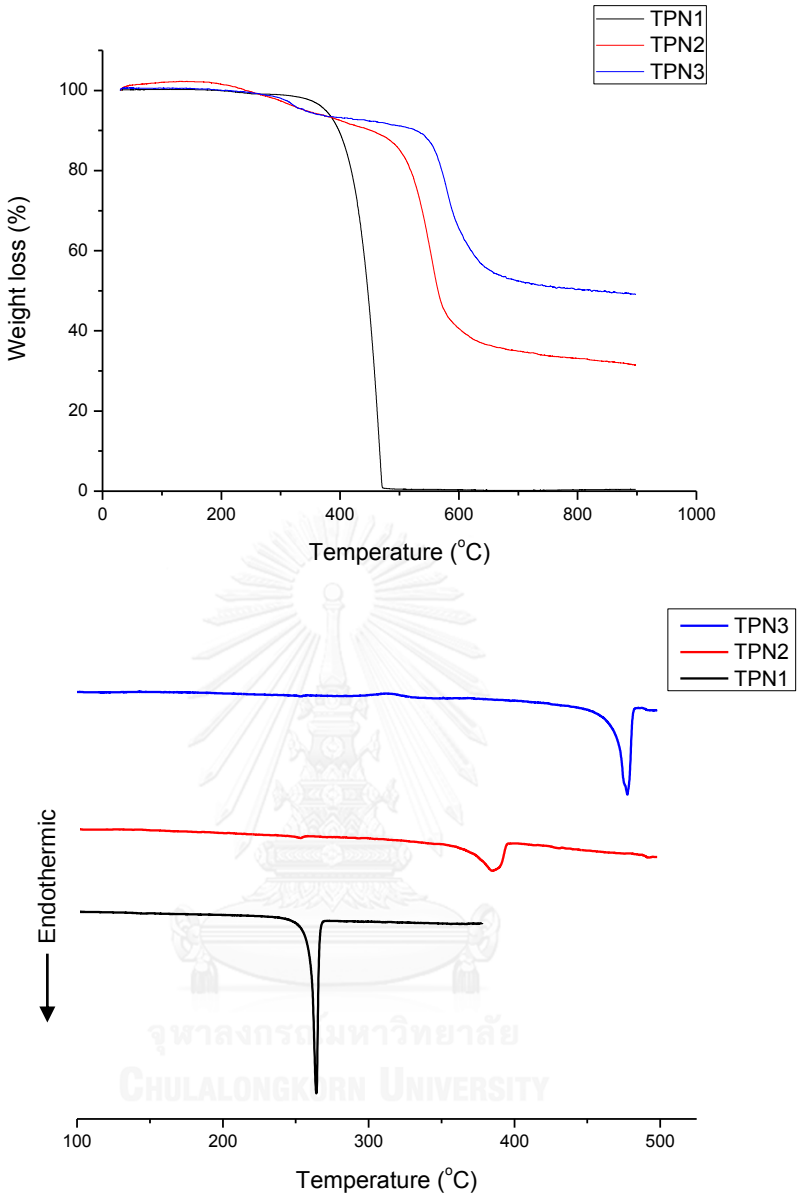

Figure 3.15. TGA (up) and DSC (down) traces of **TPN1**, **TPN2** and **TPN3** measured under N_2 atmosphere at heating rate of 10°C/min.

Table 3.2. Thermal properties of **TPN1**, **TPN2** and **TPN3**

Compounds	T_g [a] (°C)	T_m [a] (°C)	T_d [b] (°C)
TPN1	-	264	398
TPN2	254	385	453
TPN3	254	477	527

[a] Obtained from DSC measurements on the second heating cycle with a heating rate of 10°C/min under N_2. [b] 10% decomposition temperature obtained from TGA measurement with a heat rate of 10°C/min under N_2.

3.4 Electrochemical analysis

The electrochemical properties of TPN1, TPN2, and TPN3 were also studied (Figure 3.15) and their energy gaps between the highest occupied molecular orbital (HOMO) and the lowest unoccupied molecular orbital (LUMO) were obtained from cyclic voltammograms and UV-Vis absorption spectra, and the data were shown in Table 3.3.

From the UV-vis experiments, the optical band gap energy could be determined from the onset of absorption wavelength (the lowest energy that molecules absorb to excite the electron to the excited state) was estimated by $E_g = 1240/\lambda_{onset}$. The onset absorption of TPN1, TPN2, and TPN3 is 500, 493, and 488 nm respectively corresponding to band gaps energy of 2.48, 2.52 and 2.54 eV.

In this CV experiments, platinum wire was used as a counter electrode, $Ag/AgNO_3$ as a reference electrode and platinum as a working electrode, *tetra*-n-butylammoniumhexafluorophosphate ($TBAPF_6$) as an electrolyte which can solute in organic solvents. The concentration of electrolyte was 0.1 M, and the concentration of TPN1, TPN2 and TPN3 was 1.0 mM and a scan rate was 50 mV/s.

The HOMO energy levels were calculated from the onset of oxidation potential (E_{onset}) according to a formula, HOMO = $-(E_{onset} - E_{Fc/Fc+} + 4.8)$. [24] The LUMO energy levels were calculated by subtracting the HOMO energy levels with the band gaps energy estimated from the onset of UV–Vis absorption. The HOMO energy levels of all compounds were in the range of 5.21-5.25 eV, which were lower than ITO (4.80 eV) as shown in figure 3.20. Moreover, the oxidation peaks in the positive regime are influenced and shift toward more positive with the increase of naphthalimide branches, indicating the stabilization of the HOMO level due to the electron-withdrawing characteristic of naphthalimide group.

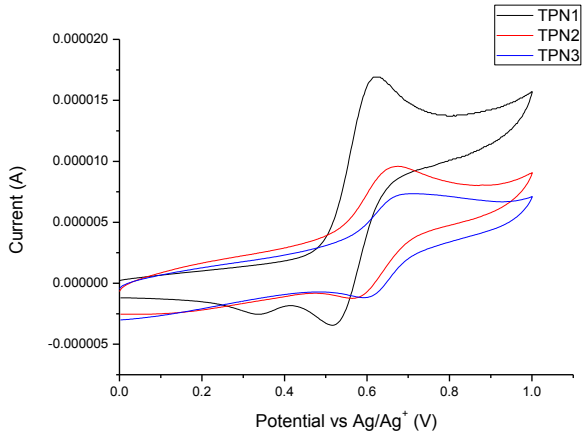

Figure 3.16. Cyclic voltammograms of **TPN1**, TPN**2** and TPN**3** in dry 20% CH_3CN:CH_2Cl_2.

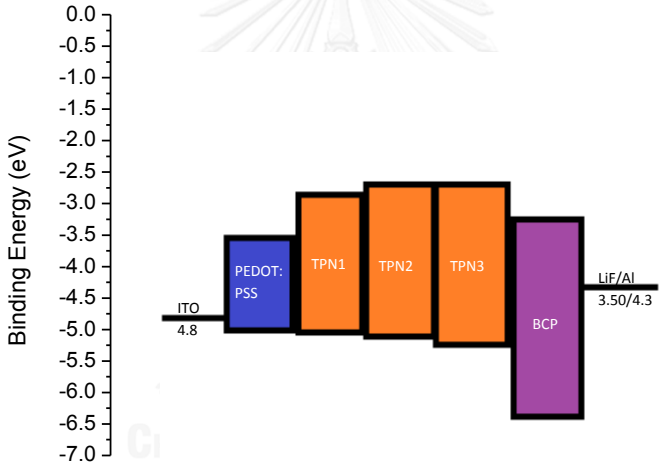

Figure 3.17. Band diagram of ITO, PEDOT:PSS, **TPN1, TPN2, TPN3**, BCP and LiF:Al.

Table 3.3. The experimental and calculated electrochemical properties of **TPN1-3**.

Cpds	Experimental data				Calculated data[e]				
	E_g (eV)[a]	E_{onset} (V)[b]	HOMO (eV)[c]	LUMO (eV)[d]	λ_{ex} (nm)[f]	E_{ex} (eV)	E_g (eV)	HOMO (eV)	LUMO (eV)
TPN1	2.48	0.51	-5.21	-2.73	487	2.54	2.92	-5.22	-2.30
TPN2	2.52	0.53	-5.23	-2.71	481	2.58	2.97	-5.42	-2.45
TPN3	2.54	0.55	-5.25	-2.71	467	2.65	3.04	-5.58	-2.53

[a] The optical energy gap estimated from the onset of the absorption spectra (E_g = $1240/\lambda_{onset}$). [b] Onset oxidation potential estimated from the cyclic voltammogram. [c]

Estimated by the empirical equation: HOMO = -(E_{onset} – $E_{Fc/Fc+}$ + 4.8). [d] Estimated from LUMO = HOMO + E_g. [e] All calculations were performed by Gaussian 09 code and geometry optimizations were done by B3LYP/6-31G(d,p) method. [f] Excitation energy (the first absorption peak) were calculated by TD-B3LYP/6-31G(d,p) method (no solvent is included).

The experimental and computationally calculated electrochemical properties are summarized in **Table 3.3**. From the onset of absorption wavelength from UV-Vis spectra, the HOMO-LUMO energy gaps (E_g) for **TPN1**-**TPN3** could be calculated to 2.48, 2.52 and 2.54 eV, respectively. The HOMO energy levels were obtained from the onset oxidation potential (E_{onset}) observed on the cyclic voltammograms, and the LUMO energy levels were estimated from the Eg and HOMO data. The E_{onset} were influenced and shifted toward more positive potentials with the increase of naphthalimides. This data indicated the stabilization of the HOMO level due to the electron-withdrawing characteristic of naphthalimide group. The experimental HOMO and LUMO levels of all three compounds were in the range of -5.21 to -5.25 eV and -2.71 to -2.73 eV, respectively. These energy levels obtained from the calculations using Gaussian 09 code with geometry optimizations using B3LYP/6-31G(d,p) method also agree with the experimental values. The orbital plots show exclusive electron localizations at the triphenylamine pendant for the HOMOs, and at the napthalimide fragments for the LUMOs (**Figure 3.18**). Since these HOMO and LUMO levels are larger than the work functions of ITO and LiF/Al (**Figure 3.17**), these materials can be fabricated into OLED devices using these electrodes. In addition, there is also a possibility of using the commercially available PEDOT:PSS as the hole-transporting layer and BCP as the hole-blocker.

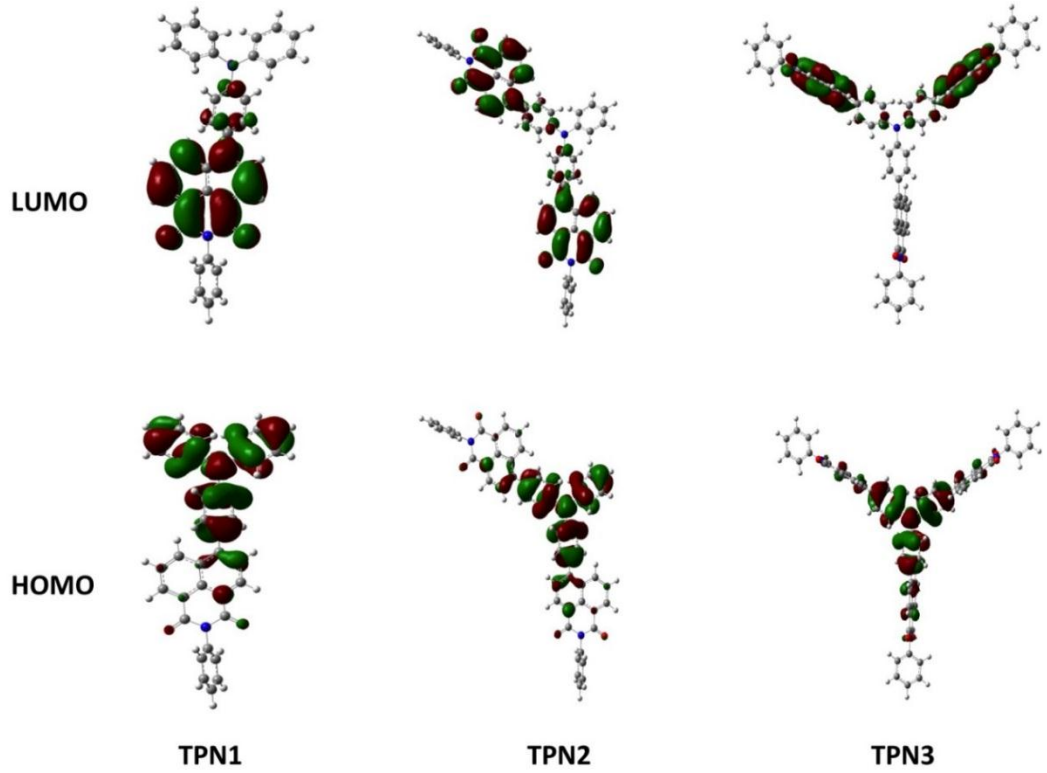

Figure 3.18. Frontier orbital plots for TPN1-3.

3.5 Electroluminescent (EL) properties

Investigation of the electroluminescent property

To investigate their light-emitting properties of TPN1, TPN2, and TPN3, double-layer OLED device was fabricated using **TPN3** as emissive material layer (EML) in devices of structure ITO /PEDOT:PSS/TPN3 (spin-coating)/LiF[0.5nm]/Al[120nm] (Device 1). Under the applied voltage, the device exhibited an orange emission but the voltage-luminance and voltage current density characteristics (*J-V-L*) of the devices is not good in term of brightness and efficiency. Because all three compound have quite low PL quantum efficiency, the device 2 was fabricated with the structure ITO /PEDOT:PSS/CBP:TPN3 (spin-coating)/LiF[0.5nm]/Al[120nm], where CBP is host material. Energy level diagrams of device 1, 2, and CBP compared with TPNs shown in figure 3. From the results, and in view of fact that the barrier for electron migration at Al/CBP:TPN3 interface was significantly high, therefore, under the present device configuration, the performance of the device is not good.

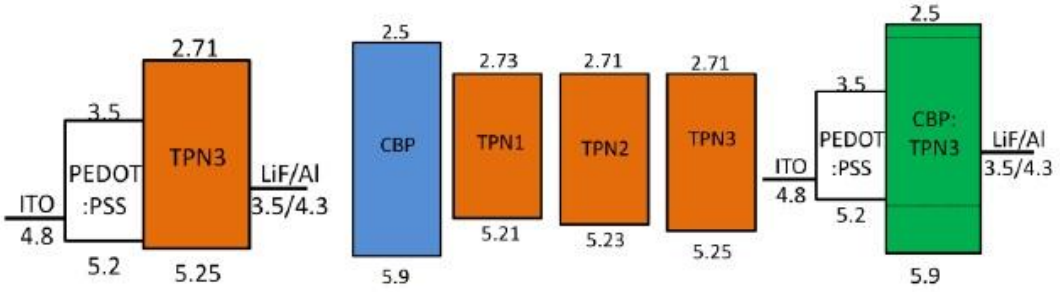

Device 1 Device 2

Figure 3.19. Energy level diagrams of device 1, 2, and CBP compared with TPNs

To improve efficiency of device, after coating the EML, 2,9-dimethyl-4,7-diphenyl-1,10-phenanthroline (BCP, 50 nm) as an hole blocking layer (HBL) was thermally deposited on top of the EML for better electron injection from cathode (figure 3.24).

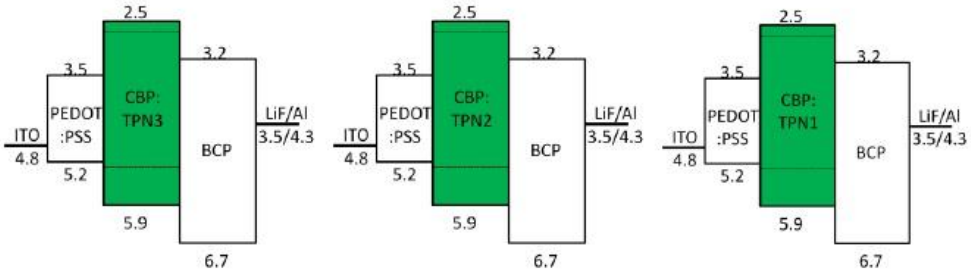

Devive 3 **Device 4** **Device 5**

Figure 3.20. Energy level diagrams of device 3-5

The results showed that device 5 exhibited the highest device performances with a maximum luminance of 10,404 cd/m^2 at 19 V, a turn-on voltage at 5.8 V. This was also corresponded to AFM results because device 5 has the best thin film. Therefore, with the AFM results, a good thin film can give a good performance of the device. Because the HOMO-LUMO of all three compounds was quite the same, the device performance might be the same. From the results, the device performances were affected from the solubility of compound in organic solvent.

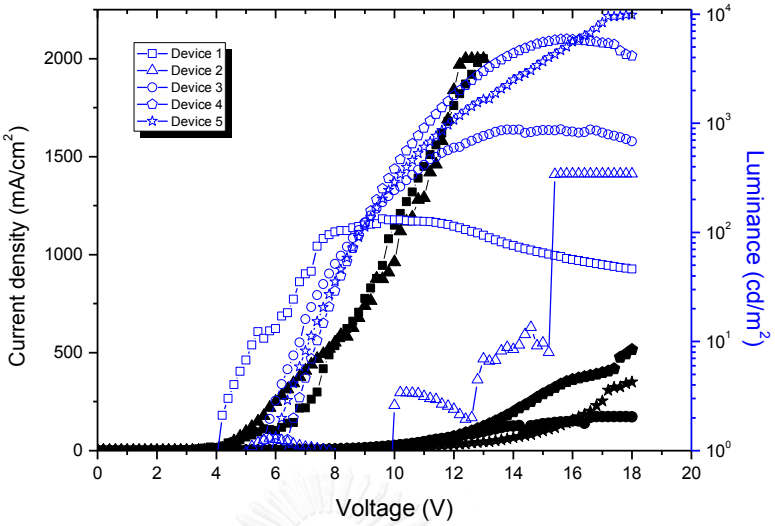

Figure 3.21. Current density and luminance VS voltage (*J-V-L*) characteristics of device 1-5

Table 3.4. Electroluminescent properties of device 3-5

Device	CBP Dopant	V_{on}	L_{max}	η_{lum}	J	CIE
3	TPN3	5.6	877 (14.2)	0.93/10.8 V	128	-
4	TPN2	6.2	5898 (15.8)	2.49/12.0 V	352	0.322, 0.575
5	TPN1	5.8	10404 (19.0)	3.77/14.0 V	410	0.299, 0.578

[a] Turn-on voltage (V). [b] Maximum luminance (cd/m^2) (at applied potential V). [c] Luminance efficiency (cd/A). [d] External efficiency (%). [e] Current density (mA/m^2). [f] Commission International d'Eclairage coordinates (*x*, *y*).

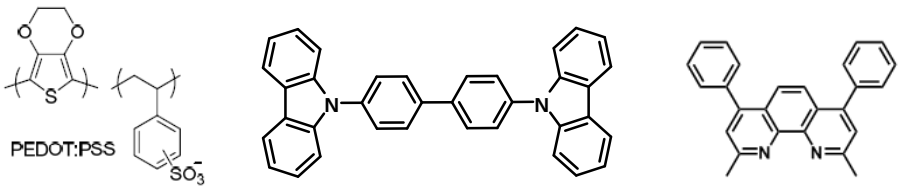

Figure 3.22. Chemical structure of PEDOT:PSS (a), CBP (b), and BCP (c)

Device fabrication by Thermal Evaporation

From the unsatisfied results of TPN3, the limitation of spin-coating process, the molecular design must consider in term of the solubility. Increase of number of naphthalimide branch, TPN3, the polarity of this compound was much higher than other compound. This brought us to change the fabrication technique to be thermal evaporation. Device 6 was introduced to fabricate; because, from the energy level diagram, HOMO of TPN3 could be candidate of hole-transporting material and also could be an emissive material, hence, the device 6 was fabricated in the configuration: ITO/TPN3/TPBi/LiF/Al which TPN3 worked as both HTL and EML (figure.). The device performance was not good because LUMO energy of TPN3 and TPBi is equal; charge recombination could occur at TPN3 incompletely.

Since the solubility of TPN3 in organic solvent, it was therefore subjected to a fabrication of a device 7 by thermal evaporation technique, a multi-layer device: ITO/ α-NPD/CBP:TPN3/TPBi/LiF/Al which used α-NPD as an HTM and TPBi as an ETM. We found that the device was improved highly with a maximum luminance of 8,400 cd/m^2 at 12 V, a turn-on voltage at 3.8 V which was lower than of spin coating, and an high external efficiency of 1.57%.

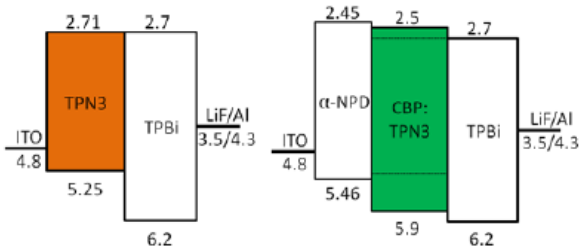

Device 6 **Device 7**

Figure 3.23. Energy level diagrams of device 6 and 7

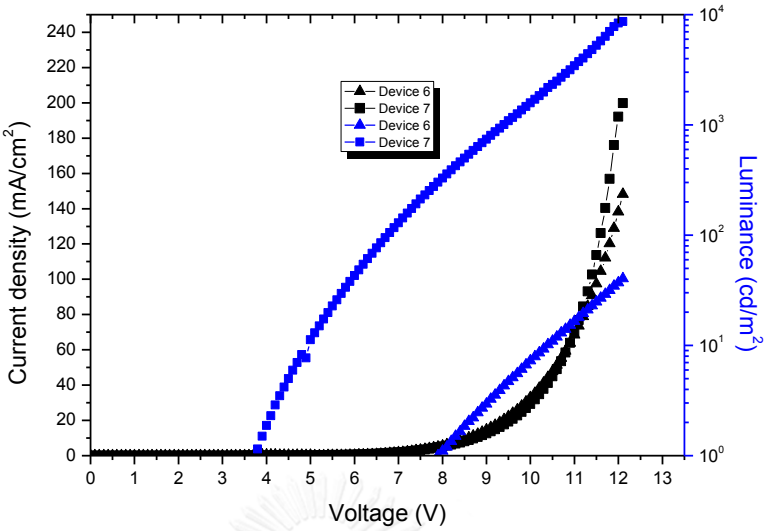

Figure 3.24. Current density and luminance VS voltage (*J-V-L*) characteristics of device 6 and 7

Table 3.5. Electroluminescent properties of device 6-7

Device		V_{on} [a]	L_{max} [b]	η_{lum} [c]	η_{ex} [d]	J [e]	CIE [f]
6	Non-doped	7.8	85.3 (12.7)	0.04/12.7 V	0.02	200	0.532, 0.395
7	doped	3.8	8400 (12)	4.3/12.0 V	1.57	200	0.258, 0.545

[a] Turn-on voltage (V). [b] Maximum luminance (cd/m^2) (at applied potential V).
[c] Luminance efficiency (cd/A). [d] External efficiency (%). [e] Current density (mA/m^2).
[f] Commission International d'Eclairage coordinates (*x*, *y*).

The electroluminescent (EL) spectra of the devices are shown in **Figure 3.27**. The EL peaks of device 4-7 were at 533, 522, 625 and 512 nm, respectively. For device 4, 5, and 7 the EL spectrum matched with the corresponding PL (thin film) emission of CBP:compound. This indicated that the same radiative excited states involved in both EL and PL processes. [47] Interestingly, for device 6, the EL spectra showed red shift compared to PL spectrum of TPN3 thin film. This could cause by the weak hole-transporting ability of this compound. No emission at longer wavelength owing to exciplex species formed at the interface of CBP:compound and

ETL, which often occurred in the devices fabricated with planar molecules was detected.

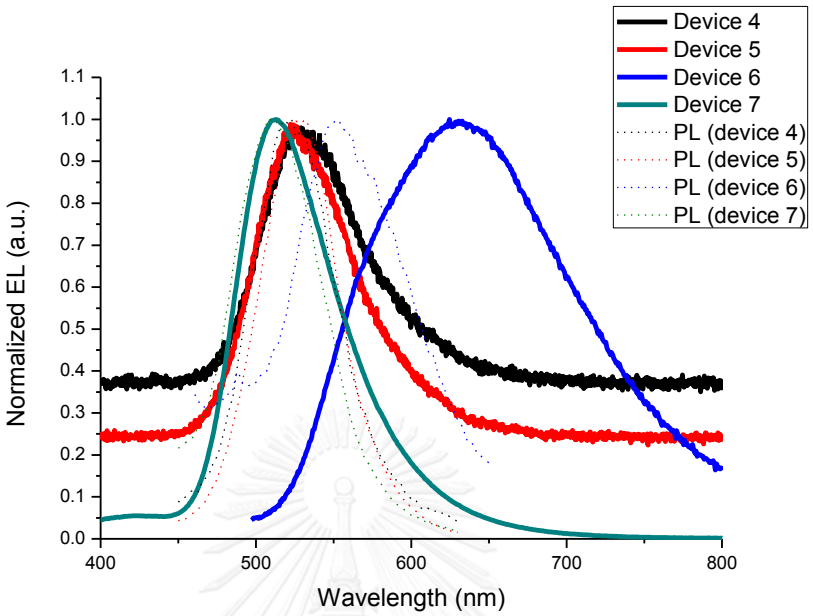

Figure 3.25. EL spectra of device 4-7

The AFM results are shown in **figure 3.26**. Spin coating, all three compounds, TPN1, TPN2 and TPN3 at concentration of 1%w/v were studied. The mixed solvent, $CHCl_3$: Toluene (4:1) was used. Toluene, high boiling point solvent was necessary to use as a mixed solvent to give a good thin film. Compared the solubility of compounds in organic solvent, TPN3 has the highest polarity followed by TPN2 while TPN1 is less. TPN1 could dissolve in mixed solvent very well and TPN2 could also dissolve moderately; but TPN3 could not dissolve well at 1%w/v concentration seen as a heterogeneous solution. Accordingly, TPN1 and TPN2 thin films could form in a good surface. While TPN3 could not form a good one, due to its solubility in organic solvent is not good. The particle which has size less than 0.45 μm could pass through the filter nylon and made the film surface not smooth.

However, for Thermal Evaporation, all compounds, TPN1, TPN2 and TPN3 at a concentration 1 %w/v could form a good thin film (**figure 3.27**). Therefore, the condition for spin coating, the solubility of material should be highly considered. These results were corresponding to device performance above. When the good thin film was formed, the performance of device was well. This suggested that the

recombination of electron and hole in the emitting layer was affected by the smoothness of thin film.

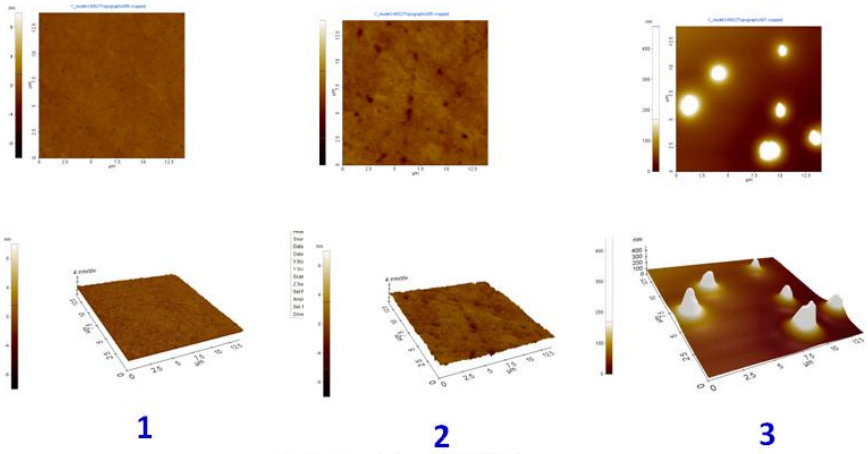

Figure 3.26. AFM images of TPN1, TPN2, and TPN3 doped with CBP by spin coating

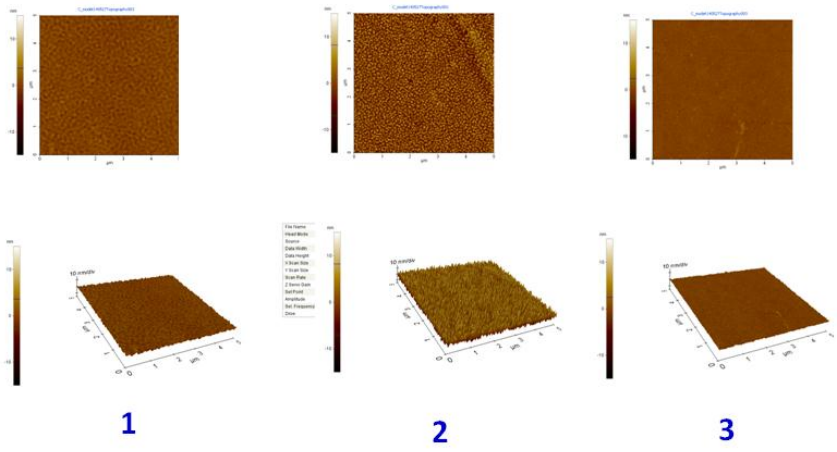

Figure 3.27. AFM images of TPN1, TPN2, and TPN3 by thermal evaporation

CHAPTER IV
CONCLUSION

Three new triphenylamine derivatives substituted by different numbers of *N*-phenylnaphthalimide units were successfully synthesized by means of Suzuki coupling in good to moderate yields. These compounds exhibited absorption maxima around 430 nm and emission maxima around 564-599 nm in $CHCl_3$ solution. The Stoke's shifts were narrower for the spectra of these compounds in solid state as a result of solid packing. With the 10% weight loss temperatures above 350 °C and glass-transition temperature at 254 °C, these compounds showed excellent thermal stability suitable for application as OLED materials. The electrochemical properties were examined by cyclic voltammetry and the data were in good agreement with those obtained from the computational calculations using Gaussian 09 code. The experimental HOMO level of the three compounds were around 5.2 eV while the LUMO levels were around 2.7 eV. When **TPN1**-doped BCP was used as a hole-transporting material in the OLED device of structure ITO/PEDOT:PSS/**TPN1**:CBP/BCP/LiF/Al, the yellowish green light with a maximum brightness of 10,404 cd/m^2 of at an applied voltage of 19 V were produced.

REFERENCES

1. Geffroy, B., P. Le Roy., and C. Prat., *Organic light-emitting diode (OLED) technology: materials, devices and display technologies.* Polymer International, 2006. **55**(6): p. 572-582.
2. Zhu, F. *OLED Activity and technology development*. in *Symposium on Sustainability Driven Innovative Technologies*. 2009.
3. Chen, C.H., et al., *Green organic electroluminescent devices*. 2000, Google Patents.
4. Lo, M.Y., et al., *Organic-inorganic hybrids based on pyrene functionalized octavinylsilsesquioxane cores for application in OLEDs.* Journal of the American Chemical Society, 2007. **129**(18): p. 5808-5809.
5. Figueira-Duarte, T.M., and K. Müllen., *Pyrene-based materials for organic electronics.* Chemical Reviews, 2011. **111**(11): p. 7260-7314.
6. Thejo Kalyani, N. and Dhoble S., *Organic light emitting diodes: Energy saving lighting technology—A review.* Renewable and Sustainable Energy Reviews, 2012. **16**(5): p. 2696-2723.
7. Duan, L., et al., *Improving the performance of OLEDs by using a low-temperature-evaporable n-dopant and a high-mobility electron transport host.* Optics express, 2011. **19**(106): p. A1265-A1271.
8. Doi, S., et al. *Novel blue light-emitting polymers for PLED*. in *Proceedings of SPIE*. 2004.
9. Sasabe, H., et al., *High-Efficiency Blue and White Organic Light-Emitting Devices Incorporating a Blue Iridium Carbene Complex.* Advanced materials, 2010. **22**(44): p. 5003-5007.
10. Lichtman, J.W. and J.-A. Conchello, *Fluorescence microscopy.* Nature methods, 2005. **2**(12): p. 910-919.
11. Chen, C.-T., *Evolution of red organic light-emitting diodes: materials and devices.* Chemistry of materials, 2004. **16**(23): p. 4389-4400.
12. Mu, H., et al., *A comparative study of electrode effects on the electrical and luminescent characteristics of Alq< sub> 3</sub>/TPD OLED: Improvements due to conductive polymer (PEDOT) anode.* Journal of luminescence, 2007. **126**(1): p. 225-229.
13. Grice, A., et al., *High brightness and efficiency blue light-emitting polymer diodes.* Applied Physics Letters, 1998. **73**(5): p. 629-631.

14. Coya, C., et al., *Synthesis and tunable emission of novel polyfluorene co-polymers with 1,8-naphthalimide pendant groups and application in a single layer–single component white emitting device.* European Polymer Journal, 2010. **46**(8): p. 1778-1789.
15. Su, S.-J., et al., *A host material with a small singlet–triplet exchange energy for phosphorescent organic light-emitting diodes: Guest, host, and exciplex emission.* Organic Electronics, 2012. **13**(10): p. 1937-1947.
16. Fu, Q., et al., *Solution-processed small molecules as mixed host for highly efficient blue and white phosphorescent organic light-emitting diodes.* ACS applied materials & interfaces, 2012. **4**(12): p. 6579-6586.
17. Song, M.-S., et al., *Synthesis of some green dopants for OLEDs based on arylamine 2, 3-disubstituted bithiophene derivatives.* Molecules, 2013. **18**(11): p. 14033-14041.
18. Burroughes, J., et al., *Light-emitting diodes based on conjugated polymers.* nature, 1990. **347**(6293): p. 539-541.
19. Heeger, A.J. and D. Braun, *Visible light emitting diodes fabricated from soluble semiconducting polymers*. 2003, Google Patents.
20. Fukuda, Y., et al. *Organic LED full color passive-matrix display*. in *SID Symposium Digest of Technical Papers*. 1999. Wiley Online Library.
21. Gudeika, D., et al., *New derivatives of triphenylamine and naphthalimide as ambipolar organic semiconductors: Experimental and theoretical approach.* Dyes and Pigments, 2014. **106**: p. 58-70.
22. Roquet, S., et al., *Triphenylamine-thienylenevinylene hybrid systems with internal charge transfer as donor materials for heterojunction solar cells.* Journal of the American Chemical Society, 2006. **128**(10): p. 3459-3466.
23. Gan, J.-A., et al., *1, 8-Naphthalimides for non-doping OLEDs: the tunable emission color from blue, green to red.* Journal of Photochemistry and Photobiology A: Chemistry, 2004. **162**(2): p. 399-406.
24. Zhu, W., et al., *A novel family of twisted molecular luminescent materials containing carbazole unit for single-layer organic electroluminescent devices.* Journal of Photochemistry and Photobiology A: Chemistry, 2003. **154**(2): p. 169-177.
25. Fang, Q., et al., *A novel fluorene derivative containing four triphenylamine groups: Highly thermostable blue emitter with hole-transporting ability for organic light-emitting diode (OLED).* Synthetic metals, 2005. **155**(1): p. 206-210.

26. Sek, D., et al., *Structure–properties relationship of linear and star-shaped imines with triphenylamine moieties as hole-transporting materials.* Optical Materials, 2010. **32**(11): p. 1514-1525.
27. Kochapradist, P., et al., *Multi-triphenylamine-substituted carbazoles: synthesis, characterization, properties, and applications as hole-transporting materials.* Tetrahedron Letters, 2013. **54**(28): p. 3683-3687.
28. Wang, S., et al., *Luminescent properties of a novel naphthalimide-fluorene molecule.* Synthetic metals, 2005. **150**(1): p. 33-38.
29. Mikroyannidis, J.A., S. Ye, and Y. Liu, *Electroluminesent divinylene-and trivinylene-molecules with terminal naphthalimide or phthalimide segments.* Synthetic Metals, 2009. **159**(5): p. 492-500.
30. Liu, Y., et al., *Synthesis and properties of starburst amorphous molecules: 1, 3, 5-Tris (1, 8-naphthalimide-4-yl) benzenes.* Synthetic Metals, 2010. **160**(19): p. 2055-2060.
31. Liu, J., et al., *Synthesis and luminescent properties of blue sextuple-hydrogen-bond self-assembly molecular duplexes bearing 4-phenoxy-1, 8-naphthalimide moieties.* Optical Materials, 2012. **34**(9): p. 1535-1542.
32. Tu, G., et al., *Highly efficient pure-white-light-emitting diodes from a single polymer: polyfluorene with naphthalimide moieties.* Advanced Functional Materials, 2006. **16**(1): p. 101-106.
33. Gudeika, D., et al., *Hydrazones containing electron-accepting and electron-donating moieties.* Dyes and Pigments, 2011. **91**(1): p. 13-19.
34. Xiao, J. and Z. Deng, *Synthesis and electroluminescent characterization of a symmetric starburst orange-red light material.* Journal of Luminescence, 2012. **132**(11): p. 2863-2867.
35. Jin, R. and S. Tang, *Theoretical study on optical and electronic properties of bipolar molecules with 1,8-naphthalimide and triphenylamine moieties as organic light-emitting materials.* Journal of Molecular Graphics and Modelling, 2013. **42**(1): p. 120-128.
36. Mei, C., et al., *Green electroluminescent polyfluorenes containing 1, 8-naphthalimide moieties as color tuner.* Polymer, 2006. **47**(14): p. 4976-4984.
37. Shi, L., et al., *High performance aniline vapor detection based on multi-branched fluorescent triphenylamine-benzothiadiazole derivatives: branch effect and aggregation control of the sensing performance.* Journal of Materials Chemistry, 2012. **22**(23): p. 11629-11635.

38. Khanasa, T., et al., *Synthesis and Characterization of 2D-D-π-A-Type Organic Dyes Bearing Bis (3, 6-di-tert-butylcarbazol-9-ylphenyl) aniline as Donor Moiety for Dye-Sensitized Solar Cells.* European Journal of Organic Chemistry, 2013. **2013**(13): p. 2608-2620.
39. Jiang, W., et al., *Synthesis and photochemical properties of novel 4-diarylamine-1, 8-naphthalimide derivatives.* Dyes and Pigments, 2008. **77**(1): p. 125-128.
40. Hosoya, T., et al., *Facile synthesis of diazido-functionalized biaryl compounds as radioisotope-free photoaffinity probes by Suzuki–Miyaura coupling.* Bioorganic & medicinal chemistry, 2009. **17**(6): p. 2490-2496.
41. Brouwer, F., et al., *Using bis (pinacolato) diboron to improve the quality of regioregular conjugated co-polymers.* Journal of Materials Chemistry, 2011. **21**(5): p. 1582-1592.
42. Mora, M., C. Jiménez-Sanchidrián, and J.R. Ruiz, *Suzuki cross-coupling reactions over Pd (II)-hydrotalcite catalysts in water.* Journal of Molecular Catalysis A: Chemical, 2008. **285**(1): p. 79-83.
43. Joshaghani, M., et al., *Efficient Suzuki cross-coupling reactions using bulky phosphines.* Journal of Molecular Catalysis A: Chemical, 2006. **259**(1): p. 35-40.
44. Kitamura, Y., et al., *Heterogeneous Pd/C-catalyzed ligand-free Suzuki–Miyaura coupling reaction using aryl boronic esters.* Tetrahedron, 2007. **63**(43): p. 10596-10602.
45. Chen, F., et al., *Near-infrared and multicolored electrochromism of solution processable triphenylamine-anthraquinone imide hybrid systems.* Electrochimica Acta, 2013. **99**: p. 211-218.
46. Pan, J.-F., S.-J. Chua, and W. Huang, *Conformational analysis (ab initio HF/3-21G*) and optical properties of poly (thiophene-phenylene-thiophene)(PTPT).* Chemical physics letters, 2002. **363**(1): p. 18-24.
47. Liu, Y., et al., *Organic light-emitting diode based on a carbazole compound.* Synthetic metals, 2006. **156**(11): p. 824-827.

APPENDIX

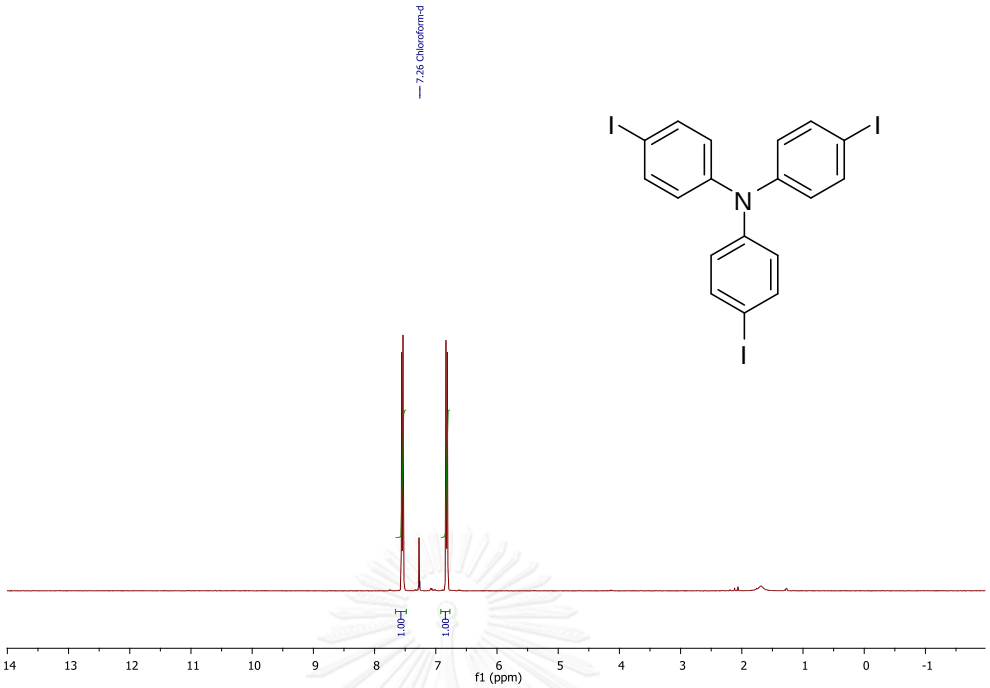

Figure A1. ^{1}H-NMR of tris(4-iodophenyl)amine in $CDCl_3$

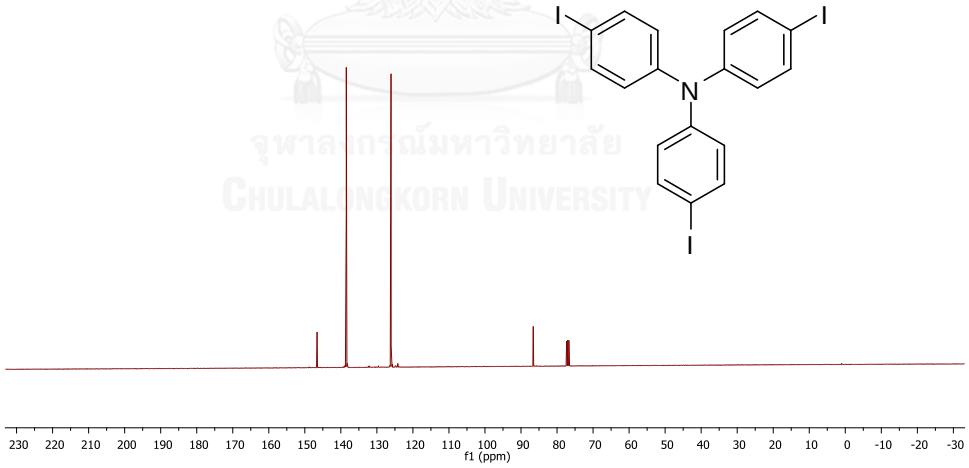

Figure A2. ^{13}C-NMR of tris(4-iodophenyl)amine in $CDCl_3$

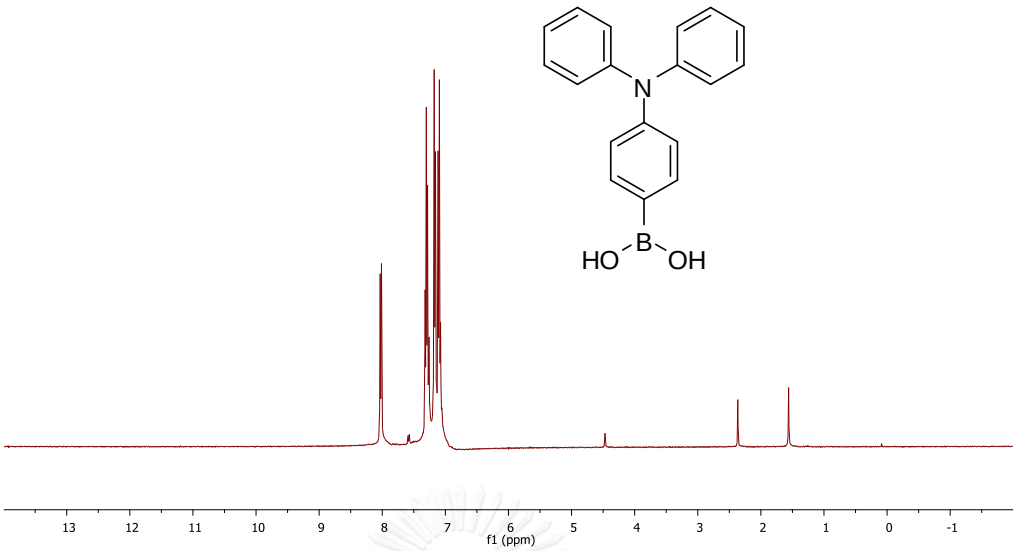

Figure A3. ^{1}H-NMR of 4-(diphenylamino)phenylboronic acid pinacol ester in $CDCl_3$

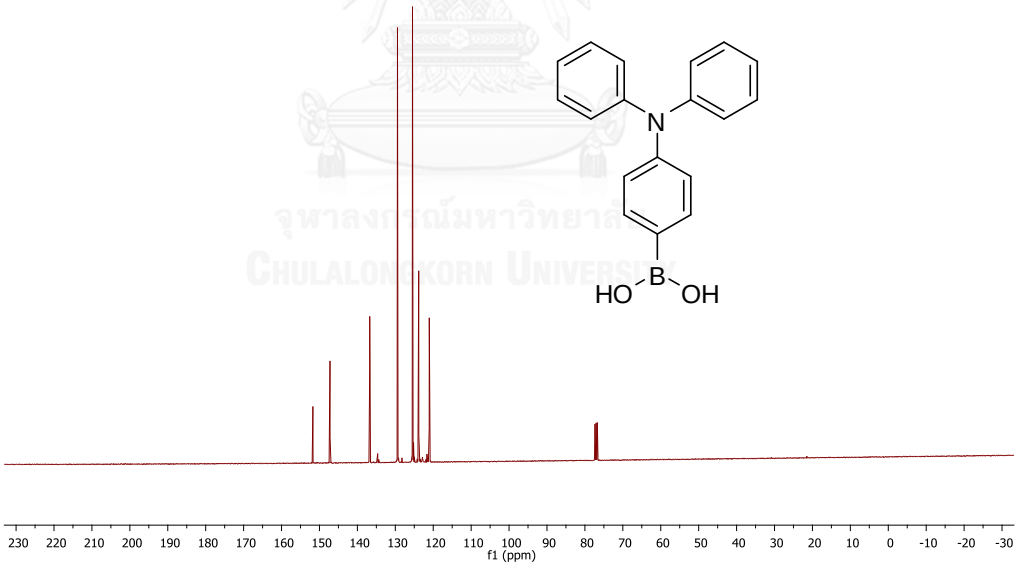

Figure A4. ^{13}C-NMR of 4-(diphenylamino)phenylboronic acid pinacol ester in $CDCl_3$

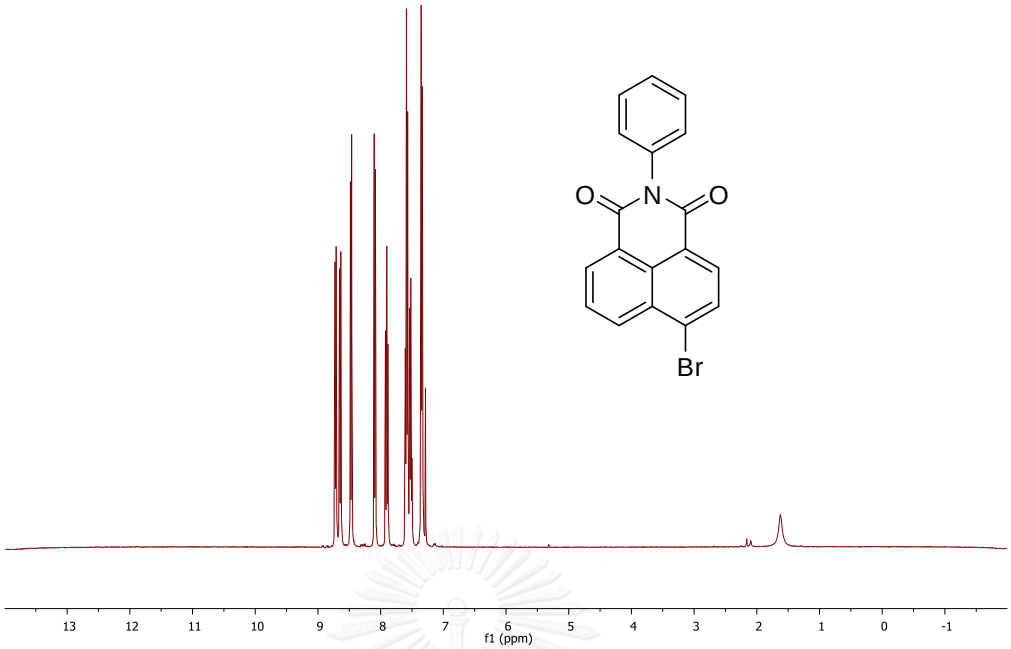

Figure A5. ^{1}H-NMR of 4-bromo-*N*-(phynyl)-1,8-naphthlimide in $CDCl_3$

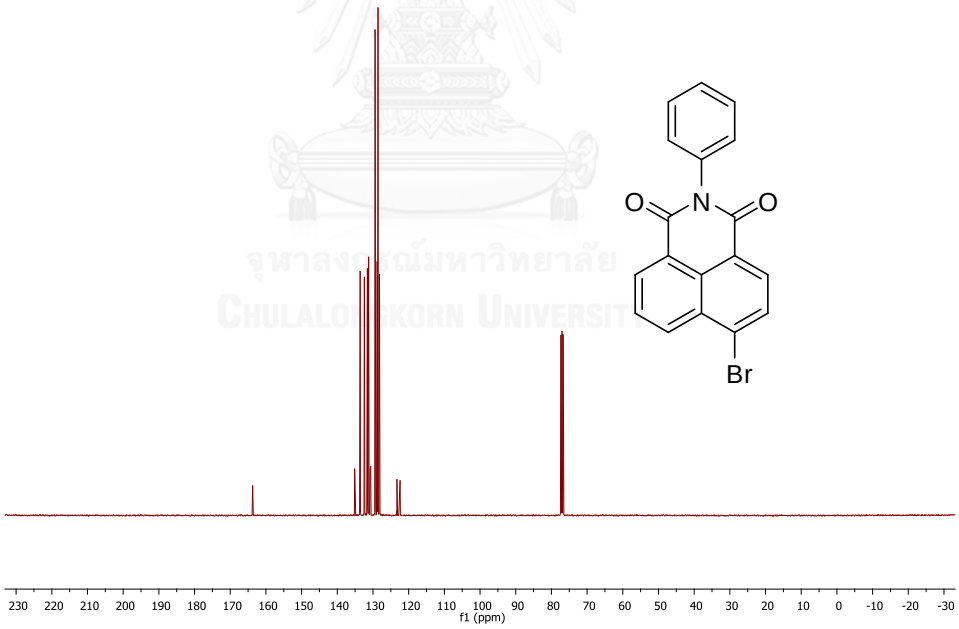

Figure A6. ^{13}C-NMR of 4-bromo-*N*-(phynyl)-1,8-naphthlimide in $CDCl_3$

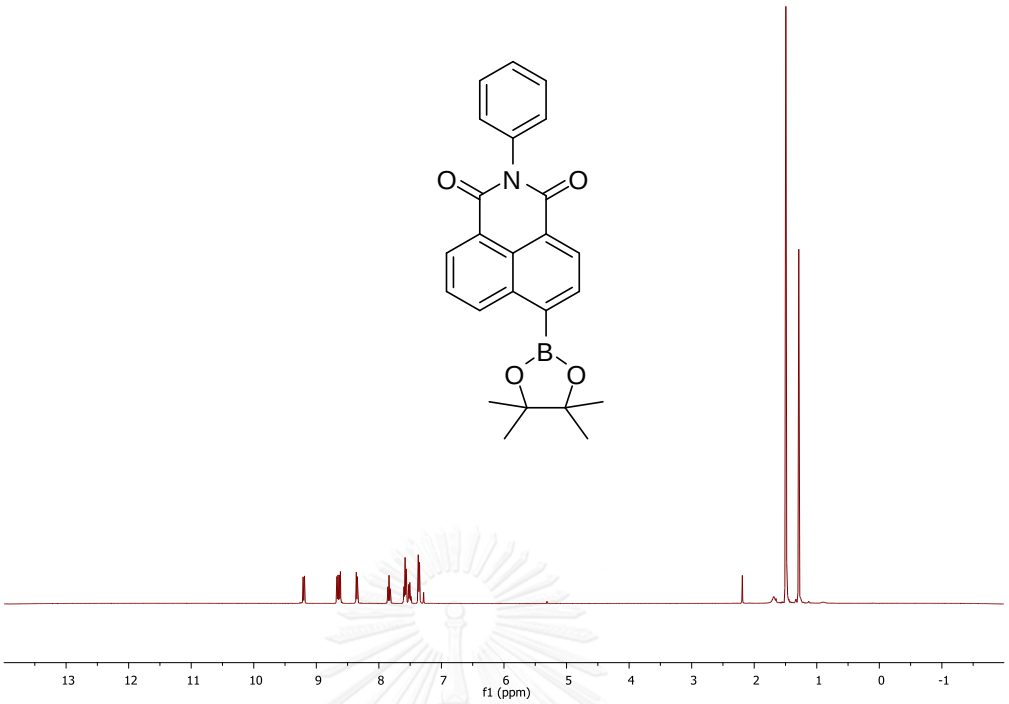

Figure A7. ^{1}H-NMR of *N*-phenyl-1,8-naphthalimide-4-boronic acid in $CDCl_3$

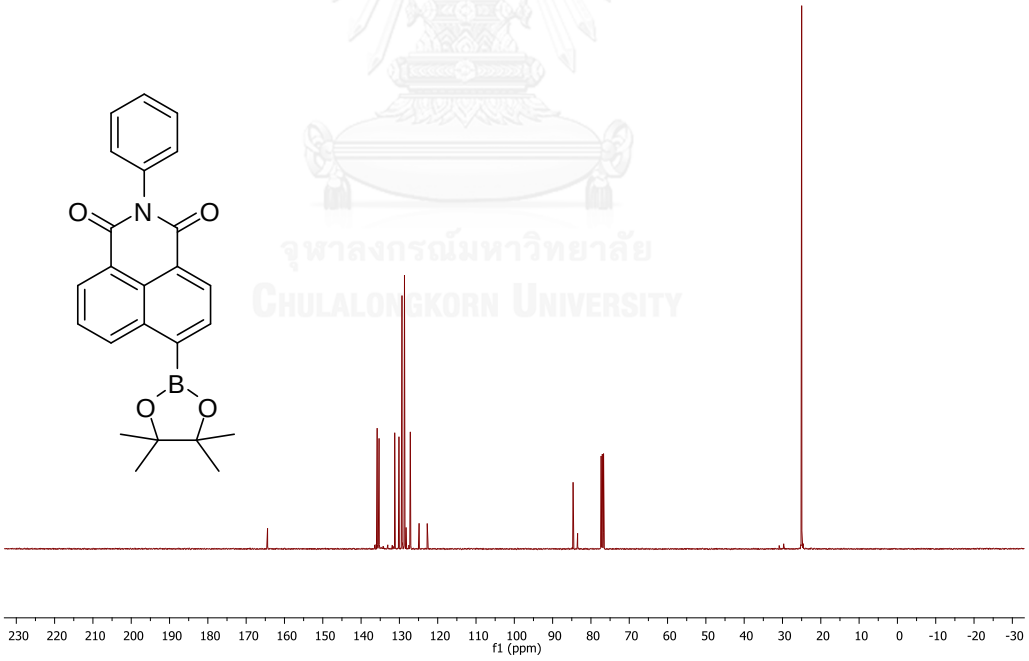

Figure A8. ^{13}C-NMR of *N*-phenyl-1,8-naphthalimide-4-boronic acid in $CDCl_3$

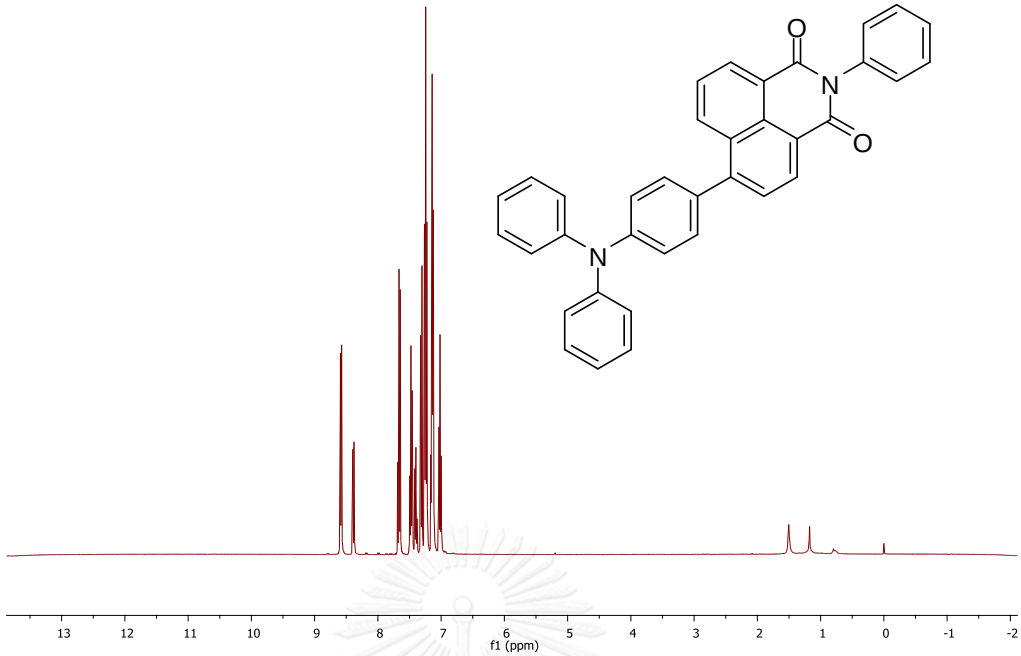

Figure A9. ^{1}H-NMR of **1** in $CDCl_3$

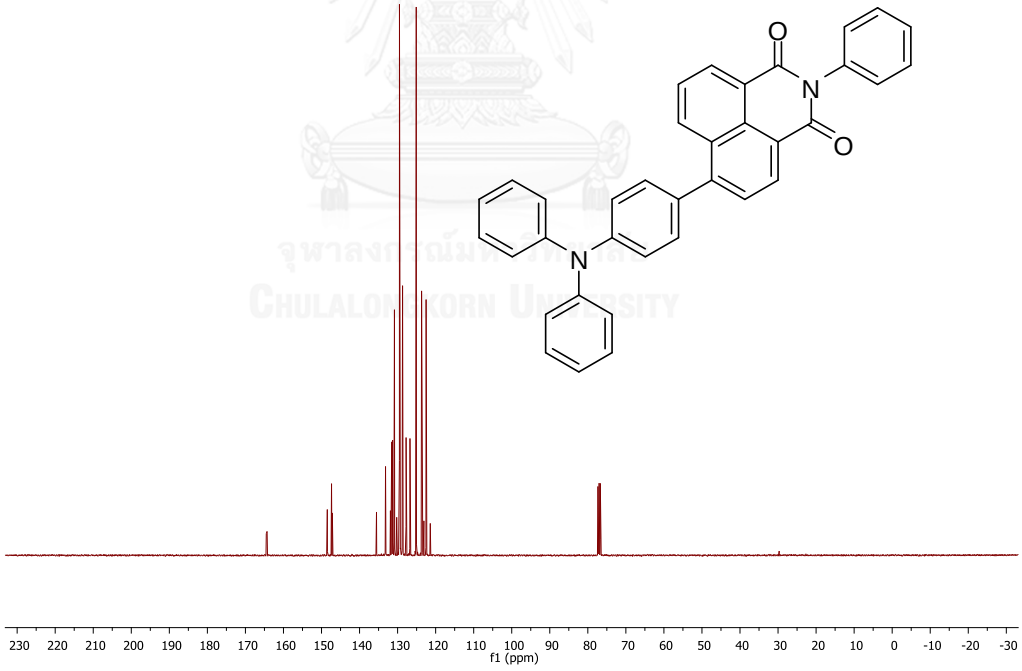

Figure A10. ^{13}C-NMR of **1** in $CDCl_3$

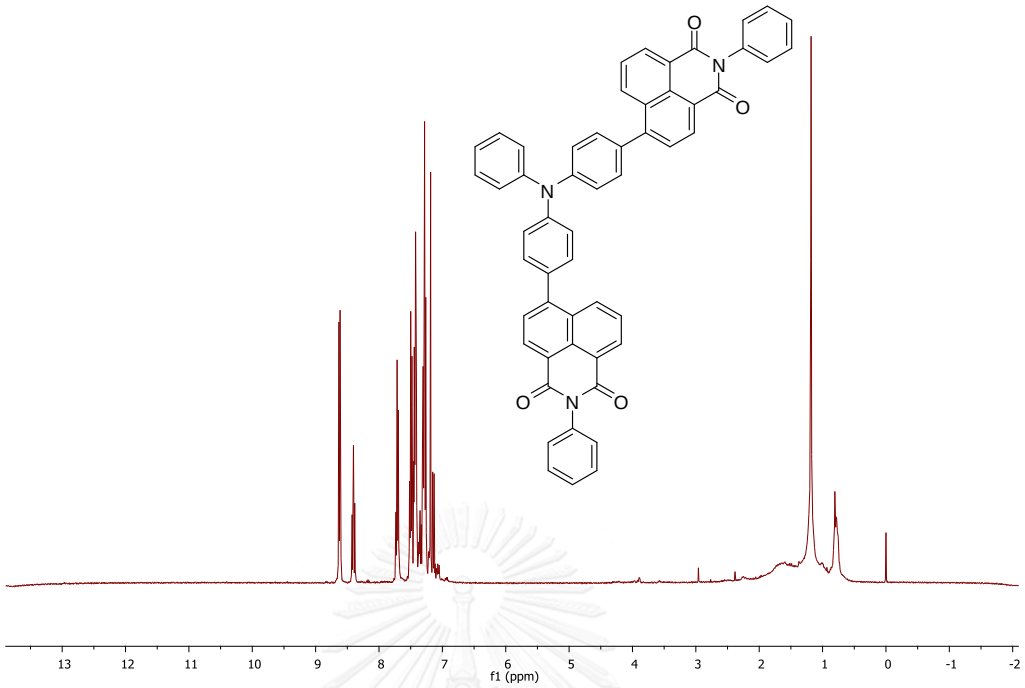

Figure A11. ^{1}H-NMR of **2** in $CDCl_3$

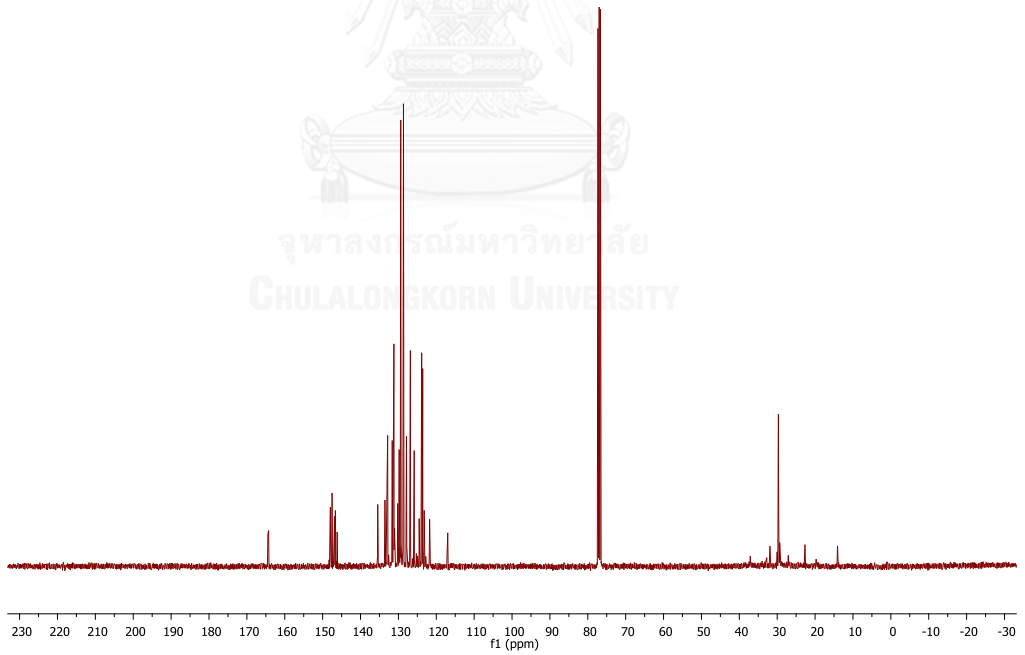

Figure A12. ^{13}C-NMR of **2** in $CDCl_3$

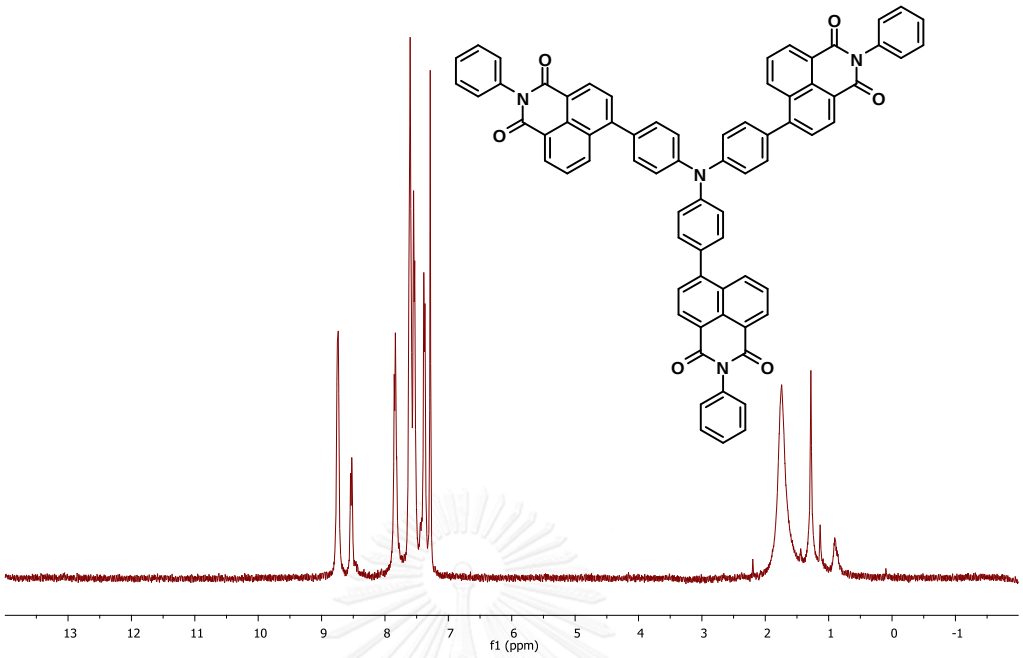

Figure A13. ^{1}H-NMR of **3** in $CDCl_3$

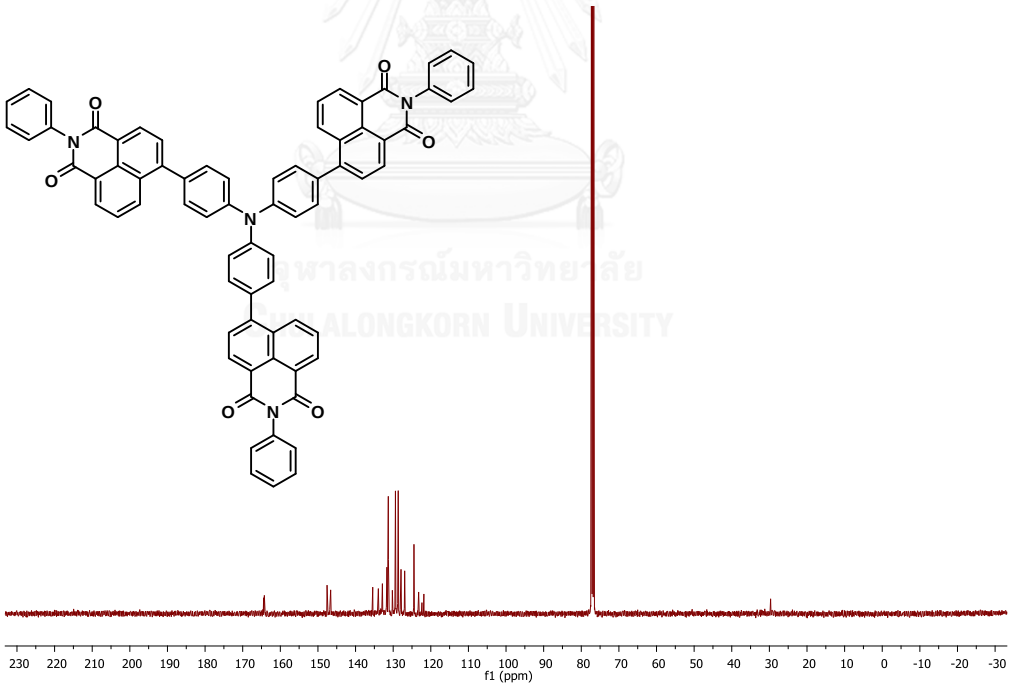

Figure A14. ^{13}C-NMR of **3** in $CDCl_3$

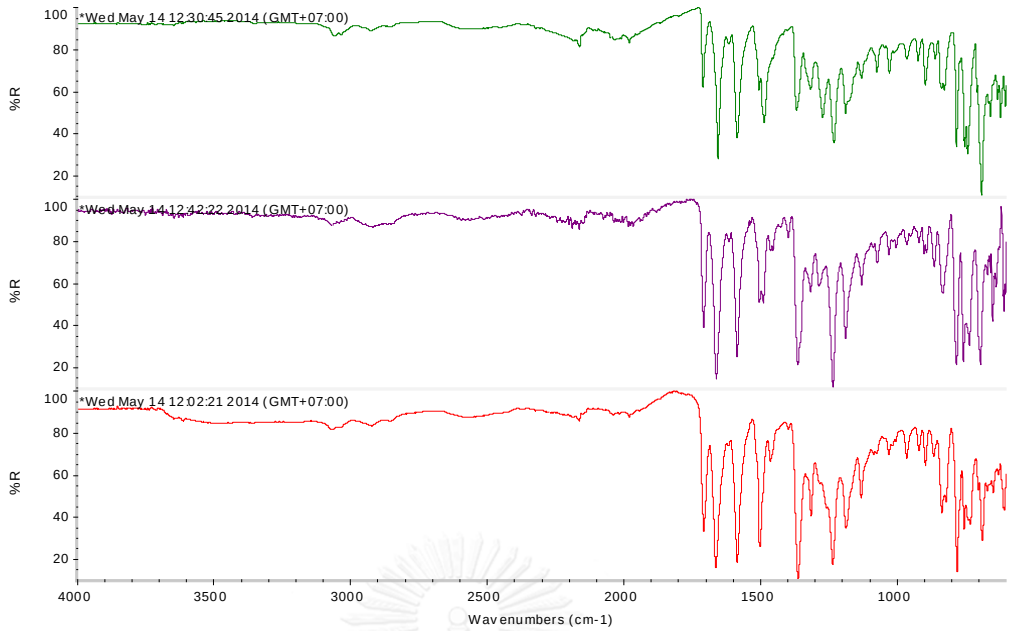

Figure A15. IR spectra of TPN1-TPN3

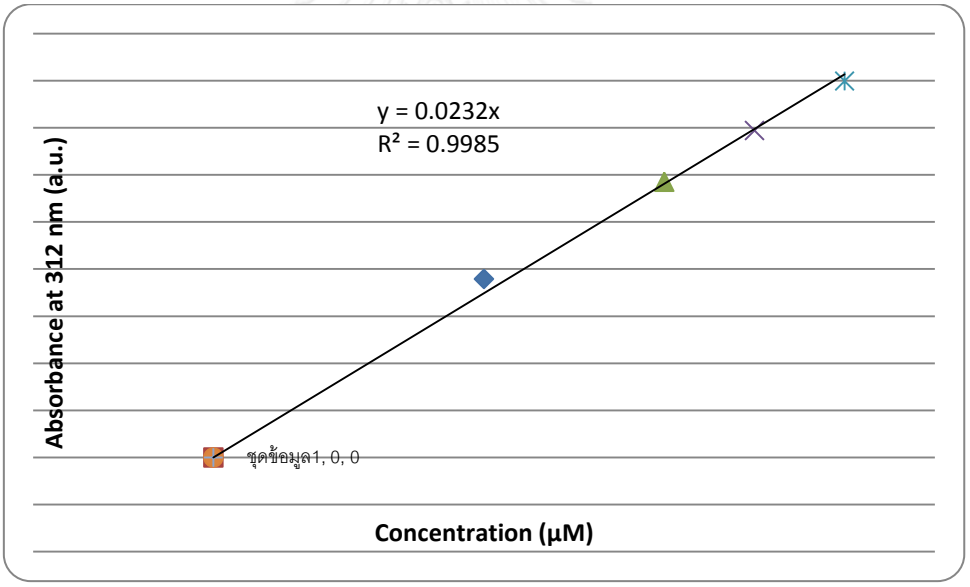

Figure A16. Molar absorption coefficient plot of target molecule **1** in $CHCl_3$

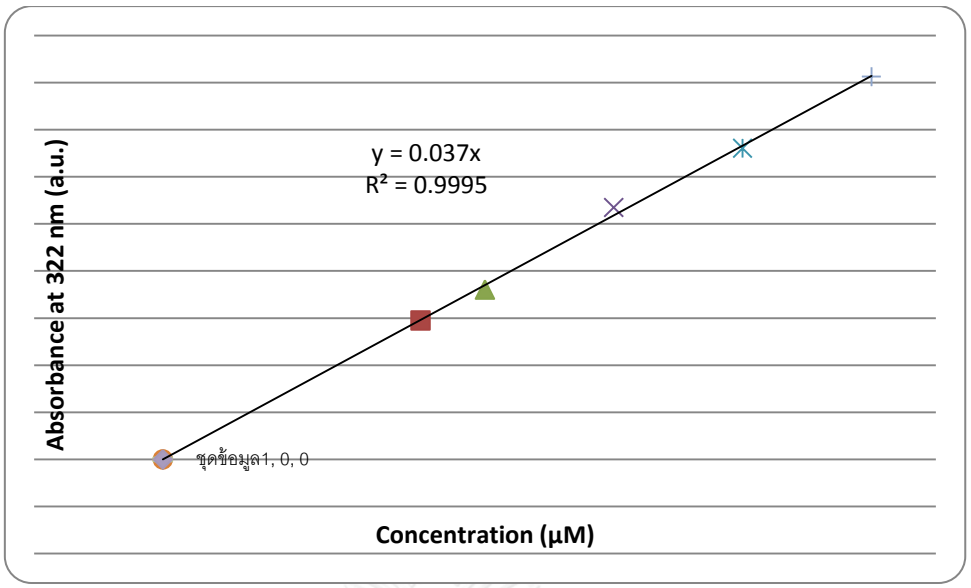

Figure A17. Molar absorption coefficient plot of target molecule **2** in $CHCl_3$

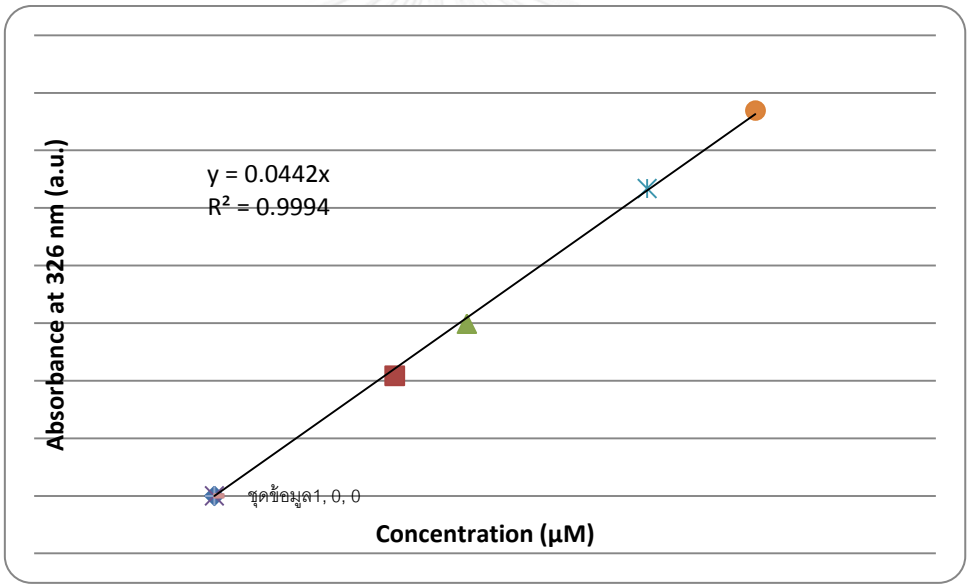

Figure A18. Molar absorption coefficient plot of target molecule **3** in $CHCl_3$

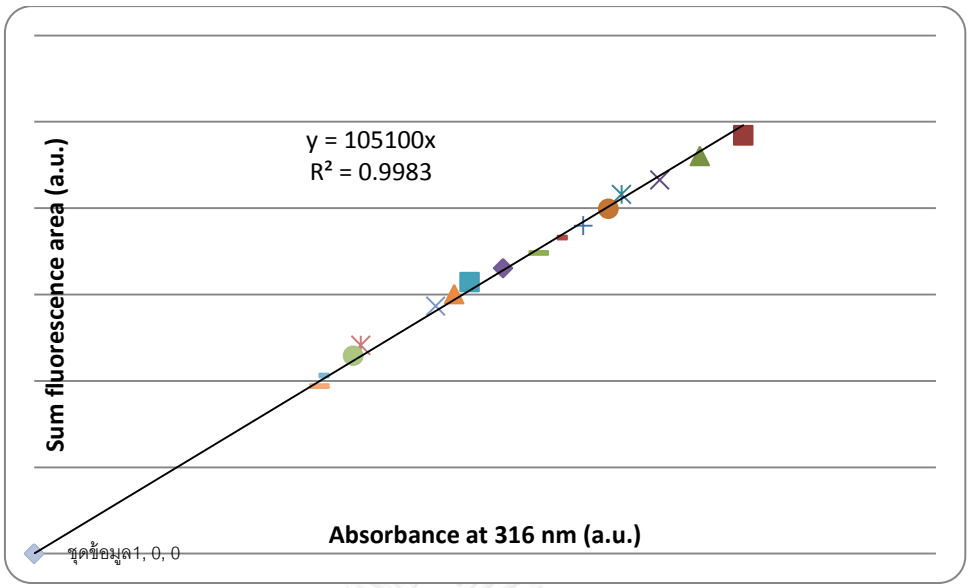

Figure A19. Quantum yield plot of target molecule **1** in $CHCl_3$

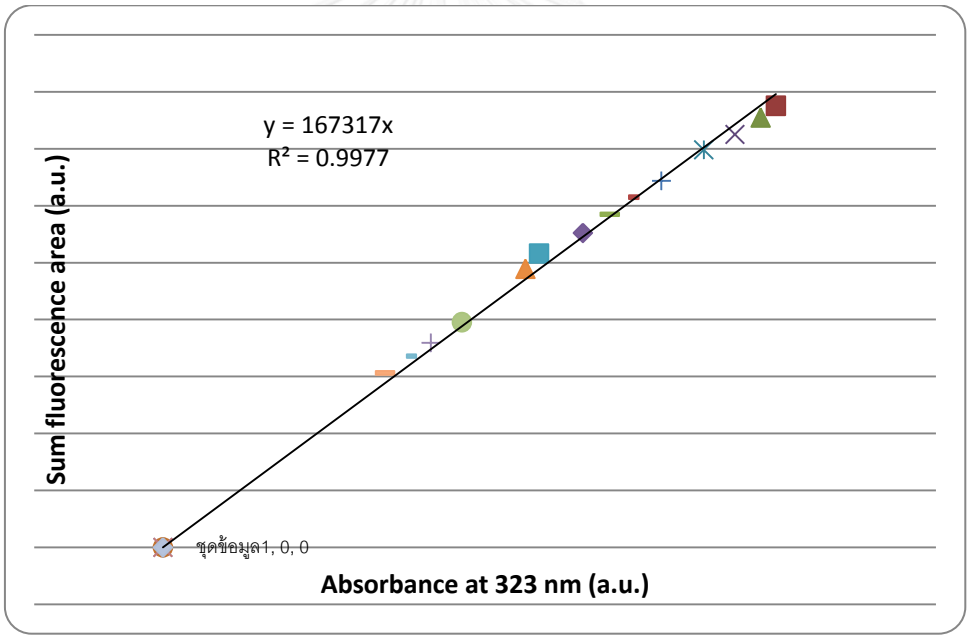

Figure A20. Quantum yield plot of target molecule **2** in $CHCl_3$

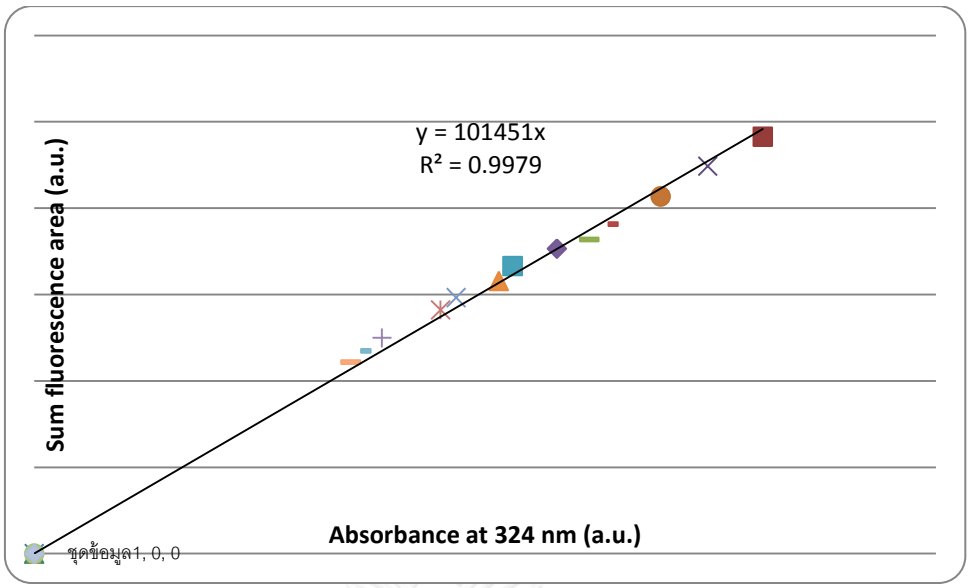

Figure A21. Quantum yield plot of target molecule **3** in $CHCl_3$

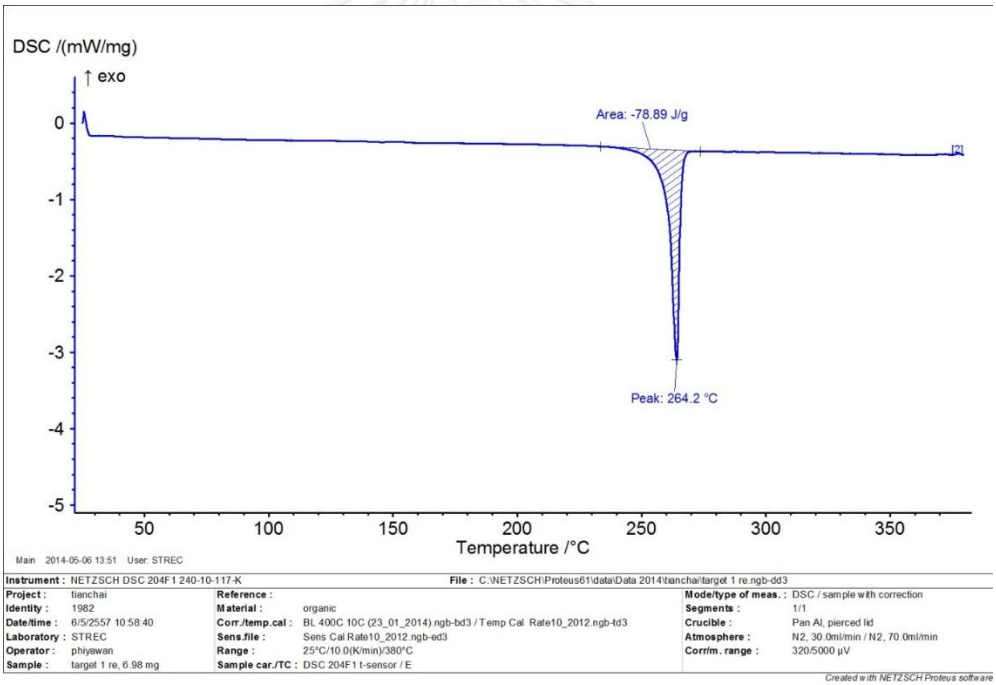

Figure A22. DSC measurement of **1** with a heating rate of 10°C per minute under N_2

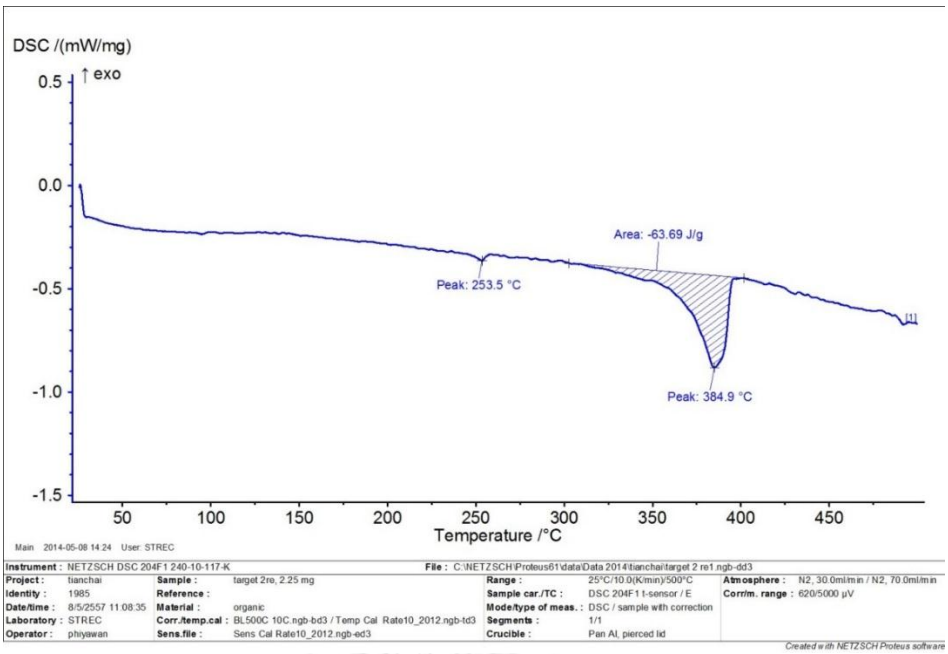

Figure A23. DSC measurement of **2** with a heating rate of 10°C per minute under N_2

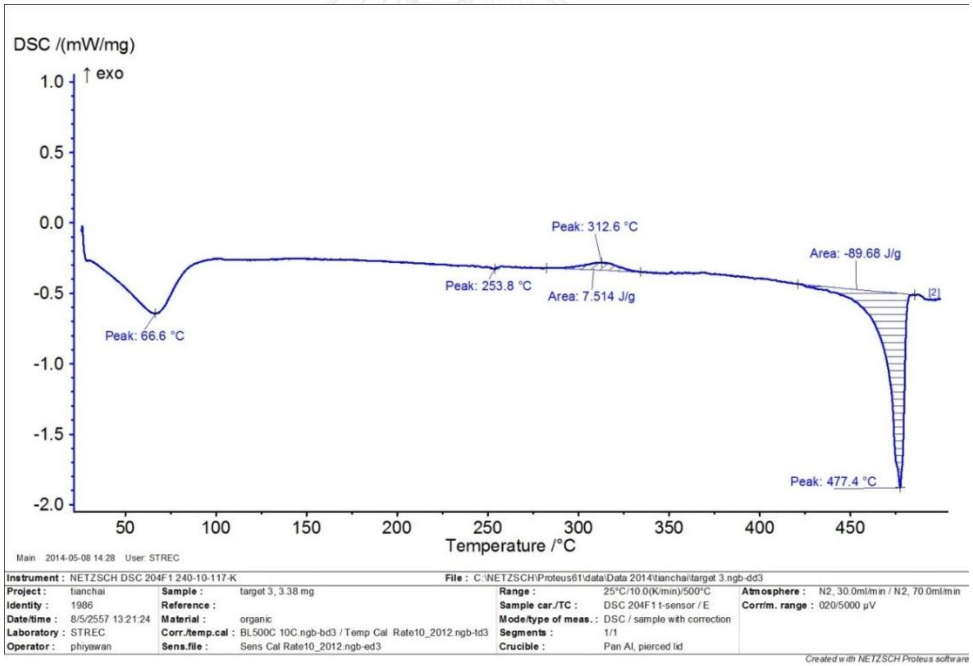

Figure A24. DSC measurement of **3** with a heating rate of 10°C per minute under N_2

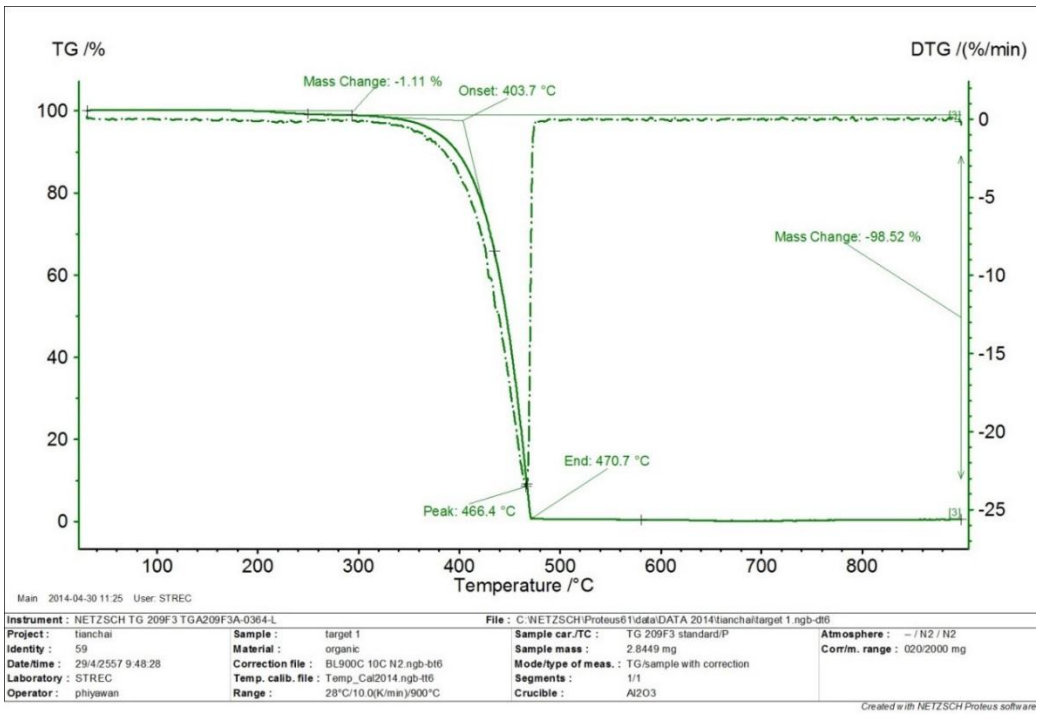

Figure A25. TGA measurement of **1** with a heating rate of 10°C per minute under N_2

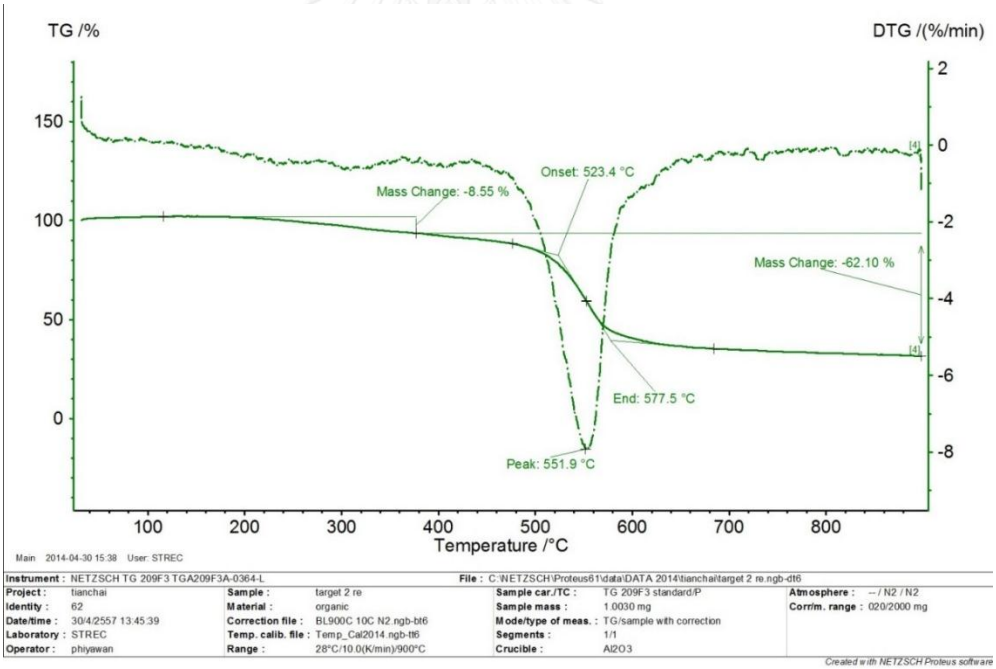

Figure A26. TGA measurement of **2** with a heating rate of 10°C per minute under N_2

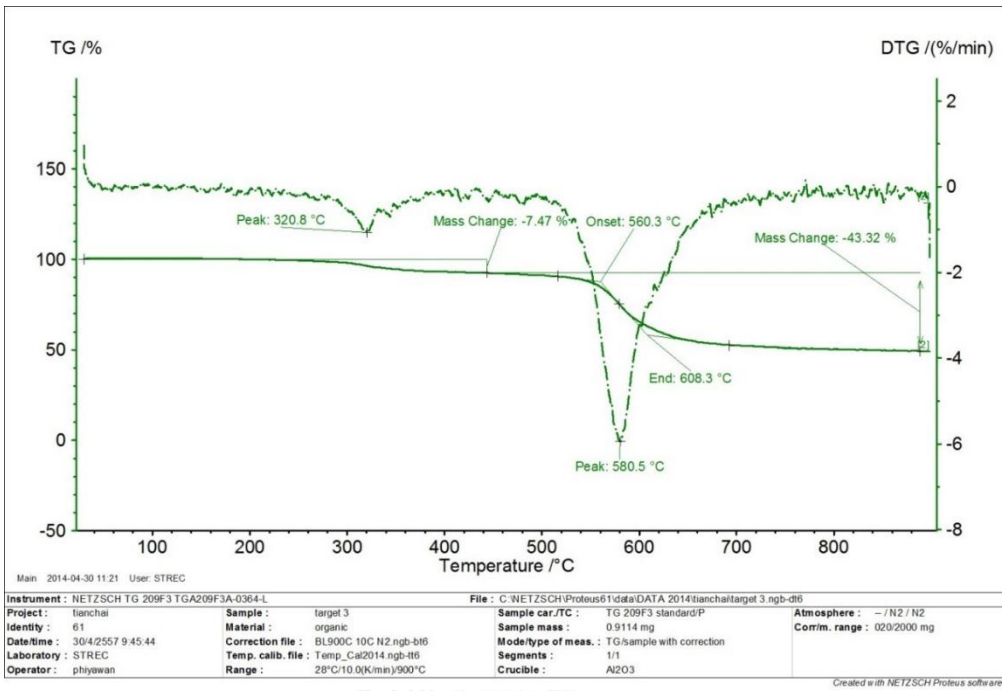

Figure A27. TGA measurement of **3** with a heating rate of 10°C per minute under N_2

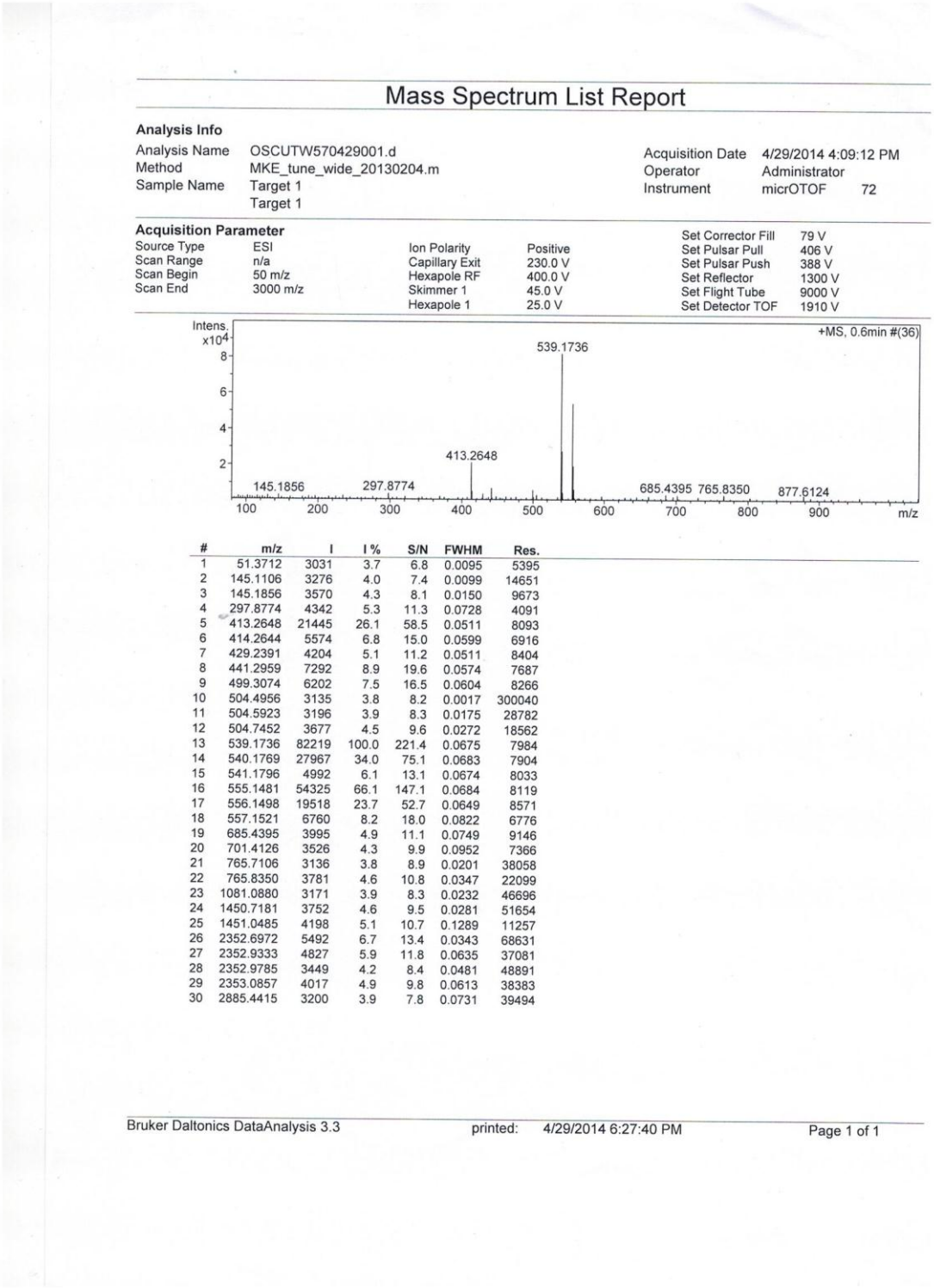

Mass Spectrum List Report

Analysis Info

Analysis Name	OSCUTW570429001.d	Acquisition Date	4/29/2014 4:09:12 PM
Method	MKE_tune_wide_20130204.m	Operator	Administrator
Sample Name	Target 1	Instrument	micrOTOF 72
	Target 1		

Acquisition Parameter

Source Type	ESI	Ion Polarity	Positive	Set Corrector Fill	79 V
Scan Range	n/a	Capillary Exit	230.0 V	Set Pulsar Pull	406 V
Scan Begin	50 m/z	Hexapole RF	400.0 V	Set Pulsar Push	388 V
Scan End	3000 m/z	Skimmer 1	45.0 V	Set Reflector	1300 V
		Hexapole 1	25.0 V	Set Flight Tube	9000 V
				Set Detector TOF	1910 V

#	m/z	I	I %	S/N	FWHM	Res.
1	51.3712	3031	3.7	6.8	0.0095	5395
2	145.1106	3276	4.0	7.4	0.0099	14651
3	145.1856	3570	4.3	8.1	0.0150	9673
4	297.8774	4342	5.3	11.3	0.0728	4091
5	413.2648	21445	26.1	58.5	0.0511	8093
6	414.2644	5574	6.8	15.0	0.0599	6916
7	429.2391	4204	5.1	11.2	0.0511	8404
8	441.2959	7292	8.9	19.6	0.0574	7687
9	499.3074	6202	7.5	16.5	0.0604	8266
10	504.4956	3135	3.8	8.2	0.0017	300040
11	504.5923	3196	3.9	8.3	0.0175	28782
12	504.7452	3677	4.5	9.6	0.0272	18562
13	539.1736	82219	100.0	221.4	0.0675	7984
14	540.1769	27967	34.0	75.1	0.0683	7904
15	541.1796	4992	6.1	13.1	0.0674	8033
16	555.1481	54325	66.1	147.1	0.0684	8119
17	556.1498	19518	23.7	52.7	0.0649	8571
18	557.1521	6760	8.2	18.0	0.0822	6776
19	685.4395	3995	4.9	11.1	0.0749	9146
20	701.4126	3526	4.3	9.9	0.0952	7366
21	765.7106	3136	3.8	8.9	0.0201	38058
22	765.8350	3781	4.6	10.8	0.0347	22099
23	1081.0880	3171	3.9	8.3	0.0232	46696
24	1450.7181	3752	4.6	9.5	0.0281	51654
25	1451.0485	4198	5.1	10.7	0.1289	11257
26	2352.6972	5492	6.7	13.4	0.0343	68631
27	2352.9333	4827	5.9	11.8	0.0635	37081
28	2352.9785	3449	4.2	8.4	0.0481	48891
29	2353.0857	4017	4.9	9.8	0.0613	38383
30	2885.4415	3200	3.9	7.8	0.0731	39494

Bruker Daltonics DataAnalysis 3.3 printed: 4/29/2014 6:27:40 PM Page 1 of 1

Figure A28. High resolution mass spectrum of **TPN1**

Mass Spectrum List Report

Analysis Info

Analysis Name	OSCUTW570429002.d	Acquisition Date	4/29/2014 4:15:47 PM
Method	Natee20130403.m	Operator	Administrator
Sample Name	Target 2 Target 2	Instrument	micrOTOF 72

Acquisition Parameter

Source Type	ESI	Ion Polarity	Positive	Set Corrector Fill	79 V
Scan Range	n/a	Capillary Exit	250.0 V	Set Pulsar Pull	406 V
Scan Begin	50 m/z	Hexapole RF	400.0 V	Set Pulsar Push	388 V
Scan End	3000 m/z	Skimmer 1	54.4 V	Set Reflector	1300 V
		Hexapole 1	21.4 V	Set Flight Tube	9000 V
				Set Detector TOF	1910 V

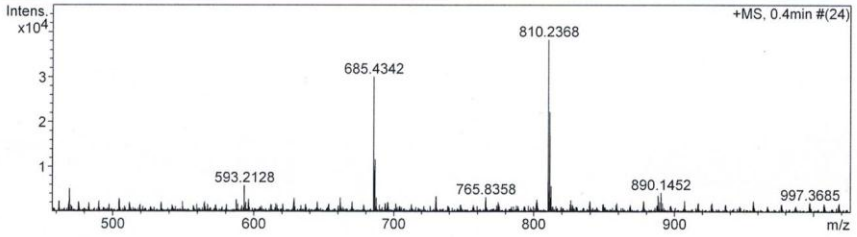

#	m/z	I	I %	S/N	FWHM	Res.
1	53.7050	3588	9.4	7.9	0.0072	7430
2	56.1455	3055	8.0	6.7	0.0303	1851
3	214.7735	3233	8.5	7.7	0.0369	5815
4	297.8772	3041	7.9	7.9	0.0768	3880
5	413.2656	13643	35.7	37.9	0.0499	8288
6	414.2626	4094	10.7	11.2	0.0573	7227
7	437.1915	3179	8.3	8.6	0.0505	8655
8	441.2959	6333	16.6	17.4	0.0582	7579
9	469.3294	5164	13.5	14.1	0.0634	7399
10	593.2128	5855	15.3	15.8	0.0672	8831
11	685.4342	30047	78.5	82.1	0.0719	9530
12	686.4397	11705	30.6	31.7	0.0801	8574
13	687.4429	3139	8.2	8.2	0.0762	9027
14	765.8358	3269	8.5	8.6	0.0346	22138
15	810.2368	38255	100.0	105.2	0.0851	9525
16	811.2390	22256	58.2	61.1	0.0855	9492
17	811.6996	3174	8.3	8.4	0.0348	23299
18	812.2437	5726	15.0	15.5	0.0902	9001
19	888.1462	3488	9.1	9.4	0.0953	9322
20	890.1452	4286	11.2	11.7	0.0911	9771
21	1081.0874	2931	7.7	8.0	0.0239	45147
22	1450.7224	3310	8.7	8.7	0.0291	49831
23	1451.0561	4150	10.8	10.9	0.1205	12044
24	1500.7067	3100	8.1	8.1	0.0310	48429
25	1874.9750	2929	7.7	7.4	0.1590	11790
26	2352.6772	5003	13.1	12.7	0.0337	69797
27	2352.9322	4194	11.0	10.6	0.0639	36815
28	2353.0777	3161	8.3	7.9	0.0662	35529
29	2369.0144	2932	7.7	7.3	0.0419	56556
30	2903.1315	3481	9.1	9.0	0.0464	62568

Figure A29. High resolution mass spectrum of **TPN2**

Mass Spectrum List Report

Analysis Info

Analysis Name	OSCUTW5704290031.d	Acquisition Date	4/29/2014 4:31:10 PM
Method	Natee20130403.m	Operator	Administrator
Sample Name	Target 3	Instrument	micrOTOF · 72
	Target 3		

Acquisition Parameter

Source Type	ESI	Ion Polarity	Positive	Set Corrector Fill	79 V
Scan Range	n/a	Capillary Exit	250.0 V	Set Pulsar Pull	406 V
Scan Begin	50 m/z	Hexapole RF	400.0 V	Set Pulsar Push	388 V
Scan End	3000 m/z	Skimmer 1	54.4 V	Set Reflector	1300 V
		Hexapole 1	21.4 V	Set Flight Tube	9000 V
				Set Detector TOF	1910 V

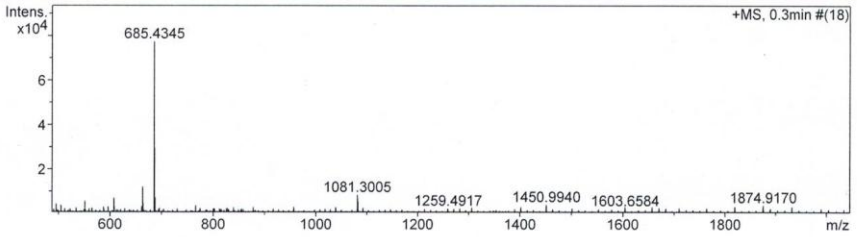

#	m/z	I	I %	S/N	FWHM	Res.
1	53.7406	3023	3.9	6.9	0.0103	5214
2	56.1504	3436	4.4	7.9	0.0410	1369
3	413.2703	12150	15.7	34.4	0.0489	8450
4	414.2668	3479	4.5	9.7	0.0629	6591
5	441.2997	6723	8.7	18.8	0.0514	8578
6	495.2673	4295	5.6	11.8	0.0554	8935
7	504.7505	3844	5.0	10.5	0.0231	21830
8	551.3277	5574	7.2	15.4	0.0566	9739
9	587.5455	3010	3.9	8.1	0.0594	9889
10	607.3887	6961	9.0	19.3	0.0628	9679
11	608.3948	3156	4.1	8.5	0.0623	9758
12	661.5486	3289	4.3	8.9	0.0570	11599
13	663.4520	12118	15.7	34.0	0.0634	10460
14	664.4571	4676	6.0	12.9	0.0768	8652
15	685.4345	77363	100.0	219.0	0.0697	9834
16	686.4384	29514	38.2	83.3	0.0741	9270
17	687.4417	7217	9.3	20.1	0.0679	10129
18	765.8466	3784	4.9	10.5	0.0336	22825
19	1081.3005	8375	10.8	25.2	0.1091	9907
20	1082.2960	5371	6.9	16.0	0.1088	9951
21	1450.7411	3451	4.5	10.1	0.0275	52817
22	1450.9940	4057	5.2	11.9	0.0723	20065
23	1874.6409	3602	4.7	10.3	0.0313	59828
24	1874.9170	3793	4.9	10.8	0.0275	68104
25	2352.7678	4957	6.4	13.7	0.0341	68897
26	2352.9969	4660	6.0	12.9	0.0608	38696
27	2353.0512	3574	4.6	9.8	0.0499	47176
28	2353.1573	3626	4.7	10.0	0.0633	37172
29	2612.1770	3235	4.2	8.8	0.0373	70045
30	2885.5369	3015	3.9	8.2	0.0684	42189

Bruker Daltonics DataAnalysis 3.3 printed: 4/29/2014 6:26:15 PM Page 1 of 1

Figure A30. High resolution mass spectrum of **TPN3**

VITA

Miss Rungthiwa Arunchai was born on April 17th, 1989 in Lopburi, Thailand. Her address is 80/427 P.Thana Tower 2 Soi Latphrao 58/1, Latphrao road, Wangthonglhang, Bangkok, 10310. To contact her, please call 0909867686 or send E-mail to thiwa_1732@hotmail.com. In 2010, she graduated her Bachelor's Degree of science in Chemistry from Chulalogkorn University. After that she continued her Master's degree of Science in Organic Chemistry at Chulalongkorn University. She has received the scholarship from the Development and Promotion of Science and Technology Talents Project from the Royal Thai Government.